Analysis of Thickness-Change Induced Local Bending Problems in CFRP-Sandwich Structures

Thomsen, Ole Thybo

Publication date:
1994

Document Version
Publisher's PDF, also known as Version of record

esa european space agency
european space research and technology centre

EXPERIMENTAL AND THEORETICAL INVESTIGATION OF PLY DROP-OFF EFFECTS IN SANDWICH PANELS WITH LAMINATED CFRP FACE-SHEETS

by

Ole Thybo Thomsen
Research Fellow
ESA/ESTEC/YME
Keplerlaan 1, P. O. Box 299
NL-2200 AG Noordwijk
The Netherlands

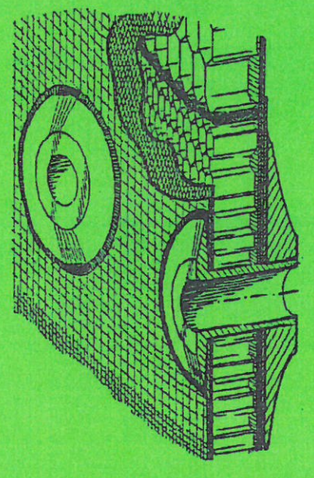

ESTEC Working Paper EWP-1839

June 1995

Printed by TIDC Reproduction

esa european space agency
european space research and technology centre

EXPERIMENTAL AND THEORETICAL INVESTIGATION OF PLY DROP-OFF EFFECTS IN SANDWICH PANELS WITH LAMINATED CFRP FACE-SHEETS

by

Ole Thybo Thomsen
Research Fellow
ESA/ESTEC/YME
Keplerlaan 1, P. O. Box 299
NL-2200 AG Noordwijk
The Netherlands

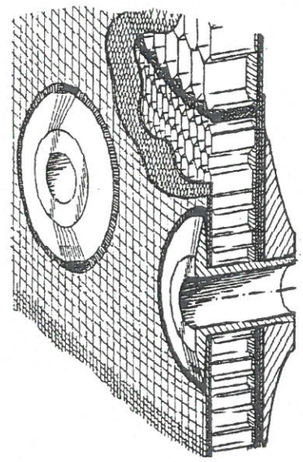

ESTEC Working Paper EWP-1839

June 1995

Front page illustration:

Design details (including ply "drop-offs" and change of honeycomb core density) around propellant-tank interface of CFRP/honeycomb satellite thrust cylinder; ESA-ASTP3 programme; demonstrator model (Courtesy of Stork Products Engineering B. V., The Netherlands).

Title:

EXPERIMENTAL AND THEORETICAL INVESTIGATION OF PLY DROP-OFF EFFECTS IN SANDWICH PANELS WITH LAMINATED CFRP FACE-SHEETS

Prepared by:

O. T. Thomsen, Research Fellow, ESTEC/YME

Summary (extended abstract):

The thickness of the face-laminates in CFRP/honeycomb sandwich panels is often increased locally in order to provide for the load transfer around highly loaded locations such as joints or inserts. Such thickness increases are accomplished by adding extra plies to the face-laminates, and a taper is produced by dropping of plies away from the area of localised loading. At all the stations where such thickness drop-offs are made, the local bending stiffness of the face-laminate changes discontinuously, thus inducing severe local bending effects. These local bending effects induce interlaminar and bending stresses in the face-laminates, as well as interlaminar stresses in the interface between the core material and the face-laminates. Thus, the induced stress concentrations may initiate delamination, core crushing or direct bending failure of the CFRP face-laminates.
This report presents the results of a combined experimental and theoretical investigation of the problem described. The objective of the experiments was to validate the theoretical approach suggested in a previous report by the author; EWP-1787, *"Analysis of Thickness-Change induced Local Bending Effects in CFRP-Sandwich Panels"*, June 1994 (ref. [1]). In this report a simple model for engineering analysis of ply "drop-off" effects in sandwich panels was developed, where the basic principle is to model the interaction between the honeycomb core and face-laminates by use of an elastic foundation model. The experimental investigation was conducted using electronic speckle pattern interferometry (ESPI), which provides very accurate surface displacement measurements ("whole field" as opposed to "discrete point" measurements).
Six CFRP/honeycomb sandwich test-specimens of three different configurations (two of each) were manufactured, where each configuration was characterised by different elastic response properties (different elastic wave-lengths). The six test-specimens provided twelve sample sides for the experiments (four sample sides of each configuration). In the experiments, the CFRP/honeycomb sandwich test-specimens were loaded in longitudinal compression, and the obtained results include the following for each of the twelve sample sides: a specklegram (image containing the interferometric data in the form of fringe patterns), selected out-of-plane deflection profiles derived from the specklegram, an averaged out-of-plane deflection profile (average of selected profiles) and a "low-pass" filtered version of the averaged deflection profile. The measured out-of-plane deflection profiles contained three contributing parts: 1. Local bending induced by the ply "drop-off's" (LB-part), 2. Local bending caused by the discrete support provided by the honeycomb core (HC-part), and 3. Speckle noise. The filtering of the averaged deflection profiles was conducted in order to isolate the LB-response parts.
Comparison of the theoretically predicted (describes the LB-response) and the measured (filtered profiles) deflection profiles revealed a good match, and it is has been demonstrated, that the elastic approach foundation suggested in ref. [1] provides a high-quality estimate of the local bending effects encountered in CFRP/honeycomb sandwich panels with tapered face-laminates.

Keywords:

CFRP/honeycomb sandwich panels, local bending, tapering, ply "drop-off" problem, elastic foundation model, honeycomb/CFRP-laminate interaction, speckle pattern interferometry, ESPI method.

Foreword:

This ESTEC Working Paper is the fourth in a series of reports presenting the main results of the work carried out under the auspices of a research fellowship awarded with the Mechanical Systems Department, Structures and Mechanisms Division, Structural Engineering Section at ESTEC in Noordwijk, the Netherlands. The overall theme of the research fellowship was entitled *"Discontinuities and Load Introduction Aspects of CFRP-Sandwich Structures"*, and the subject of analysis and design of structural sandwich panels with tapered (i.e., with ply "drop-off's") laminated CFRP face-sheets comprised one of the areas addressed during the period (18 months) of the research fellowship.

This report is devoted to the presentation of result obtained from an experimental investigation of ply "drop-off" effects in CFRP/honeycomb sandwich panels. The objective of the investigation was to check/validate a simple model for engineering analysis of such problems suggested by the author in a previous ESTEC Working Paper (EWP-1787, *"Analysis of Thickness-Change induced Local Bending Effects in CFRP-Sandwich Panels"*, June 1994; ref. [1]). As the local bending problem is characterised by very short wave-lengths, it was necessary to adopt an extremely sensitive measuring technique, and the experiments were carried out using electronic speckle pattern interferometry (ESPI).

The content of this report is organised such, that the local bending problem associated with ply "drop-off's" in CFRP/honeycomb sandwich panels is introduced along with a very brief description of the theoretical approach described in EWP-1787, ref. [1] (to which the reader is referred for details of the theoretical modelling of the problem).
Following this introduction, the main part of the report is devoted to the specification of the experimental investigation (including objectives, requirements and selection of experimental technique), description of the experimental procedure, presentation of the experimental results as well as comparison between the experimental results and the theoretical predictions (based on ref. [1]).
The report is concluded with a discussion of the obtained comparative results, as well as a discussion of possible future experimental investigations of ply "drop-off" effects in sandwich panels (i.e., "lessons learned").

Noordwijk, June 1995

O. T. Thomsen

LIST OF CONTENTS

PRINCIPAL NOTATION

Abbreviations:

C.R.I.F.:	Centre de Recherches scientifiques et techniques de l'Industrie de Fabrications métalliques, Section Technologie des Matériaux, Liège, Belgium.
ESPI:	Electronic speckle pattern interferometry.
HC:	Honeycomb core induced bending response (with wave-length equal to the honeycomb cell size S_c).
HI:	Holographic interferometry.
LB:	Local bending response induced by face-laminate thickness "drop-off".
MRC:	Microgravity Research Center, Université Libre de Bruxelles, Bruxelles, Belgium.
PSSI:	Phase shifting speckle interferometry.

Latin symbols:

$[\boldsymbol{A}_{11}(x)]$:	(6,6)-matrix of stiffness coefficients for the governing system of differential equations in the interval $0 \le x < L_1$.
$[\boldsymbol{A}_{ij}^{*}(x)]$ $(i,j=1,2)$:	(6,6)-matrices of stiffness coefficients for the governing system of differential equations in the interval $L_1 \le x \le L_2$.
b:	Width of face-laminates used in ref. [1]: $b=1.0\ mm$ (unit width); (mm).
$\{\boldsymbol{B}_1(x)\}$:	(6,1)-matrix of non-homogeneous load-terms for the governing system of differential equations in the interval $0 \le x < L_1$.
$\{\boldsymbol{B}_i^{*}(x)\}$ $(i=1,2)$:	(6,1)-matrices of non-homogeneous load-terms for the governing system of differential equations in the interval $L_1 \le x \le L_2$.
c:	Honeycomb core thickness (mm).
D_i $(i=1,2)$:	Principal bending stiffnesses of the base-line and reinforcing laminates; (Nmm).
E_a:	Elastic modulus of adhesive/"resin-rich" layer interfacing the base-line and reinforcing laminates; (MPa).
E_c:	Elastic modulus (out-of-plane) of honeycomb core material; (MPa).
E_x, E_y:	In-plane elastic moduli (face-laminates or plies); (MPa).
E_0:	Effective out-of-plane elastic modulus of honeycomb core; (MPa).
G_L, G_W:	Honeycomb core shear moduli in L- and W-directions, respectively; (MPa).
G_{xy}:	Shear modulus (face-laminates or plies); (MPa).
K_z, K_x:	Out-of-plane and shear foundation moduli ; $(MPa/mm=N/mm^3)$.
$F_j(\phi)$ $(j=1,2)$:	"Coefficient functions" for elastic foundation moduli.
L_i $(i=1,2)$:	Lengths of face-laminates in base-line and reinforced regions; (mm).
M_i $(i=1,2)$:	Bending moment resultants in face-laminates; (Nmm/mm).
N_i $(i=1,2)$:	Normal stress resultants in face-laminates; (N/mm).
P:	In-plane stress resultant in face-laminates; (N/mm).
P_{tot}:	Total in-plane load on test-specimens: $P_{tot}=2\times$"*specimen width*"$\times P$; (N).
P_1, P_2:	"Off-set" and "maximum load" in-plane stress resultants in face-laminates ; (N/mm).
Q_i $(i=1,2)$:	Out-of-plane shear stress resultants in face-laminates; (N/mm).

S_c:	Honeycomb core cell size: largest circle-diameter which can be inscribed in the honeycomb cells; (*mm*).
t_a:	Thickness of adhesive/"resin-rich" layer interfacing the base-line and reinforcing laminates; (*mm*)
t_i $(i=1,2)$:	Thicknesses of face-laminates; (*mm*).
u_i $(i=1,2)$:	Longitudinal displacements of face-laminates; (*mm*).
u_{0i} $(i=1,2)$:	Longitudinal displacements of mid-surfaces of face-laminates; (*mm*).
w:	Out-of-plane deflections of test-specimen surfaces; (*mm*).
w_i $(i=c \text{ or } i=1,2)$:	Out-of-plane deflections of core or face-laminates; (*mm*).
$\|w\|$:	Amplitude of out-of-plane deflection profiles; $\|w\|=w(maximum)-w(minimum)$; (*mm*).
x:	Longitudinal coordinate; (*mm*).
x_{peak}:	Distance between minimum ("valley") and maximum ("peak") points of filtered (experimental) and theoretical out-of-plane deflection profiles; (*mm*).
Δx:	Phase difference between filtered (experimental) and theoretical out-of-plane deflection profiles; (*mm*).
Δx_{avg}:	Average phase difference between filtered and theoretical out-of-plane deflection profiles, $\{\Delta x(\text{"}max.points\text{"})+\Delta x(\text{"}min.points\text{"})\}/2$; (*mm*).
y:	"Width"-direction coordinate; (*mm*)
$\{y_i(x)\}$ $(i=1,2)$:	$(6,1)$-matrix of fundamental variables for face-laminates: $\{y_i(x)\}=\{u_{0i}(x), w_i(x), \beta_i(x), N_i(x), M_i(x), Q_i(x)\}$.
z:	Out-of-plane coordinate; (*mm*).

Greek symbols:

α:	Characteristic decay distance; (*mm*).
β_i $(i=1,2)$:	Rotation of the midsurface normals of face-laminates; (*rad*).
ϕ:	Non-dimensional geometric coefficient (foundation model).
γ:	Non-dimensional coefficient (foundation model); $(\gamma=1.5)$.
λ:	Wave-length of elastic response; (*mm*).
ν_a:	Poisson's ration of adhesive/"resin-rich" layer interfacing the base-line and reinforcing laminates.
ν_c:	Poisson's ratio (out-of-plane) of honeycomb core material.
ν_0:	Effective Poisson's ratio of honeycomb core material.
ν_{xy}:	In-plane Poisson's ratio (face-laminates or plies).
σ_c:	Honeycomb core transverse normal stress (interface between core and face-laminates); (*MPa*).
τ_c:	Honeycomb core shear stress (interface between core and face-laminates); (*MPa*).
$\psi(z)$:	Decay function for through-the-thickness core deflections.
$\Psi_j(\phi)$ $(i=1,2)$:	"Coefficient functions" for elastic foundation moduli ("exponential decay" formulation).

Superscripts:

$(\,)'$:	Differentiation with respect to the x-coordinate: $(\,)'=d(\,)/dx$.

1.0 INTRODUCTION

The originating problem for this study was the specific failure mode experienced with a wet filament wound CRFP sandwich structure (with aluminium honeycomb core), representing the central thrust cylinder of a telecommunications satellite designed and manufactured under the ESA-ASTP3 programme; see Fig. 1. In this programme, a full scale demonstration model thrust cylinder was loaded to failure in a static test with the objective of verifying the strength margin. It was not possible to identify precisely which failure mechanism initiated the onset and development of the final failure, but eventually the face-laminates of the thrust cylinder failed completely at a location where the face-laminate thickness changed abruptly. This change of face-thickness was located on the inner side of the cylinder at the junction between the propellant tank interface reinforcements, and the laminates at the lower end of the cylinder (see Fig. 1). Most likely, the phenomenon causing failure to occur at this location was local bending induced by the abrupt change of the face bending stiffness associated with the thickness change.

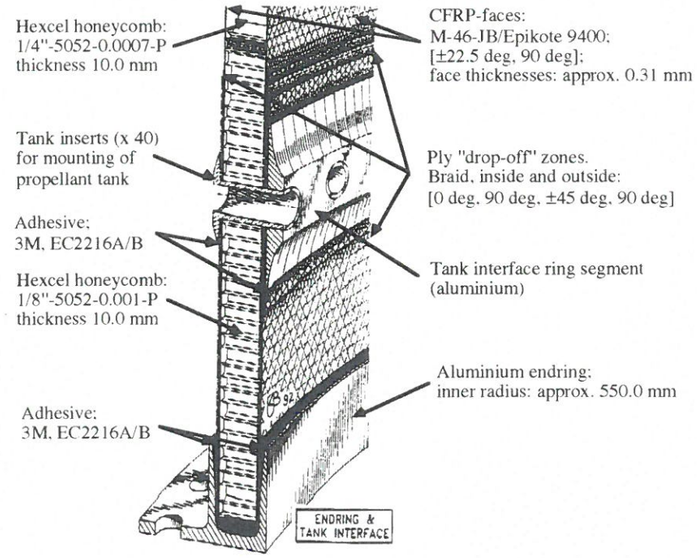

Figure 1. Design details of lower endring and tank interface of CFRP-sandwich satellite thrust cylinder; ESA-ASTP3 programme; demonstrator model (Courtesy of Stork Products Engineering B.V., The Netherlands).

In general, the thickness of face-laminates in CFRP-sandwich panels is often increased locally in order to provide for the load transfer around highly loaded locations such as joints or inserts. Such thickness increases are accomplished by adding extra plies to the face-laminates, and a taper is produced by dropping of plies away from the area of localised loading. At all the stations where such thickness "drop-off's" are made, the local bending stiffness of the face-laminate changes discontinuously, thus inducing severe local bending effects. These local bending effects, in which the face-laminate/core interaction plays an important role, induce interlaminar and bending stresses in the face-laminates, as well as stresses in the core/face-laminate interface. Thus, the stress concentrations induced in the regions near the dropped plies may initiate delamination, core crushing or direct bending failure of the face-laminates.

The general problem described briefly above was treated theoretically by the author in ref. [1], where a simple model for engineering analysis of local bending effects induced by

tapering of CFRP-laminates acting as sandwich panel face-sheets was suggested (note that unsupported CFRP-laminates can also be treated with the suggested model). The model suggested in ref. [1] is based on the assumption, that the interaction between the laminated CFRP face-sheets and the core material, which is assumed to be of honeycomb type, can be modelled by adopting an elastic foundation approach. This approach has been successfully adopted previously for the study of local bending effects in *foam-cored* sandwich panels subjected to localised out-of-plane loads; Thomsen ref. [2] and [3] (the latter reference contains an experimental verification of the approach).

2.0 OBJECTIVES

The work reported in ref. [1] (containing model definition, mathematical formulation, examples collection and a parametric study) is purely theoretical, and as the elastic foundation approach suggested has not been verified for honeycomb-cored sandwich panels in general and thickness "drop-off" problems in particular, it was decided to plan and carry out an experimental investigation. The objectives of the experimental investigation were decided to comprise the following sub-tasks:

- Establishing a base of experimental data for the evaluation and adjustment of the predicted values of the elastic foundation moduli K_x and K_z, which express the foundation transverse normal and shear stiffnesses in terms of the geometric and elastic coefficients of the constituent face-sheet and core materials. In other words, establishing whether the expressions suggested for K_x, K_z in ref. [1] are appropriate or need some adjustment.
- General evaluation of the elastic foundation approach for typical space application honeycomb-cored CFRP-sandwich panels with thickness "drop-off's". Several CFRP-sandwich panel configurations with different local bending characteristics (according to the elastic foundation approach) should be included in the investigation.
- Establishing, if possible, to what extent the discrete nature of the support of the face-sheets provided by the honeycomb cells (characterised by their cell-size S_c) influences the local bending response around face-sheet thickness "drop-off's" in CFRP-sandwich panels.

3.0 BRIEF REVIEW OF THEORETICAL BACKGROUND

In the following a brief review of the features of the mechanical model suggested in ref. [1] will be given. The mathematical details pertaining to the derivation and subsequent numerical solution of the governing set of equations will not be given, and the reader is instead referred to ref. [1].

3.1 Elastic foundation approach - fundamentals

The mechanical model suggested in ref. [1] can be considered as a general beam/plate/shell model. This is to be understood in the way, that the system of governing equations for each type of model, or the field equations, can be stated mathematically in the exact same form, thus enabling the use of the same solution procedure independent of the nature of the problem addressed.
The problem is illustrated in Fig. 2a, which shows a part of a honeycomb-cored CFRP-sandwich panel loaded in compression. The thickness of the face-laminates varies

stepwise over the length of the sandwich panel. The local area around one such thickness "drop-off" is shown schematically in Fig. 2b, where the sandwich panel face is considered as elastically supported on the core material, and subjected to a compressive load *P*.

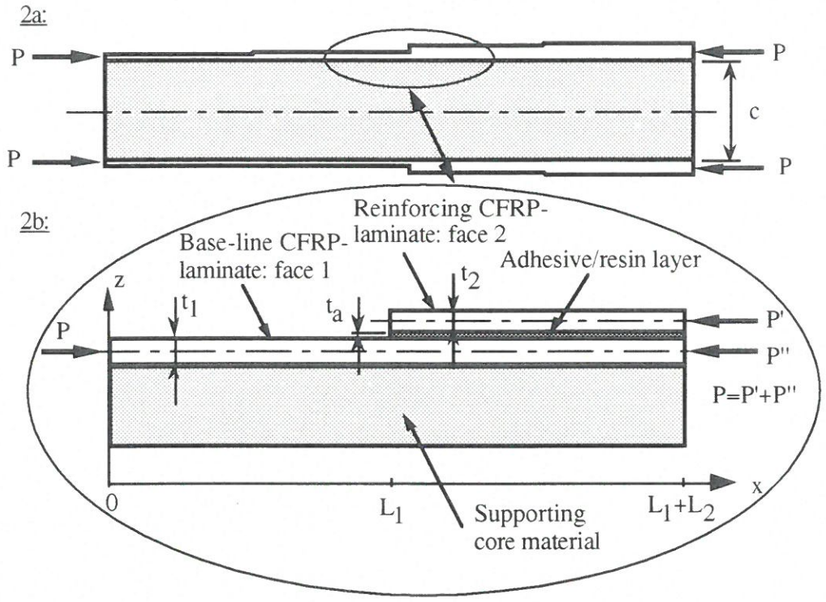

Figure 2. Definition of mechanical model:
2a: Honeycomb-cored sandwich panel with tapered CFRP face-laminates.
2b: Local zone around "drop-off" of face-laminate thickness.

The mechanical model suggested in ref. [1] comprises the following constituent parts (as seen from Fig. 2b):

- Face-laminate 1 (also referred to as the base-line laminate) of thickness t_1, which can be composed of an arbitrary number of plies. Face-laminate 1 is considered as a laminated beam or a plate in cylindrical bending (adopting "Bernoulli-Euler" beam theory or "Kirchhoff" plate theory), where the elastic laminate behaviour is modelled using classical laminate theory ("CLT").
- Face-laminate 2 (also referred to as the reinforcing laminate) of thickness t_2, which is considered in the same way as face-laminate 1.
- An adhesive/"resin-rich" layer of thickness t_a interfacing face-laminates 1 and 2. The adhesive/"resin-rich" layer is modelled as continuously distributed tension/compression and shear springs, thus coupling the mechanical responses of face-laminates 1 and 2.
- The honeycomb core material of thickness c is considered as an elastic foundation for the face-laminates on each side of the sandwich panel. Effectively this means that it is assumed, that the local bending responses induced by thickness "drop-off" effects on either side of the sandwich panel do not interfere with each other. In other words it is assumed, that the decay of the local bending effects is complete a very short depth into the core material. Fig. 2a displays a symmetric sandwich panel, but the sandwich panel under consideration does not have to be symmetric, given that the above assumption of complete decay of the local bending effects through the depth of the core is fulfilled.
  The elastic foundation (honeycomb core) is modelled using a two-parameter elastic foundation model. Thus, the elastic interaction between the face-laminates

and the core material is characterised by two constants K_x and K_z, which are referred to as the elastic foundation moduli. K_z is the transverse (out-of-plane) elastic foundation modulus, and K_X is the foundation shear modulus.

Very briefly, the set of differential equations for the local bending problem outlined above was derived by setting up the equilibrium, kinematic and constitutive equations for face-laminates 1 and 2. The response of face-laminate 1 is coupled with the honeycomb core response through the assumed elastic foundation model, and the responses of face-laminates 1 and 2 are coupled through the interfacing adhesive/"resin-rich" layer. The resulting set of differential equations can be expressed in the following general form:

$$0 \le x \le L_1: \qquad \{y_1(x)\}' = [A_{11}(x)]\{y_1(x)\} + \{B_1(x)\},$$

(1)

$$L_1 \le x \le L_1 + L_2: \quad \begin{Bmatrix} \{y_1(x)\} \\ \{y_2(x)\} \end{Bmatrix}' = \begin{bmatrix} [A^*_{11}(x)] & [A^*_{12}(x)] \\ [A^*_{21}(x)] & [A^*_{22}(x)] \end{bmatrix} \begin{Bmatrix} \{y_1(x)\} \\ \{y_2(x)\} \end{Bmatrix} + \begin{Bmatrix} \{B^*_1(x)\} \\ \{B^*_2(x)\} \end{Bmatrix}$$

where $\{y_i(x)\} = \{u_{0i}(x), w_i(x), \beta_i(x), N_i(x), M_i(x), Q_i(x)\}$[1] $(i=1,2)$ are the (6,1) matrices of so-called fundamental variables, $[A_{11}(x)]$, $[A_{ij}{}^*(x)]$ $(i,j=1,2)$ are (6,6) matrices of stiffness coefficients; and $\{B_1(x)\}$, $\{B_i{}^*(x)\}$ $(i=1,2)$ are vectors of non-homogeneous load terms (zero in this problem as there are no surface loads specified).
The boundary conditions are suggested as follows (see Fig. 2b):

(2) $x = 0$: $\{w_1 = 0, \quad N_1 = -P, \quad M_1 = 0$ ("simple support");

(3) $x = L_1$: $\begin{cases} \textit{Face 1:} & \{\text{"continuity" across junction at } x = L_1; \\ \textit{Face 2:} & \{N_2 = 0, \quad M_2 = 0, \quad Q_2 = 0 \quad (\text{"free edge"}); \end{cases}$

(4) $x = L_1 + L_2$: $\begin{cases} \textit{Face 1:} & \{u_{01} = 0, \quad \beta_1 = 0, \quad Q_1 = 0 \quad (\text{"symmetry"}); \\ \textit{Face 2:} & \{u_{02} = 0, \quad \beta_2 = 0, \quad Q_2 = 0 \quad (\text{"symmetry"}). \end{cases}$

The statement of the boundary conditions at the ends of the modelled thickness "drop-off" zone contains an element of arbitrariness (the "mathematical" argument for imposing the "symmetry" conditions is to suppress rigid body deformations). However, the actual boundary conditions imposed at $x=0$ and $x=L_1+L_2$ are not very important, as the local bending effects only extends a short distance to each side of the thickness "drop-off".

The "multiple-point" boundary value problem constituted by eqs. (1)-(4) was solved using the "multi-segment method of integration" (ref. [1]). This method is based on a transformation of the original "multiple-point" boundary value problem into a series of initial value problems. The principle behind the method is to divide the original problem into a finite number of segments, where the solution within each segment can be accomplished by means of any method of direct integration. Continuity of the solution vectors at the boundaries, and at the segment separation points, is ensured by formulating and solving a set of linear algebraic equations. For more detailed information reference is made to ref. [1]. The implementation of the solution was carried out using a UNIX-version of MATLAB®, version 4.1, implemented on a HP9000/700 workstation.

---

1 u_{0i} : In-plane (x-axis) displacement of midsurface of face-laminates ($i=1$: face-laminate 1; $i=2$: face-laminate 2).
w_i : Out-of-plane (z-axis) displacement of face-laminates ($i=1,2$).
β_i : Rotation of midsurface normals of face-laminates ($i=1,2$).
N_i : In-plane normal stress resultants in face-laminates ($i=1,2$).
M_i : Bending moment resultants in face-kaminates ($i=1,2$).
Q_i : Transverse shear stress resultants in face-laminates ($i=1,2$).

3.2 Determination of elastic foundation moduli K_x, K_z

As mentioned in the previous section, the mechanical model adopted in ref. [1] was based on the assumption, that the face-laminate/core-interaction can be modelled by the adoption of a two-parameter elastic foundation model. This two-parameter foundation model, which represents the simplest possible extension of the well-known Winkler foundation model (one-parameter model), assumes the existence of two elastic foundation moduli:

K_z: which determines the compressive/tensile strain in the foundation (core);
K_x: which determines the shearing strain in the foundation (core), and thus defines the load-spreading capacity of the foundation.

Of the two foundation moduli K_z is of most importance in describing the foundation response, and it is similar to the foundation modulus adopted in the "classical" Winkler foundation model.
In the present problem (see ref. [1]), the implementation of the two-parameter elastic foundation model is achieved by modelling the core/CFRP-face interaction by stipulating the following equations, which relate u_1 (in-plane displacement of face-laminate 1) and w_1 to the core transverse normal and shear stress components σ_c and τ_c (see Fig. 2b):

$$(5) \qquad \sigma_c = K_z w_1, \quad \tau_c = K_x \underbrace{\left\{u_1(x, -\frac{t_1}{2})\right\}}_{\text{BENDING CONTRIBUTION}} = -K_x \frac{t_1}{2} \beta_1.$$

From the above it is recognised, that a very essential issue pertaining to the quality of the suggested approach is the accuracy, with which K_x, K_z can be expressed in terms of the elastic and geometric properties of the constituent materials (i.e., of the face-laminates and the honeycomb core). Several suggestions for such expressions can be found in the literature (mostly "soil mechanics" related literature such as refs. [4], [5], [6] and [7]), but unfortunately there are considerable difficulties associated with the establishment of generally valid expressions.
The most thorough approach to the treatment of this problem was presented by Vlasov and Leon'tev in ref. [4], which derives the characteristics of "single-layer" and "multiple-layer" foundations from 3-D theory of elasticity. According to this approach, the behaviour of a "single-layer" foundation (characterised by its depth c) can be described in terms of two constants of which one defines the foundation compressive/tensile strains (corresponding to K_z adopted in [1]) and the other defines the foundation shearing strains (corresponding to K_x adopted in ref. [1]).
According to ref. [4] it is necessary to assume a function for the decay of the through-the-thickness displacement w_c through the elastic foundation. The simplest possible way to accomplish this is to assume, that the decay is linear:

$$(6) \qquad w_c(x,z) = w_c(x, z=0)\,\psi(z) = w_1(x)\,\psi(z) \quad \text{where} \quad \psi(z) = \frac{c - z}{c};$$

where z is the through-the-thickness (out-of-plane) coordinate and c is the foundation depth (core thickness). By adopting the simple linear "decay function" $\psi(z)$ it can be shown for the present problem, that K_z and K_x can be expressed as follows:

$$(7) \qquad K_z = \frac{E_0}{c(1 - \nu_0^2)}; \quad K_x = \frac{E_0}{3\,t^*(1 + \nu_0)} \quad \text{where}$$

$$E_0 = \frac{E_c}{1 - \nu_c^2}, \quad \nu_0 = \frac{\nu_c}{1 - \nu_c}, \quad t^* = \begin{cases} t_1 & \text{for} \quad 0 \le x < L_1, \\ t_1 + t_a + t_2 & \text{for} \quad L_1 \le x \le L_1 + L_2. \end{cases}$$

In eqs. (7) E_c and ν_c are the Young's modulus and the Poissons's ratio of the core material.
The simple linear decay assumption described above is generally believed (ref. [4]) to represent a good approximation for foundations of relatively small depth, but for foundations of more considerable depth it is recommended to use the following "exponential" (or "hyperbolic") decay assumption, ref. [4]:

$$(8) \qquad w_c(x,z) = w_c(x,z=0)\psi(z) = w_1(x)\psi(z) \quad \text{where} \quad \psi(z) = \frac{\sinh\left(\frac{\gamma(c-z)}{\alpha}\right)}{\sinh\left(\frac{\gamma c}{\alpha}\right)};$$

where γ is a coefficient depending of the elastic properties of the foundation, and α is a "characteristic decay length" of the considered problem. It is seen from eqs. (8), that the quantity (γ/α) determines the rate of decrease of the displacements over the depth of the foundation. By adopting the "exponential" decay function presented in eqs. (8) it can be shown, that the elastic foundation moduli for the thickness "drop-off" problem can be expressed as follows (where E_0, ν_0 and t^* are specified in eqs. (7)):

$$K_z = \frac{E_0}{c(1-\nu_0^2)}\Psi_1(\phi), \quad K_x = \frac{E_0}{3t^*(1+\nu_0)}\Psi_2(\phi) \quad \text{where}$$

$$(9) \qquad \Psi_1(\phi) = \frac{\phi}{2}\frac{\sinh(\phi)\cosh(\phi)+\phi}{\sinh^2(\phi)}, \quad \Psi_2(\phi) = \frac{3}{2\phi}\frac{\sinh(\phi)\cosh(\phi)-\phi}{\sinh^2(\phi)},$$

$$\phi = \frac{\gamma c}{\alpha}.$$

The value of the parameter γ in eqs. (8) and (9) is recommended to $\gamma=1.5$, ref. [4], whereas the value of the "characteristic decay length" α has to be selected carefully from problem to problem. Thus it is seen, that the success of the elastic foundation approach (at least when the "exponential decay" assumption is adopted) is highly dependent on the correct "choice"/"selection" of α.

In ref. [1], the "characteristic decay length" α was chosen in accordance with the recommendations pertaining to plate problems given in ref. [4], as well as with the results obtained from the combined theoretical and experimental investigations of local bending effects experienced in polymeric foam-cored sandwich plates reported in refs. [2] and [3]. Thus, in ref. [1] α was chosen to one half "beam/plate width" ($\alpha=b/2$) which for the thickness "drop-off" case yields (where E_0, ν_0 and t^* are specified in eqs. (7)):

$$K_z = \frac{E_0\gamma}{b(1-\nu_0^2)}F_1(\phi), \quad K_x = \frac{E_0 b}{4t^* c\gamma(1+\nu_0)}F_2(\phi) \quad \text{where}$$

$$(10) \qquad F_1(\phi) = \frac{\sinh(\phi)\cosh(\phi)+\phi}{\sinh^2(\phi)}, \quad F_2(\phi) = \frac{\sinh(\phi)\cosh(\phi)-\phi}{\sinh^2(\phi)},$$

$$\alpha = \frac{b}{2}, \quad \phi = \frac{\gamma c}{\alpha} = \frac{2\gamma c}{b} \quad \text{and} \quad b = 1.0\,mm \text{ ("unit width").}$$

It should be noted, that the unit "beam/plate width", i.e., "$b=1$ mm", assumed in eqs. (10) is a consequence of the fact, that the thickness "drop-off" problem is treated as a "unit width beam"/"plate in cylindrical bending" problem.

From the above brief introduction to one of the most important problems associated with the use of elastic foundation models it is clear, that an important outcome of the experimental investigation described herein is the evaluation of the expressions for the elastic foundation moduli K_x, K_z adopted in ref. [1]. Thus, the experimental investigation should provide answers to the following questions:

- Does the "exponential decay" approach (corresponding to eqs. (9)-(10)) adopted in ref. [1] provide a good description, and is the "characteristic decay length" α chosen appropriately ?
- If the answers to the above questions are negative, does the simpler "linear decay" approach (corresponding to eqs. (7)) provide a feasible alternative ?

3.3 Characteristics of predicted local bending response

In the previous sections a brief discussion of the elastic foundation approach as applied to the analysis of face-laminate thickness "drop-off" problems in CFRP/honeycomb sandwich panels was presented. Pertaining to the completion of this discussion, the most important features of the local bending phenomena induced by tapering of CFRP sandwich panel face-sheets are summarised below (for more elaborate details see ref. [1]):

- A short wave-length local bending pattern is induced in the immediate vicinity of the thickness "drop-off".
- The local bending pattern is displaying a strongly damped wavy harmonic nature, and a complete decay is observed a short distance away on each side of the "drop-off".
- Two local deflectional (out-of-plane) extrema are seen; one on each side of the thickness "drop-off". Considering the compressive load case, and referring to Fig. 2b for geometry, the peak local bending deflection is seen on the left hand side of the "drop-off" in the form of an indentation into the honeycomb material (i.e., inducing local compressive transverse normal stresses in the core). On the right hand side of the thickness "drop-off", a slightly smaller local deflection peak of opposite sign is induced (i.e., inducing tensile transverse normal stresses in the face-laminate/core interface).
- The local bending pattern induced locally is displaying small amplitudes, but as the complete raise and fall of the local bending deflections usually takes place over a very limited distance it is clear, that very severe local deflection gradients (i.e., rotations and curvature changes) can be present. This again reveals, that severe local bending and transverse shear stresses can be induced in the face-laminates, that severe stresses can be induced in the interface between the base-line and reinforcing laminates, and finally that severe stresses can be induced in the face-laminate/core interface. Thus it is seen, that the local bending effects induced by an abrupt face-laminate thickness change can cause the occurrence of severe stress concentrations in all the constituent parts, and the result might be a premature structural failure.

According to ref. [1], the elastic wave-length of the locally induced bending deflection pattern can be calculated from the following simple expression (see Fig. 2b):

$$(11) \qquad \lambda = 2\pi\sqrt[4]{\frac{D^*}{K_z}} \quad \textit{where} \quad D^* = \begin{cases} D_1 \text{ (i.e., the bending stiffness of face - laminate 1) for } 0 \le x < L_1. \\ \text{Combined bending stifness of face - laminates 1 and 2 for } L_1 \le x \le L_1 + L_2. \end{cases}$$

From eq. (11) it is observed that the elastic wave-length λ does not have the same magnitude in the two intervals $0 \leq x < L_1$ (base-line laminate) and $L_1 \leq x \leq L_1 + L_2$ (reinforced region); see Fig. 2b.
Typical space application CFRP/honeycomb sandwich panels are characterised by having "high stiffness"/"low thickness" CFRP face-laminates in conjunction with "low stiffness"/"low density" honeycomb cores, and typical values of the elastic wave-length are in the approximate range of $8\text{-}10\ mm \leq \lambda \leq 25\ mm$. The peak out-of-plane deflections will be located about $\lambda/4$ from the thickness "drop-off", corresponding to $2\text{-}2.5\ mm \leq \lambda/4 \leq 6.25\ mm$ which reveals, that very sensitive methods must be used in order to measure the local bending effects (i.e., local deflections or strains) accurately.

4.0 SPECIFICATION OF EXPERIMENTS

It was decided to perform the experimental investigation of local bending effects in CFRP/honeycomb cored sandwich panels on test-specimens loaded in compression (as illustrated in Fig. 2b), and from the characteristic features of the local bending problem obtained by application of the elastic foundation approach (presented in the brief review of the theory given in the previous chapter) the requirements for the experimental method were specified. These requirements, possible "candidate methods", selection of experimental method, selection of test-specimen configurations, test set-up as well as the experimental procedure will be discussed in the following.

4.1 Requirements for and selection of experimental technique

From section 3.3 the requirements for the experimental method to be adopted can be summarised as follows:

- The method should be capable of detecting the very short wave-length elastic local bending response experienced in typical space application CFRP/honeycomb sandwich panels with face-laminate thickness "drop-offs". This requirement implies that the method should be sensitive enough for measuring the complete raise and fall of out-of-plane deflections (or surface strains) within a distance-range limited to *8-25 mm*, where the complete raise will be seen to occur within an approximate distance-range of *2.5-6.25 mm*.
- In order to detect the deflection/strain gradients accurately, the method should be capable of providing "point" measurements rather than measurements conducted (and averaged) over a "finite area".
- In order to collect as many details as possible from the deflection/strain curves, the method should be capable of providing "whole field" measurements rather than "discrete point" measurements.

It is readily recognised, that the only experimental techniques, which are capable of complying with the requirements, are optical interferometric measurement methods[2]. Several different optical interferometric measurement methods have been developed, and without giving a full over-view some of the most well-known are listed below:

[2] The smallest commercially available strain gauges have a grid size of about *0.2 mm* (with a carrier size of about *3 mm*), but as strain gauges of this size are unsuitable for measuring strains on CFRP-laminates (due to their heterogeneous nature), the grid size should be at least *2-3 mm* (and preferably larger). Thus it is concluded, that strain gauge measurements are completely out of the question in the present context, as none of the mentioned requirements can be fulfilled.

- Moiré fringe interferometry.
- Holographic interferometry or "HI".
- Speckle interferometry, where especially electronic speckle pattern interferometry or "ESPI" is of interest.

Of these methods the first was discarded in the present context for three reasons: 1. It is usually necessary to coat the test-specimens with a surface grating using a photographic reproduction technique; 2. The measurement of out-of-plane displacements is rather complicated; 3. The sensitivity of the method is not likely to be sufficient.
Comparing the two latter methods, the major difference between holographic and speckle interferometry is the way in which the fringe pattern is formed, ref. [8]. In holographic interferometry usually a photosensitive plate is used to record a wave front, which is reconstructed afterwards in order to enable interference of two wave fronts emanating from the same object (the test-specimen). In ESPI the basic idea is to use the speckle pattern correlation to create fringes. The resolution of the recording medium used for this technique needs only to be relatively low, compared to the requirements for the recording of a HI-image, as it is only necessary to resolve the speckle pattern (instead of the very fine fringes formed by the interference of the object and reference "beams" in HI). In ESPI the fringe pattern is created by digital image processing of two subsequent video recordings (one displaying the speckle pattern of the not loaded object and one displaying the speckle pattern of the loaded object). The information displayed in the resulting ESPI image (specklegram) only represents relative displacements.
Both the holographic interferometry and the ESPI methods were considered applicable in the present context, but the ESPI technique was believed to offer some advantages:

- No need for chemical developing and fixing of a photosensitive layer.
- The stability requirements for the test set-up are less critical as the recording frequency is as large as *30* per second.

The only disadvantage of ESPI as compared to holographic interferometry is that the ESPI recorded fringes contain an unavoidable amount of speckle noise. In the present context, however, it was considered that ESPI (or an other speckle interferometry method) was most suitable.

4.2 Test-specimens

The test-specimens to be used for the experimental investigation were requested to fulfil the following requirements:

- The test-specimens should possess mechanical properties similar to those of CFRP/honeycomb sandwich panels typically used for spacecraft applications.
- Different test-specimen configurations, characterised by different elastic wave-lengths λ of the local bending response, should be included in the investigation.
- In order to ascertain the gathering of a reasonable amount of experimental data, several samples of each test-specimen configuration should be produced.

The exact specification of the test-specimen configurations (materials selection and geometry) was decided after consultations with the contracting organisations[3]. The details are given in the work statement (the work statement is enclosed as appendix for this report), but will be reviewed in the following.

[3] As will be described later, the contract for the experimental investigation was given to Microgravity Research Center, Université Libre de Bruxelles, Belgium with C.R.I.F., Section Technologie de Materiaux, Liège also Belgium as sub-contractor for the manufacturing of test-specimens and the measurement of engineering constants of the manufactured CFRP-laminates.

The selected test-specimen geometry is shown in Fig. 3.

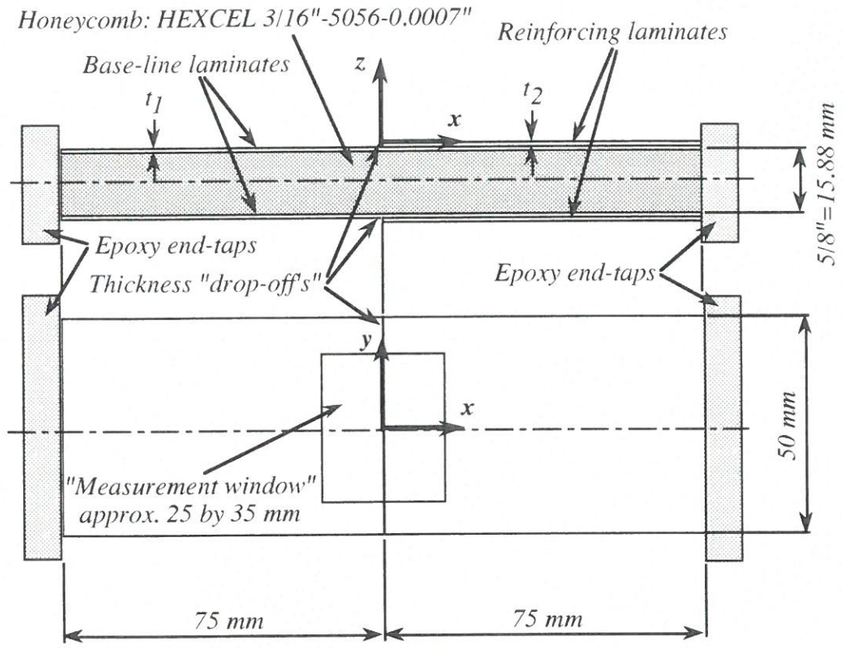

Figure 3. Test specimen geometry including the position and approximate size of the "window" where the ESPI measurements are to be carried out.

The end-taps mounted at the ends of the test-specimen in Fig. 3 were required in order to ascertain a proper in-take of the external compression load. No specific requirements were specified for the end-taps except, that the end-faces of the taps should be perpendicular to the CFRP face-laminates. The end-taps were cast from epoxy resin mixed with aluminium powder and glued to the end surfaces of the sandwich specimens.

The following material systems were specified in the work statement for the CFRP-laminates and the honeycomb core material:

Face-laminates: UD-prepregs from HEXCEL: *6T6-145F500* carbon fibre/epoxy system (type of carbon fibres: T300/3000 fibres).
Curing temperature: *120 °C*.
Cured ply thickness: *0.0054"=0.137 mm* (*61.1* fibre vol. %)

Honeycomb core: HEXCEL aluminium core: *3/16"-5056-0.0007"*.
Core thickness: *c=5/8"=15.88 mm*

It was decided to produce a total of six CFRP/honeycomb sandwich panels with geometry as shown in Fig. 3; two samples of each of the following three panel configurations (with the *L*-direction of the honeycomb core parallel with the *x*-axis):

Configuration 1:

Base-line laminate:	3-ply symmetric laminate:	$[0°/90°/0°]$.
	Cured laminate thickness:	$t_1=0.411$ *mm*.
Reinforcing laminate:	2-ply asymmetric laminate:	$[\pm 45°]$.
	Cured laminate thickness:	$t_2=0.274$ *mm*.

Configuration 2:

Base-line laminate:	6-ply symmetric laminate:	$[0°_2/90°]_S$.
	Cured laminate thickness:	$t_1=0.822$ *mm*.
Reinforcing laminate:	4-ply symmetric laminate:	$[\pm 45°]_S$.
	Cured laminate thickness:	$t_2=0.548$ *mm*.

Configuration 3:

Base-line laminate:	6-ply symmetric laminate:	$[0°_2/90°]_S$.
	Cured laminate thickness:	$t_1=0.822$ *mm*.
Reinforcing laminate:	2-ply asymmetric laminate:	$[\pm 45°]$.
	Cured laminate thickness:	$t_2=0.274$ *mm*.

In the work statement it is specified, that the CFRP-laminates with thickness "drop-offs" should be cured separately, and that the CFRP-laminates subsequently should be bonded to the honeycomb in a separate cure cycle[4].

In order to verify the material data supplied by HEXCEL for the CFRP/epoxy system used, it was further decided to measure the in-plane elastic engineering constants E_x, E_y and ν_{xy} for the base-line laminates of configurations 1 and 2 (see above). Thus, two series of tests were require: 1. a series of tensile "longitudinal axis" tests, and 2. a series of tensile "off-axis" tests.

4.3 Experimental set-up and experimental procedure

The experimental investigation of thickness change induced local bending effects in compression loaded CFRP/honeycomb sandwich panels, for which the work statement is included as an appendix to this report, was given to Microgravity Research Center, Université Libre de Bruxelles, Belgium under ESTEC Contract No. 10.983/94/NL/PP. As sub-contractor for the manufacturing of test-specimens as well as for the measurement of engineering constants Microgravity Research Center engaged C.R.I.F.[5], Section Technologie de Materiaux, Liège also in Belgium.

As part of the contract Microgravity Research Center (hereinafter referred to as MRC) designed and manufactured a special test-rig for the mounting and the application of compressive axial loads to the sandwich test-specimens. The test-rig designed and manufactured is displayed in Fig. 4.
The compressive axial load was applied through a hydraulic actuator with a pressure range from *0* to *80 kg/cm²* (*0* to *80 bar*). The compressive load was transferred from the hydraulic actuator to the test-specimen through two plates (see Fig. 4) in between which, a piezoelectric pressure transducer was mounted. The test-specimen was mounted between the lower of the above mentioned plates and the bottom of the test-rig.
The displacements (axial) of the the actuator arm of the hydraulic jack (and thereby of the "plate arrangements", the piezoelectric transducer as well as the test-specimen) were guided by three bars clamped into the top of the test-rig (see Fig. 4).

---

[4] Unfortunately the specified production sequence with two subsequent cure cycles was abandoned in the manufacturing of the specimens, as it was agreed to allow co-curing instead. As will be described later the result of this was, that one surface on each specimen was manufactured with a very poor surface quality (the CFRP-laminates were indented into the core cells, and the resulting surfaces displayed distinct doubly-curved topographical patterns).

[5] C.R.I.F. is an abbreviation for "Centre de Recherches scientifiques et techniques de l'Industrie de Fabrications métalliques".

centred around the thickness "drop-off". Before this calculation, the recorded images were filtered (high-pass filter) in order to increase the fringe quality (by eliminating the speckle aspect).

- For each of the recorded specklegrams, four out-of-plane deflection profiles parallel with the x-axis (longitudinal direction, see Fig. 3) were stored. Two out-of-plane deflection profiles were chosen at local "maximum"-deflection points and two at "minimum"-deflection points in the transverse direction (y-direction) near the thickness "drop-off". The recorded variation of the out-of-plane deflection amplitudes in the transverse direction (y-direction) was due to the cellular structure of the honeycomb core (this issue will be discussed later).

5.0 RESULTS

In this chapter the results of the experimental work carried out by MRC in association with C.R.I.F. will be presented. Furthermore, the experimentally obtained out-of-plane deflection profiles will be compared with the ones predicted theoretically by use of the elastic foundation approach derived in ref. [1].

5.1 Manufactured test-specimens

As mentioned, C.R.I.F. Liège, acting as sub-contractor for MRC, undertook the manufacturing of the six CFRP-sandwich test-specimens specified in the work statement (see appendix). The CFRP-laminates were made of carbon fibre/epoxy UD-prepregs 6T6-145F600 from Hexcel. The honeycomb core used in all three test-specimen configurations was Hexcel *3/16"-5056-0.0007"* with a thickness of *5/8"*. As mentioned in section 4.2, the production sequence for the sandwich specimens specified in the work statement (see appendix) was not followed. According to the work statement, each face-laminate (including reinforcing laminates) should be cured individually, and subsequently the face-laminates should be bonded to the honeycomb core in a separate cure cycle. This sequence would have ensured the best possible "flatness" and surface quality of the sandwich specimens.
However, it was decided to allow the sandwich specimens to be manufactured by co-curing in a vacuum-bag (i.e., the face-laminates and the sandwich panels were cured in one cycle) in order to overcome potential difficulties with warping of the asymmetric laminates. The resulting sandwich test-specimens displayed two types of "irregularities":

- The CFRP-laminates, which were located on the top of the sandwich test-specimens during co-curing (i.e., in direct contact with the rubber-sheet of the vacuum-bag), displayed a distinct doubly-curved topographical pattern corresponding to the cell-spacing of the honeycomb core (i.e., a spacing of S_c=*3/16"≈4.76 mm*). This "golf-ball" aspect topography was caused by the pressure of the vacuum bag (i.e., atmospheric pressure), which indented the top prepregs into the core cells. A photo of the "golf-ball" aspect surface (denoted as side A) of one of the manufactured CFRP-sandwich test-specimens is displayed in Fig. 5.
- A photo of a typical "flat" test-specimen surface is displayed in Fig. 6. The "flat" surfaces were obtained on the bottom specimen surfaces, i.e., the surfaces that were facing the "hold plate" of the mould during co-curing. These surfaces displayed the second type of surface "irregularity" encountered. The typical geometry of the "flat" specimen surfaces is illustrated (in exaggerated form) in Fig. 7. Thus, the "flat" aspect surfaces of the specimens (denoted as side B of the specimens) were slightly curved (in the out-of-plane or z direction) close to the thickness "drop-off".

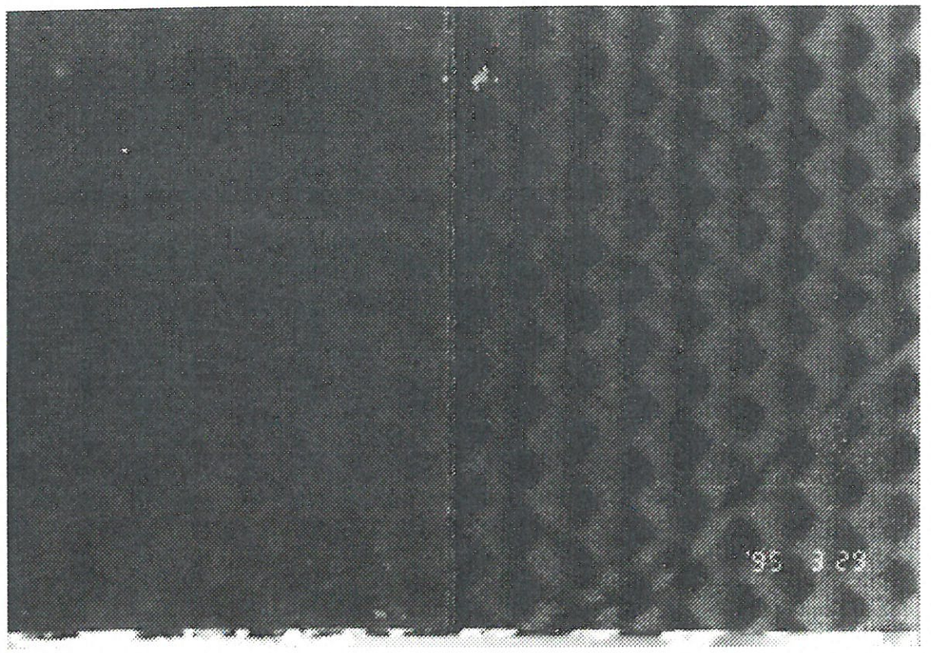

Figure 5. Typical "golf-ball" aspect surface (side A) of CFRP/honeycomb sandwich test-specimen.

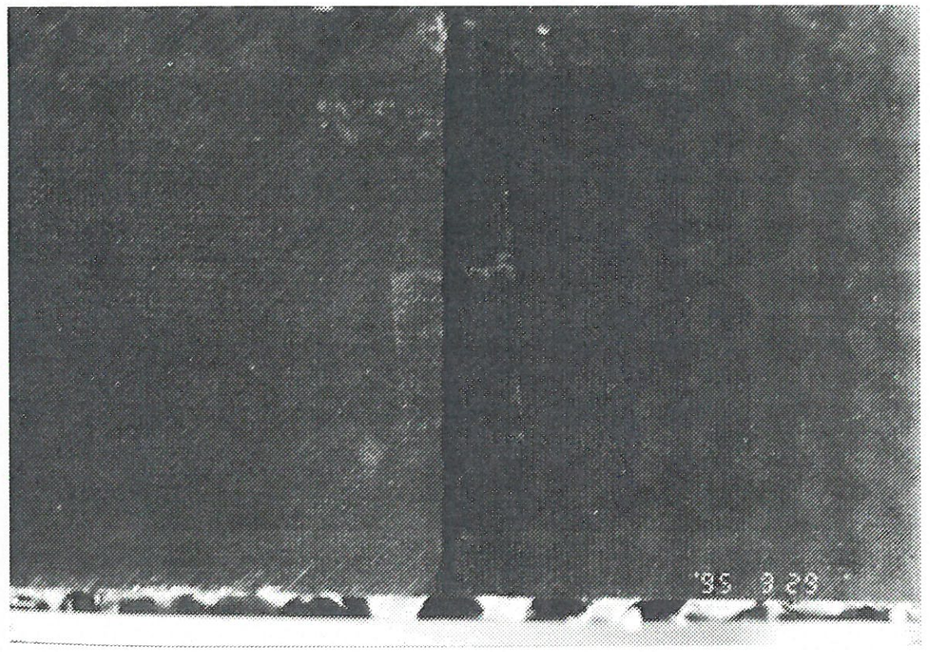

Figure 6. Typical "flat" aspect surface (side B) of CFRP/honeycomb sandwich test-specimen.

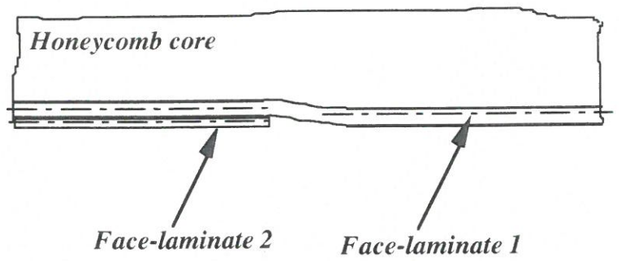

Figure 7. Exaggerated illustration of typical geometry around thickness "drop-off" of "flat" aspect CFRP-sandwich test-specimen surfaces (side B).

Despite the relatively poor quality of the manufactured test-specimens (especially the "golf-ball"/A surfaces) it was decided to accept the specimens as they were. The reason for this being, that the test results obtainable from the surfaces of poor quality would reflect surface properties that are quite realistic from a practical point of view, as the co-curing process is used for the manufacturing of sandwich panels for many applications. In order to identify each of the twelve test-specimen surfaces precisely, the following notation was adopted by MRC:

Configuration 1:	Specimen 1-1:	Sides s11A and s11B.
	Specimen 1-2:	Sides s12A and s12B.
Configuration 2:	Specimen 2-1:	Sides s21A and s21B.
	Specimen 2-2:	Sides s22A and s22B.
Configuration 3:	Specimen 3-1:	Sides s31A and s31B.
	Specimen 3-2:	Sides s32A and s32B.

5.2 Measured engineering constants and input-data for theory

As part of the contract, C.R.I.F. was requested to measure the effective engineering constants E_x, E_y and ν_{xy} for the base-line laminates of test-specimen configurations 1 and 2. The testing was carried out using two different techniques:

- Combined longitudinal and transverse strain measurements using an extensometer of the type INSTRON Statique 2630-036 (longitudinal measurements; reference length *50 mm*) and an extensometer of the type INSTRON Statique 2640-008 (transverse measurements; reference length *12-16 mm*).
- Strain gauge measurements using *0°-90°* strain gauges of the type TOKIO SOKKI KENKYUJO TML-FCA-5-23 (grid length *5 mm*)

The testing was performed on the following "base-line" laminate configurations:

3-ply laminate, $[0°/90°/0°]$: Four tensile "longitudinal axis" and four tensile "off-axis" tests; specimens: *25 mm* (width) by *270 mm* (length).

6-ply laminate, $[0°_2/90°]_S$: Four tensile "longitudinal axis" tests, and four tensile "off-axis" tests; specimens: *25 mm* by *270 mm* .

The obtained values of E_x, E_y, ν_{xy} as well as the specimen thicknesses and widths are displayed in Tables 1 to 4[10] (mean values, standard deviations and variation coefficients).

10 Note that the values for E_x, E_y and ν_{xy} for the 3-ply and the 6-ply laminates should be exactly the same according to classical laminate theory (CLT).

	E_x	E_y	ν_{xy}	*Thickness*	*Width*
Mean value	*89850 MPa*	*48630 MPa*	*0.079*	*0.46 mm*	*25.62 mm*
Standard deviation	*7361 MPa*	*8250 MPa*	*0.016*		
Variation coefficient	*8.18*	*16.96*	*20.06*		

Table 1. Engineering constants of 3-ply laminate $[0°/90°/0°]$ measured using INSTRON extensometers (tensile tests), ref. [9].

	E_x	E_y	ν_{xy}	*Thickness*	*Width*
Mean value	*82297 MPa*	*44609*	*0.076*	*0.46 mm*	*25.62 mm*
Standard deviation	*5651 MPa*	*3668*	*0.003*		
Variation coefficient	*6.87*	*8.20*	*3.59*		

Table 2. Engineering constants of 3-ply laminate $[0°/90°/0°]$ measured using strain gauges (tensile tests), ref. [9].

	E_x	E_y	ν_{xy}	*Thickness*	*Width*
Mean value	*88636 MPa*	*51467 MPa*	*0.069*	*0.87 mm*	*25.18 mm*
Standard deviation	*6137 MPa*	*1569 MPa*	*0.004*		
Variation coefficient	*6.92*	*3.05*	*5.84*		

Table 3. Engineering constants of 6-ply laminate $[0°_2/90°]_S$ measured using INSTRON extensometers (tensile tests), ref. [9].

	E_x	E_y	ν_{xy}	*Thickness*	*Width*
Mean value	*84561 MPa*	*49751 MPa*	*0.071*	*0.87 mm*	*25.18 mm*
Standard deviation	*3583 MPa*	*779 MPa*	*0.005*		
Variation coefficient	*4.24*	*1.57*	*6.66*		

Table 4. Engineering constants of 6-ply laminate $[0°_2/90°]_S$ measured using strain gauges (tensile tests), ref. [9].

Pertaining to the results obtained using the two Instron extensometers some problems were encountered with instability, where especially the transverse (i.e., the width direction) measurements caused problems; ref. [9]. These instability problems, which were most pronounced for the measurements on the 3-ply laminates, were caused by slight out-of-plane warping of the test-specimens during loading (could indicate that the manufactured laminates were not symmetric). The problems described are reflected by the relatively high standard deviations observed for the measured values of ν_{xy} (especially the 3-ply laminate; Table 1).
Pertaining to the values of E_x and E_y measured using the two methods it is seen from the tables, that there is a systematic difference between the obtained results. Thus, the values of E_x, E_y measured with the extensometers were about *5-10 %* larger than the values of E_x, E_y obtained with strain gauges. Furthermore it is seen, that the standard deviations on the extensometer measurements were relatively large (about twice as large as the standard deviations on the strain gauge measurements).
Based on the above considerations it is believed, that the strain gauge measurements provided the best results. Accordingly, the measurements of the elastic moduli as well as the Poisson's ratio for the laminates obtained using the extensometers are discarded.

The test results displayed in Tables 1 to 4 all represents effective engineering constants on the laminate level, whereas the engineering constants needed as input for the theoretical model (elastic foundation approach) needs to be specified on the ply level. Theoretically it is possible to compute the ply level engineering constants from the laminate level constants, given that the thicknesses as well as the orientations of the individual plies are known accurately. This, however, has not been attempted, as the test programme undertaken by C.R.I.F. was not intended to include these aspects.
Instead, the measured effective laminate engineering constants (the strain gauge measurements) have been compared to theoretical predictions (using CLT) based on ply-data obtained from material data-sheets. Given that the predicted and the experimentally obtained (mean values) laminate engineering constants were reasonably close (i.e., that they match each other within less than *5 %*), it was decided to use the data-sheet ply-data as input for the theoretical predictions throughout this report.
The assumed ply-data for the used carbon fibre/epoxy UD-prepreg system (T6T-145F500) are given in Table 5. The ply-data quoted in Table 5 have not been taken from the data-sheets provided from Hexcel (as these are unsatisfactory), but were instead taken from ref. [1] where a similar carbon fibre/epoxy system was referred to (based on T300 carbon fibres and an epoxy resin system with curing temperature *120 °C*).

$(E_x)_{ply}$	$(E_y)_{ply}$	$(\nu_{xy})_{ply}$	$(G_{xy})_{ply}$	t_{ply}
118500 MPa	*10200 MPa*	*0.35*	*4000 MPa*	*0.145 mm*

Table 5. Assumed ply-data for UD-prepreg T6T-145F500 (fibre vol. *60 %*), ref. [1].

Using the ply-data quoted in Table 5 for the computation of the in-plane engineering constants of $[0°/90°/0°]$- and $[0°_2/90°]_S$-laminates yielded the results displayed in Table 6, which should be compared with the results shown in Tables 2 and 4.

$(E_x)_{laminate}$	$(E_y)_{laminate}$	$(\nu_{xy})_{laminate}$	$(G_{xy})_{laminate}$	$t_{3\text{-}ply}/t_{6\text{-}ply}$
83000 MPa	*46637 MPa*	*0.077*	*4000 MPa*	*0.435/0.87 mm*

Table 6. Predicted laminate properties for $[0°/90°/0°]$- and $[0°_2/90°]_S$ -laminates using the ply-data of Table 5.

Comparing the results shown in Table 6 with the results displayed in Tables 2 and 4 (strain gauge measurements) reveals a very close match[11]. Thus, the ply-data given in Table 5 have been used for the theoretical prediction of the laminate properties throughout the report.

With respect to the material properties for the honeycomb core material, the data supplied from Hexcel (and used in ref. [1]) have been used for the theoretical predictions. The assumed honeycomb properties are displayed in Table 7 .

Hexcel core type	*Density*	*Core thickness*	*Elastic Modulus; out-of-plane;* E_c	*Poisson's ratio; out-of-plane;* $\nu_c{}^{12}$	*Shear Modulus; W-direction;* G_W	*Shear modulus; L-direction;* G_L
3/16"-5056-0.0007"	*32 kg/m³*	*5/8" =15.875 mm*	*310 MPa*	*0.3*	*90 MPa*	*186 MPa*

Table 7. Material data for Hexcel honeycomb core.

11 Comparison of $(E_x)_{experimental}$ and $(E_x)_{theory}$ yields the following differences between strain gauge measurements and theoretical predictions:
- 3-ply laminate: $[(E_x)_{experimental}-(E_x)_{theory}]/(E_x)_{experimental}$=*-0.9 %*.
- 6-ply laminate: $[(E_x)_{experimental}-(E_x)_{theory}]/(E_x)_{experimental}$=*1.8 %*.

12 The "out-of-plane" Poisson's ratio for the honeycomb core must equal that of the solid from which the cell walls are built up (ref. [10]), i.e., aluminium in this case.

Finally, the properties assumed for the adhesive/"resin-rich"[13] layer interfacing the base-line laminate (face 1) and the reinforcing laminate (face 2) are given in Table 8 (ref. [1]).

Epoxy type	*Thickness of layer;* t_a	*Elastic modulus;* E_a	*Poisson's ratio;* ν_a
Same as in UD-prepregs (curing temperature 120 °C)	*0.01 mm*	*2350 MPa*	*0.4*

Table 8. Assumed properties for the adhesive/"resin-rich" layer interfacing the base-line and the reinforcing laminates, ref. [1].

5.3 Adjustment of theory

As discussed in section 3.2, an important part of the results of the experimental investigation was to evaluate which type of "decay" assumption was most suitable (if any at all) in the elastic foundation approach. It should be recalled, that the choice of "decay-function" (through the thickness of the core material) effectively determined the expressions (derived from 3-D theory of elasticity) relating the elastic and geometric properties of the constituent materials to the elastic foundation moduli K_z, K_x. Two types of functions for the decay of the out-of-plane deflections were discussed in section 3.2 (see ref. [4] for details of the elastic foundation description):

- Linear decay function, which provides the simplest possible approach. Using the linear decay assumption, the elastic foundation moduli are expressed as given in eqs. (7). The linear decay function approach provides a good description for elastic foundations with small to "moderate" depths, ref. [4].
- Exponential decay function, which is generally believed to provide better results than the linear approach for "deep" foundations. The elastic foundation moduli derived from the exponential decay assumption are given in eqs. (9). Using the exponential decay approach involves the choice of a "characteristic decay length", denoted α in eqs. (9), which determines the rate of decrease of the displacements through the elastic foundation. It is therefore clear, that a correct "choice"/"selection" of α is very important, in order for the elastic foundation approach to provide good predictive results[14].

In ref. [1], the exponential decay assumption was used together with a "characteristic decay length" chosen to $\alpha=0.5$ *mm* ("one half plate width" in accordance with results derived in refs. [2], [3] and [4]), and the corresponding expressions for K_z and K_x were given in eqs. (10) (section 3.2).

---

13 Obviously, the specific elastic properties of very thin adhesive/"resin-rich" layer exert virtually no influence on the local out-of-plane deflection pattern of the base-line and reinforcing face-laminates. The elastic properties of this layer determine the magnitude of the stress concentrations at the interface between the two face-laminates. Thus, the elastic properties of the adhesive/"resin-rich" layer are given here merely because, they are required as input-data for the theoretical solution procedure derived in ref. [1].

14 The sensitivity of elastic foundation models to the correct specification of a decay function "a priori" often provides the impression, that the use of elastic foundation models is an art rather than an action based on purely rational reasoning.

Thus, the first task in the evaluation of the results provided by MRC was to compare the measured and theoretically predicted deflection amplitudes and wave-lengths in order to evaluate the choice of K_z, K_x suggested in ref. [1].

From the experimentally obtained deflection profiles (the details of these will be given later) it was clear, that the choice of K_z, K_x suggested and implemented in ref. [1] "under-predicted" the out-of-plane deflection amplitudes quite significantly (a factor between 3 and 4), whereas the shape and general characteristics of the deflection profiles were predicted quite well. As the size of the "under-prediction" (i.e., the predicted amplitude deviation) was approximately the same for all the three test-specimen configurations, it was clear, that the mispredictions were caused by a systematic "error" in the expressions for K_z, K_x (eqs. (10)). Furthermore, as the observed and predicted overall deflection patterns matched each other well (at least evaluated superficially), it seemed apparent, that the choice of "characteristic decay length" α in ref. [1] was the cause of the problem.
As described, the exponential decay function approach is very sensitive to the specification of α (which might change from problem to problem), and as the amount of experimental data was considered as being to small for providing a reasonable confidence in an empirical expression for α (to be used for the analysis of thickness "drop-off" problems in CFRP/honeycomb sandwich panels), the use of the linear decay function was investigated instead (where no choice of decay length is necessary; eqs. (7)).
The result of using eqs. (7) instead of eqs. (10), at least for the purposes of a preliminary comparison, was that of a much better correlation (in terms of match between amplitudes as well as elastic wave-lengths) between the experimentally and theoretically obtained out-of-plane deflection profiles. In fact, for some of the test-specimen configurations, the correlation turned out to be excellent (again based on a preliminary comparison). Thus, it was decided to use eqs. (7) throughout this report for deriving the theoretical out-of-plane deflection profiles.

Probably it would be possible to derive an empirical expression for α, which would enable better predictive results based on an exponential decay approach. It is even likely, that the results would be superior to those derived by use of the linear decay function. However, the successful implementation and use of the exponential decay approach would require, that a systematic test campaign was planned and undertaken in order to provide enough data for suggesting a generally valid expression for α (for the class of possible/realistic CFRP/honeycomb panels).

Using eqs. (7) and (11) together with the input data given in Tables 6 and 7 provided the following values of the elastic foundation moduli and the elastic wave-lengths for the three test-specimen configurations (see Fig. 2b for notation):

Configuration 1: $K_z=26.29\ N/mm^3$;
$K_x(0\le x<L_1)=211.97\ N/mm^3$; $K_x(L_1\le x\le L_1+L_2)=125.18\ N/mm^3$;
$\lambda(0\le x<L_1)=13.04\ mm$; $\lambda(L_1\le x\le L_1+L_2)=16.78\ mm$.

Configuration 2: $K_z=26.29\ N/mm^3$;
$K_x(0\le x<L_1)=105.98\ N/mm^3$; $K_x(L_1\le x\le L_1+L_2)=63.09\ N/mm^3$;
$\lambda(0\le x<L_1)=21.93\ mm$; $\lambda(L_1\le x\le L_1+L_2)=28.22\ mm$.

Configuration 3: $K_z=26.29\ N/mm^3$;
$K_x(0\le x<L_1)=105.98\ N/mm^3$; $K_x(L_1\le x\le L_1+L_2)=78.70\ N/mm^3$;
$\lambda(0\le x<L_1)=21.93\ mm$; $\lambda(L_1\le x\le L_1+L_2)=24.64\ mm$.

5.4 Processing and presentation of results

The experimental results provided by MRC includes a very large amount of data. Thus, for each sample side (the notation for sample side identification was given in section 5.1, p.16) the following data are available in ref. [9]:

- Precise sample identification.
- Two pictures of each surface (one with a graph paper in order to identify the "measurement window"; see Fig. 3).
- A table summarising the results for each load level:
  1. Date, test number, the position of the "drop-off" (pixel), the load.
  2. Data for the digital image analysis of the fringe patterns of the specklegrams: the sensitivity ($\lambda/2$ of the laser diode used in the ESPI equipment: $\lambda=780\ nm$), the calibration of the deflections as function of the number of "grey-levels" of the picture (the "grey-level" vary from *0* to *255*), the maximum (peak) and minimum (valley) deflections, the zero-order "grey-level" (arbitrarily chosen), the number of fringes in the measurement window.
     As the specimens invariably were "tilted" slightly in the test-rig (see Fig. 4), the specklegrams display a large number of fringes associated with rigid body or "global" deformations. The rigid body displacements and rotations were removed by identifying and subtracting a compensating plane. The *x*- and *y*-inclinations as well as the off-set of the compensating plane calculated by the digital image analysis software are given in the tables (see Fig. 3 for orientations of the *x*- and *y*-axes). The relative point of the compensating plane is the centre of the "measurement window".
     The results (sensitivity, calibration, peak-valley distance) of the digital image analysis after correction with the "best fit compensating plane" are given in the tables.
  3. Four out-of-plane deflection profiles parallel with the *x*-axis were selected from each specklegram, and the positions of these are identified precisely by their pixel-value in the *y*-direction (see Fig. 3 for orientations of the *x*- and *y*-axes).
- The phase picture and the filtered phase picture for each load level.
- The fringe image (specklegram) displaying the total deformations (including rigid body deformations) and the fringe image displaying the deformations derived by subtraction of a compensating plane (rigid body deformations removed).
- The four out-of-plane deflection profiles (without rigid body deformations) selected for each load level (as specified in the test procedure given in section 4.3); two profiles corresponding to "maximum" (peak) deflections at the position of the "drop-off"; and two profiles corresponding to "minimum" (valley) deflections at the position of the "drop-off".
- The averaged out-of-plane deflection profile computed from the selected four deflection profiles for each load level.

All the data mentioned above, which takes up about 260 A4 pages, will not be included in the present report. Instead only data obtained at the *highest load levels* (as the patterns are most clear here) will be given for each specimen surface, and it was decided to include the following data in this report (for the complete set of experimental data, reference is made to ref. [9]):

- The fringe image (specklegram) displaying the local deformations around the thickness "drop-off" (i.e., influence of rigid body deformations have been removed).
- The four out-of-plane deflection profiles (parallel with the *x*-axis) selected from the specklegram. These deflection profiles (also referred to as the "raw data") formed the basis for the comparison with the theoretical predictions.

- The averaged out-of-plane deflection profile computed from the selected four deflection profiles (i.e., from the "raw data").
- The theoretically predicted out-of-plane profile (displayed in the same figure as the averaged deflection profile).

The specklegrams, the selected out-of-plane deflection profiles as well as the averaged out-of-plane deflection profiles displayed rather complicated patterns (at least at first glance). Thus, these images included (as will be apparent later) three different characteristic "signal" sources superimposed on each other:

- A local bending response induced by the thickness "drop-off" displaying an asymmetric, wavy harmonic and strongly damped pattern. This response part will be referred to as the ***LB***-response. The wave-lengths (as there are two: one on each side of the thickness "drop-off") of this pattern were predicted at the end of section 5.3 (using the adjusted foundation moduli).
- A deflection response corresponding to the cell size of the honeycomb core ($S_c=3/16"=4.76\ mm$). This part of the total response, which (obviously) is not included in the theoretical predictions, was caused by the discrete nature of the support provided for the face-laminates by the core material. This response part will be referred to as the "honeycomb cell"- or ***HC***-response.
  As will be demonstrated later, the HC-response was most apparent for the test-specimen surfaces with "golf-ball" aspect surfaces (i.e., the A-sides of the test-specimens as described in section 5.1). The reason for this being, that the initial curviness induced by the co-curing process tended to amplify the tendency for the CFRP- sandwich face-laminates to "select" an out-of-plane deflection pattern with wave-length equal to the cell size S_c.
- Finally, the specklegrams and the out-of-plane deflection profiles contained "high-frequency" irregular speckle noise. The presence of speckle noise is an unfortunate but unavoidable part of using the ESPI-technique (as well as any other technique based on speckle pattern interferometry). Part of the noise was removed in the digital image processing of the specklegrams, but (as will be seen later from the display of experimental data) it was not possible to remove the speckle noise completely.

Of the above mentioned three signal sources the former two represented structural responses, whereas the latter represented a "high-frequency" signal disturbance.
Pertaining to the two structural response parts, the LB-response induced by the thickness "drop-off" was the one of interest in the present context, and it was characterised (or rather expected to be characterised) by wave-lengths as given in section 5.3, i.e., wave-lengths ranging from about *13 mm* (base-line laminate; configuration 1) to about *28 mm* (base-line + reinforcing laminates = reinforced laminate; configuration 2). The HC-response was characterised by a wave-length very close to $S_c=4.76\ mm$.
Considering the amplitudes of the recorded LB- and HC-responses, respectively, the overall tendency was that the LB-responses displayed the largest amplitudes. This tendency was most pronounced for the specklegrams recorded at the highest load levels, but was not as clear for the "golf-ball" aspects surfaces (A-sides) as for the "flat" aspect surfaces (B-sides) of the test-specimens. Increasing load levels tended to strengthen the LB-response part, but when the load levels were increased above a certain value, the resulting specklegrams simply contained so many closely spaced fringes that no interferometric measurements were possible (even through digital image processing). Thus, it was impossible to apply sufficiently large external loads to ensure a "dominating" LB-response for all the test-specimen configurations included in the investigation. Consequently, the specklegrams and the selected out-of-plane deflection profiles included in this report represents the highest load levels, where it was possible to create specklegrams containing interferometric data of reasonable quality.

Based on the arguments presented above, it was decided to perform an additional digital filtering of the recorded out-of-plane deflection profiles in order to identify (as clearly as

possible) the LB-response part of the recorded out-of-plane deflection profiles. From a principal point of view, such a filter could have been designed as a "two-band" pass filter which effectively removed the parts of the recorded signals having wave-lengths close to the honeycomb cell size S_C. This would provide a filtered signal containing the LB-response as well as the speckle noise.
It was decided, however, to design and apply a "low pass" filter that removed the parts of the recorded signals corresponding to wave-lengths below the honeycomb cell size S_C (approximately). The signals derived by the application of such a filtering process only contained the LB-responses, and were therefore directly comparable with the theoretically predicted out-of-plane deflection profiles.
The "low pass" digital filter was designed and the filtering conducted using the MATLAB®, version 4.1, Signal Processing TOOLBOX. The designed digital filter was a so-called 3'rd order Butterworth filter, and the actual filtering of the signals was performed using a MATLAB routine performing zero-phase digital filtering; refs. [11], [12]. The order of the digital Butterworth filter (3) was chosen as the lowest possible providing a "smooth" filtered signal with no higher-order harmonics present (purely "visual inspection"). The "cut-off" frequency for the filter was chosen to half the "cell-frequency" (i.e., to $0.5\times(1/S_C)=0.105\ mm^{-1}$) in order to ascertain, that the response parts above the "cell-frequency" were effectively filtered out.
The performance of the filter was checked by ensuring (for each test-specimen configuration), that filtering of the theoretically predicted deflection profiles did not cause any signal distortions (i.e., no visible differences).
Pertaining to the shape of the filtered deflection profiles it should be noted, that the filtered signals were not expected to display "reasonable" behaviour at the ends of the sampling intervals. The reason for this being, that the sampling intervals in the x-direction were fairly short (usually they comprised less than one full elastic wave-length), thus providing the filtering algorithm with insufficient data for the identification of the LB-response parts (no information about the "repetition"-sequence of the averaged signals).

In the forthcoming sections, the averaged out-of-plane deflection profiles are displayed together with the filtered averaged and the theoretically predicted out-of-plane deflection profiles. In order to establish a systematic procedure for conducting the comparisons, the following three quantities will be used throughout for comparing the filtered (experimental) and theoretical out-of-plane deflection profiles:

- Peak distance x_{peak}:

(12) $$x_{peak} = abs\{\, x(maximum\ deflection) - x(minimum\ deflection)\,\}.$$

- Phase difference Δx:

(13) $$\Delta x = \begin{cases} abs\left\{ [x(minimum\ deflection)]_{theory} - [x(minimum\ deflection)]_{filtered} \right\}; \\ abs\left\{ [x(maximum\ deflection)]_{theory} - [x(maximum\ deflection)]_{filtered} \right\}. \end{cases}$$

- Amplitude $|w|$:

(14) $$|w| = w(maximum) - w(minimum).$$

The "minimum" and "maximum" deflections used in the above expressions are defined as the extreme values encountered on each side of the thickness "drop-offs". Pertaining to the "phase difference" Δx, the two definitions may result in different values if the filtered and theoretical wave-lengths are different. Thus, both values (referred to as "minimum point"/"maximum point" values) will be given in the presentation of the results for each sample side of the test-specimens.

5.5 Comparison between experimental and theoretically predicted deflection profiles

In the following sections the experimental data as well as the theoretical predictions will be presented. The results will be presented individually for each test-specimen surface, and the sequence of the presentation of results will follow the specimen surface identification system defined in section 5.1.

5.5.1 Configuration 1: [0°/90°/0°] + [±45°]

Configuration 1 of the test-specimens represented the most "extreme" CFRP/honeycomb sandwich panels included in the investigation (see section 4.2 for reference), where the word "extreme" refers to the fact, that the base-line laminates were very thin (3 plies; $t_1 \approx 0.46\ mm$). As the reinforcing laminates were also thin (2 plies; $t_2 \approx 0.29\ mm$), the predicted elastic wave-lengths were very short (see section 5.3), and it was expected "a priori" that the separation of the LB- and HC-reponses for these test-specimens would prove to be more difficult than for the other two configurations.
As described previously, the specklegrams of best quality were obtained at the highest load levels. The specklegrams for the specimen surfaces corresponding to configuration 1 were recorded under the load conditions specified in Table 9[15].

Specimen surface	*Reference image recorded at total load: P_{tot}(reference)*	*"Maximum load" image recorded at total load: P_{tot}(maximum)*	*In-plane normal stress resultant corresponding to specklegram: $P=\Delta P_{tot}/(2\times 50\ mm)$*
s11A	*-436 N*	*-619 N*	*-1.83 N/mm*
s11B	*-329 N*	*-555 N*	*-2.26 N/mm*
s12A	*-462 N*	*-564 N*	*-1.02 N/mm*
s12B	*-418 N*	*-562 N*	*-1.44 N/mm*

Table 9. Load conditions for recording of specklegrams for ***configuration 1*** CFRP/honeycomb sandwich test-specimens.

15 In the forthcoming, the total load acting on each CFRP/honeycomb sandwich test-specimen is referred to as P_{tot}, whereas the in-plane normal stress resultant acting in each face-laminate is referred to as P (following the notation introduced in Fig. 2). P can be related to P_{tot} through the relation:

$$P = \frac{P_{tot}(maximum) - P_{tot}(reference)}{2\times "width\ of\ test\text{-}specimen"} = \frac{\Delta P_{tot}}{2\times 50\ mm}.$$

5.5.1.1 Specimen 1-1 (sides s11A and s11B)

s11A:

The specklegram obtained for sample side s11A is displayed in Fig. 8, where the "measurement window" size is *24.0 mm* (*x*-direction) by *31.7 mm* (*y*-direction). The thickness "drop-of" is positioned along a horizontal line going through the middle of Fig. 8, where the part of the plot below the middle corresponds to the "thin" face-laminate. Sample side s11A is a "golf-ball" aspect surface (as explained in section 5.1; see Fig. 5), and a deflection pattern with doubly-curved local perturbations is clearly recognised in Fig. 8 (especially in the lower part). The absolute deflection magnitudes displayed in Fig. 8 do not represent the actual out-of-plane displacements, as a specklegram only provides information about the relative differences between maximum and minium displacements. Thus, Fig. 8 only provides information about the relative differences between the minimum and maximum values of the out-of-plane deflection pattern encountered.

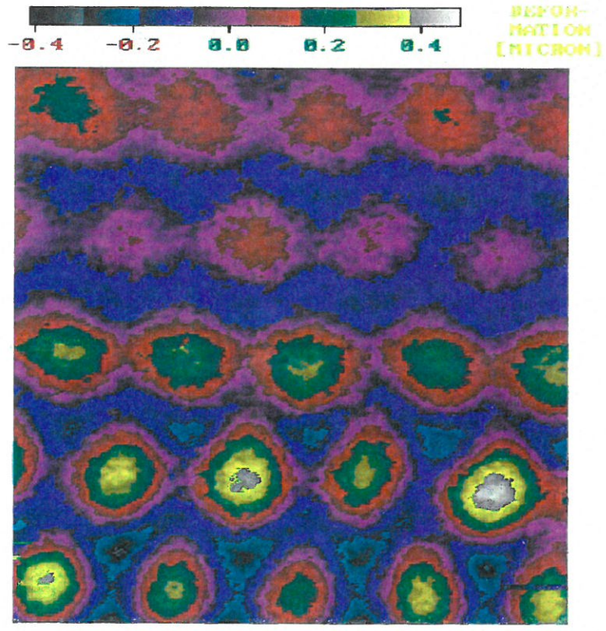

Figure 8. Specklegram (including *440×320* pixels) of sample side s11A recorded for *P=-1.83 N/mm*. "Measurement window": *24.0 mm* (*x*) by *31.7* (*y*) *mm*. The "thin-laminate" part corresponds to the lower half of the image.

From the data contained in Fig. 8, four out-of-plane deflection profiles were selected; two profiles representing maximum deflections (peaks), and two profiles representing minimum deflections (valleys). The selected profiles are displayed in Fig. 9, where the scaling of the *x*-axis was chosen such that *x=0* corresponds to the location of the thickness "drop-off" as shown in Fig. 3.
From Fig. 9 the HC-response (i.e., the part of the bending pattern with wave-length equal or close to the honeycomb cell size S_c=*4.76 mm*) seems to be very dominant, and it is very difficult to identify any LB-response (i.e., local bending response induced by the presence of the thickness "drop-off") by pure visual inspection. The reason for the HC-response to be so dominant is primarily, that the surface quality of the specimen was poor

(i.e., the "golf-ball" aspect problem), and secondly that the LB-response at the applied load level was of very small amplitude.

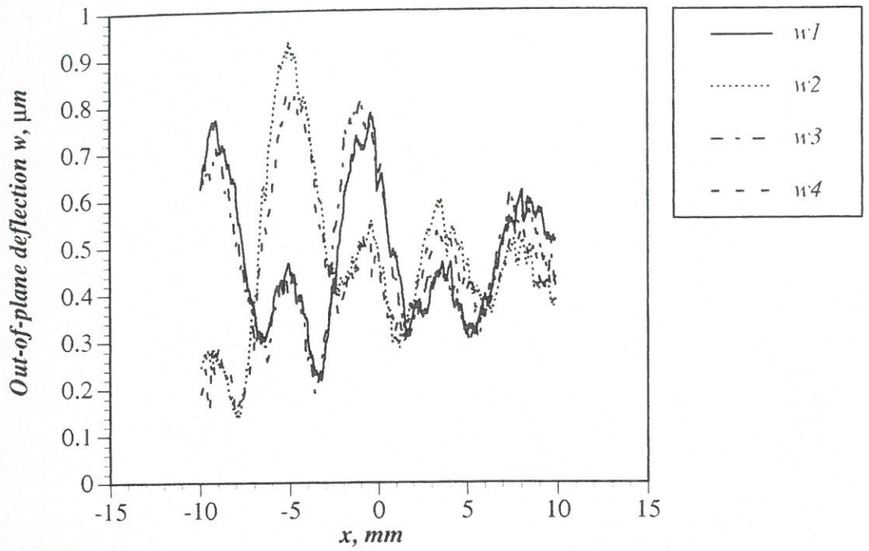

Figure 9. Selected out-of-plane deflection profiles for sample side s11A (*x=0* corresponds to the position of the thickness "drop-off"), where *w1*="*y*-pixel *195*", *w2*="*y*-pixel *229*", *w3*="*y*-pixel *266*" and *w4*="*y*-pixel *299*".

In Fig. 10, the averaged out-of-plane deflection profile (obtained as the average of the four profiles shown in Fig. 9) is displayed together with the "low-pass" filtered average and the theoretically predicted out-of-plane deflection profiles. The experimentally obtained out-of-plane deflection profiles (averaged and filtered) included in Fig. 10 have been attributed a negative "off-set" deflection amplitude of *-0.475 µm* compared with the results shown in Figs. 8 and 9[16].
Considering the averaged profile at first, it is possible to identify what seems to be a LB-response superimposed to the HC-response (or vice versa). Considering the filtered deflection profile reveals, that a LB-response is present, and that the overall shape of this response is close to the expected shape. It is also seen, however, that a significant phase difference between the filtered and theoretically predicted deflection profiles is present[17].
The following three key-figures can be given for the comparison of the filtered (experimental) and theoretical out-of-plane deflection profiles:

- Peak distance x_{peak} (filtered profile/theoretical profile): *6.1 mm / 5.5 mm.*
- Phase difference Δx (minimum points/maximum points): *5.7 mm / 6.3 mm.*
- Amplitude |w| (filtered profile/theoretical profile): *0.11 µm / 0.31 µm.*

---

16 The chosen "off-set" value for the averaged and "low-pass" filtered deflection profiles is chosen (arbitrarily) in order to facilitate the comparison with the theoretical results.

17 The magnitude of the observed phase difference is close to half the wave-length of the elastic response (i.e., the filtered and theoretically predicted out-of-plane deflection profiles are effectively of opposite phases). This surprising result is a special feature of the "golf-ball" aspect sample sides, and no such "opposite phase" deflection patterns were observed for the "flat" aspect sample sides (as will be demonstrated later).

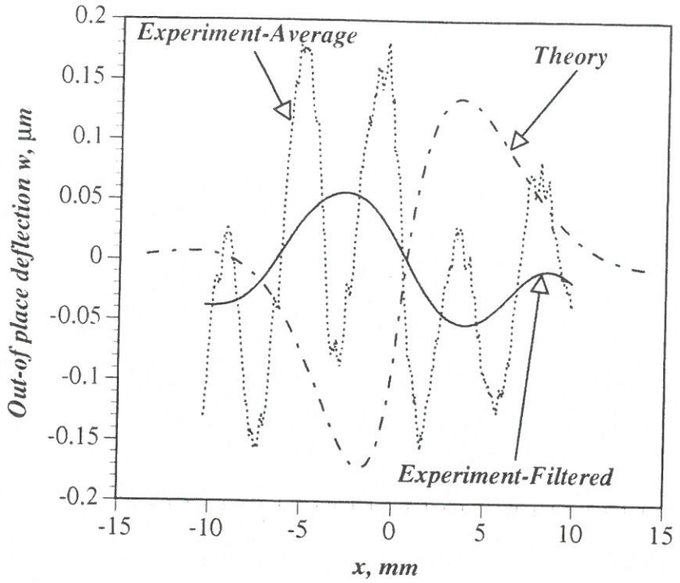

Figure 10. Averaged, "low-pass" filtered and theoretically predicted out-of-plane deflection profiles for sample side s11A. "Off-set" value for averaged and "low-pass" filtered deflection profiles: *-0.475 μm*.

Thus, the comparison of the filtered signal with the theoretically predicted deflection profile shows that the shape patterns are very close, that the wave-lengths are very close, but that the predicted deflection amplitudes are almost three times as large as the deflection amplitudes of the filtered signal. Moreover, there is a considerable phase difference (about one half elastic wave-length) between the predicted and filtered deflection profiles.

s11B:

The specklegram obtained for side s11B is displayed in Fig. 11, and the size of the "measurement window" is the same as for sample side s11A, i.e., *24.0 mm* (*x*-direction) by *31.7 mm* (*y*-direction). The thickness "drop-of" is positioned along a horizontal line going through the middle of the image, where the part of the plot below the middle corresponds to the "thin" face-laminate. Sample side s11B is a "flat aspect" surface (see section 5.1; Fig. 6) with the characteristic irregularity displayed in Fig. 7. As for all the specklegrams included in this report, the absolute deflection magnitude level attributed in Fig. 11 represents an arbitrary choice, as only the "relative" deflections can be determined.

From Fig. 11, it is seen that the overall deflectional pattern does not display the same dominating role of the HC-response part as was the seen in Fig. 8 (showing sample s11A). The presence of a HC-response is, however, clearly observed.

It is further observed that particular large deflections are present below the "drop-off" in the left part of the specklegram (shown by a "dark grey"/"black" hole). The presence of this area of extraordinary large (negative) deflections is probably caused by some sort of imperfection/irregularity in the honeycomb/face-laminate interface.

From the data contained in Fig. 11, four out-of-plane deflection profiles were selected (all of them selected away from the "dark grey"/"black" hole observed in the left part of the specklegram"): two profiles representing maximum deflections (peaks), and two profiles representing minimum deflections (valleys). The selected profiles are shown in Fig. 12, where *x=0* corresponds to the thickness "drop-off" as shown in Fig. 3.

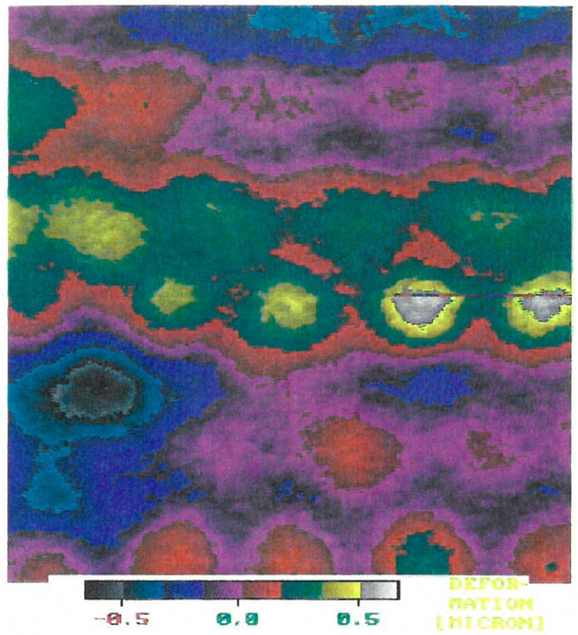

Figure 11. Specklegram (including *440×320* pixels) of sample side s11B recorded for *P=-2.26 N/mm*. "Measurement window": *24.0 mm* (*x*) by *31.7* (*y*) *mm*. The "thin-laminate" part corresponds to the lower half of the image.

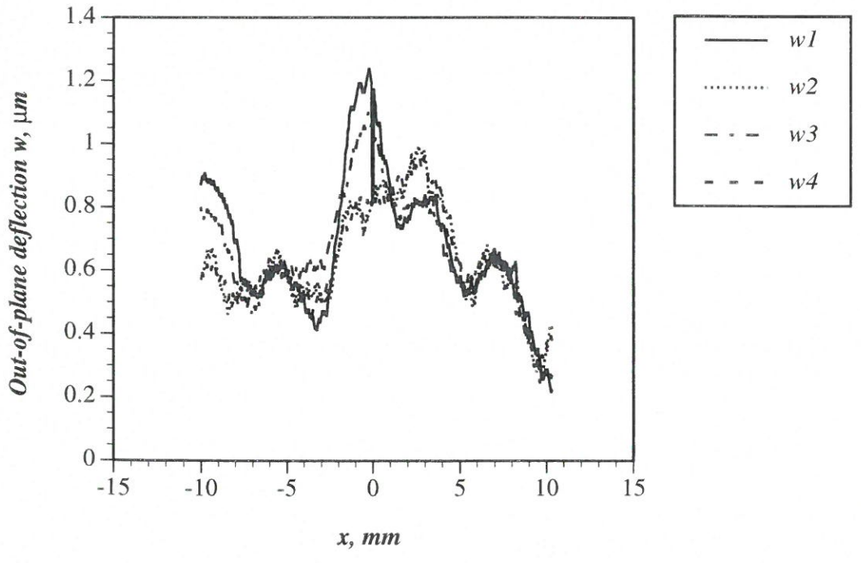

Figure 12. Selected out-of-plane deflection profiles for sample side s11B (*x=0* corresponds to the position of the thickness "drop-off"), where *w1*="*y*-pixel *331*", *w2*="*y*-pixel *291*", *w3*="*y*-pixel *257*" and *w4*="*y*-pixel *219*".

From Fig. 12 it is clear, that a LB-response is present, and that the overall deflection pattern is much more homogeneous than was observed for side s11A (see Fig. 9). The reason why the LB-response in Fig. 12 is more apparent than in Fig. 9 is primarily, that the surface quality of side s11B was much better than of side s11A, and secondly that the load level was somewhat higher (about 24 %; see Table 9).
The average out-of-plane deflection profile, derived from the four deflection profiles shown in Fig. 12, is shown in Fig. 13, which also displays the filtered out-of-plane and theoretically predicted deflection profiles. The averaged and filtered deflection profiles have been attributed (arbitrarily) an "off-set" value of *-0.75 μm* as compared with the results shown in Figs. 11 and 12.

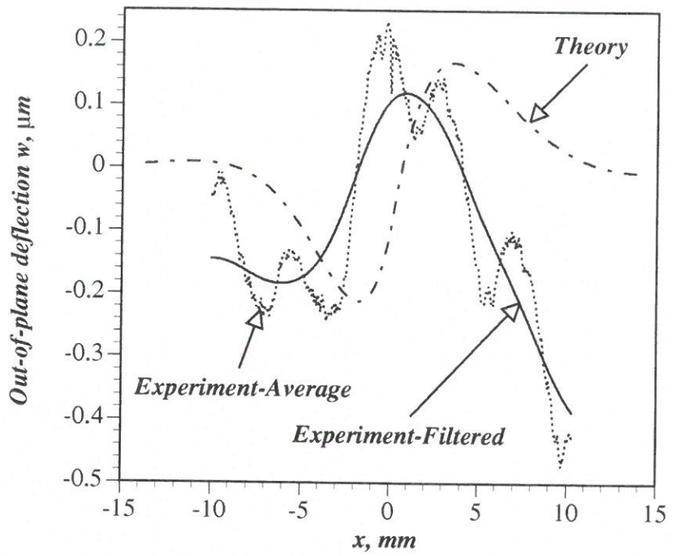

Figure 13. Averaged, "low-pass" filtered and theoretically predicted out-of-plane deflection profiles for sample side s11B. "Off-set" value for averaged and "low-pass" filtered deflection profiles: *-0.750 μm*.

From Fig. 13 it is seen, that the filtered and theoretical deflection profiles resemble each other very much except close to the ends of the sampling interval. The deviations registered at the ends of the sampling interval (especially on the right side of the sampling interval) are probably a consequence of the lack of information about the "repetition"-sequence of the averaged deflection profile due to the limited size of the ESPI "measurement window". Within the sampling interval the resemblance is very good with respect to the signal shapes and amplitudes. It is also seen, that the filtered and theoretically predicted deflection profiles display a slight phase difference. This phase difference, however, is much smaller than was seen for sample side s11A. From Fig. 13, the following three key-quantities has been derived for the comparison of the filtered and theoretical out-of-plane deflection profiles:

- Peak distance x_{peak} (filtered profile/theoretical profile): *6.4 mm / 5.5 mm.*
- Phase difference Δx (minimum points/maximum points): *3.5 mm / 2.6 mm.*
- Amplitude |w| (filtered profile/theoretical profile): *0.30 μm / 0.38 μm.*

Thus it is seen, that especially the wave-lengths as well as the amplitudes compare well (disregarding the amplitude differences encountered at the ends of the sampling interval as explained above).

Comments for sample sides s11A and s11B:

The results presented for test-specimen 1-1, have shown, that the theoretical model was able to predict the overall deflectional behaviour around the thickness "drop-off's" with reasonable accuracy (at least for sample side s11B). However deviations between experiment and theory were observed.
With respect to sample side s11A it was seen, that a considerable phase difference between the filtered and theoretical deflection profiles was present (opposite phases), and even though the exact reason for this phenomenon is (yet) unknown, it turns out only to be associated with the "golf-ball" aspect sample sides. Thus, the problem is (must be) a consequence of the poor surface quality of the A-sides of the test-specimens.
With respect to sample side s11B, the deviations between experiments and theory can be attributed to problems caused by the limited size of the ESPI "measurement window".

5.5.1.2 Specimen 1-2 (sides s12A and s12B)

s12A:

The specklegram recorded for sample side s12A is shown in Fig. 14. The size of the "measurement window" is *23.5 mm* (*x*-direction) by *31.3 mm* (*y*-direction). The thickness "drop-off" is positioned along a horizontal line dividing the specklegram in two half's, where the "thin" laminate part corresponds to the lower part of the image. Sample side s12A is a "golf-ball" aspect surface (see section 5.1, Fig. 5), and it is seen, that the specklegram in Fig. 14 is almost identical to the specklegram recorded for sample side s11A (Fig. 8). Thus, a deflection pattern with doubly-curved local perturbations is clearly recognised in Fig. 14. As for all the specklegrams, only information about the relative differences between the local minima and maxima is contained in the image.

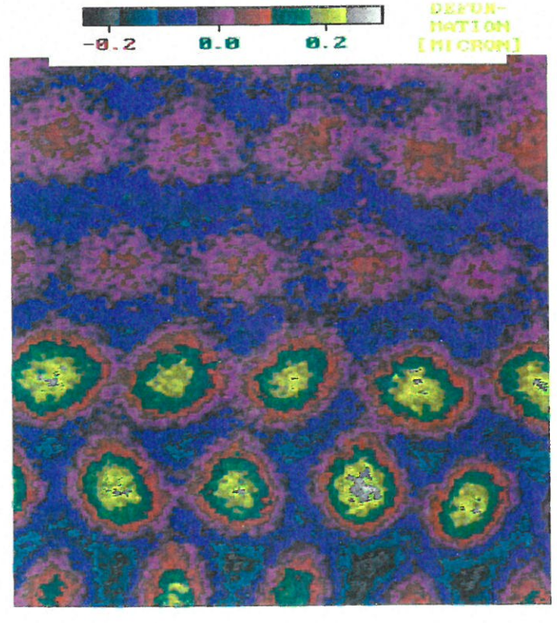

Figure 14. Specklegram (including *440×320* pixels) of sample side s12A recorded for *P=-1.02 N/mm*. "Measurement window": *23.5 mm* (*x*) by *31.3* (*y*) *mm*. The "thin-laminate" part corresponds to the lower half of the image.

From the data contained in Fig. 14, four out-of-plane deflection profiles were selected (following the same procedure as previously: two "peak"-profiles and two "valley"-profiles). The four deflection profiles are shown in Fig. 15.

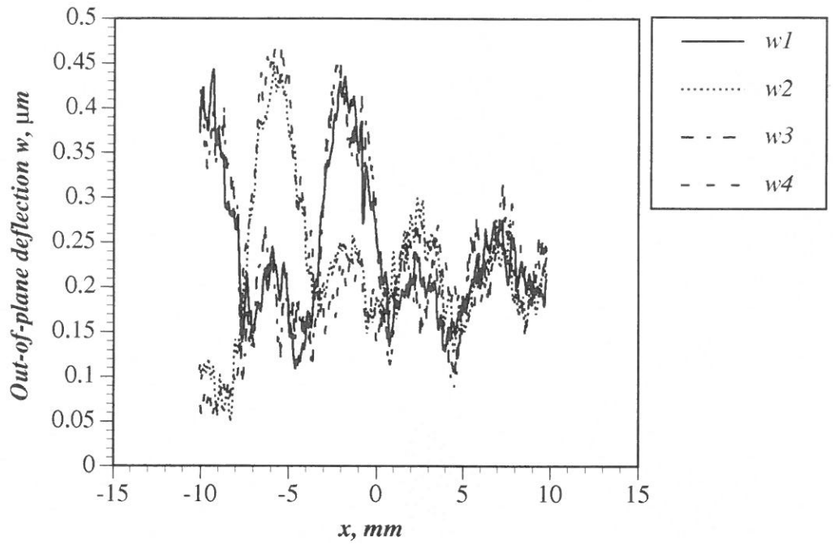

Figure 15. Selected out-of-plane deflection profiles for sample side s12A (*x=0* corresponds to the position of the thickness "drop-off"), where *w1*="*y*-pixel *193*", *w2*="*y*-pixel *226*", *w3*="*y*-pixel *262*" and *w4*="*y*-pixel *297*".

From Fig. 15 it is seen, that the HC-response part is very dominating in all the deflection profiles, and it is extremely difficult to identify the presence of any LB-response parts. As for sample side s11A, the reason for the HC-response to be so dominant is, that the surface quality of the specimen was poor (i.e., the "golf-ball" aspect problem), and that the LB-response at the applied load level was of very small amplitude.
From the selected deflection profiles displayed in Fig. 15 an averaged deflection profile was computed. The derived averaged deflection profile is displayed in Fig. 16 together with the "low-pass" filtered and theoretically predicted deflection profiles. The experimentally obtained out-of-plane deflection profiles (averaged and filtered) included in Fig. 16 have been attributed a negative "off-set" deflection amplitude of *-0.23 µm* compared with the results shown in Figs. 14 and 15.
By considering the averaged profile, it is just about possible to identify the LB-response part. The presence of the LB-response is revealed by the "low-pass" filtered signal, and it is seen, that the LB-response (filtered) is very close to the theoretically predicted signal with respect to overall shape and wave-length. It is seen, however, that the predicted and measured amplitudes differ by a factor of between two and three, and that the theoretical and filtered signals are of almost opposite phases (i.e., a phase difference of about one half elastic wave-length). Thus, the features of sample side s12A resembles those observed for sample side s11A. The following three key-quantities have been derived from the information contained in Fig. 16 for the comparison of the filtered (experimental) and theoretical out-of-plane deflection profiles:

- Peak distance x_{peak} (filtered profile/theoretical profile): *7.5 mm / 5.5 mm.*
- Phase difference Δx (minimum points/maximum points): *6.2 mm / 6.8 mm.*
- Amplitude |w| (filtered profile/theoretical profile): *0.07 µm / 0.17 µm.*

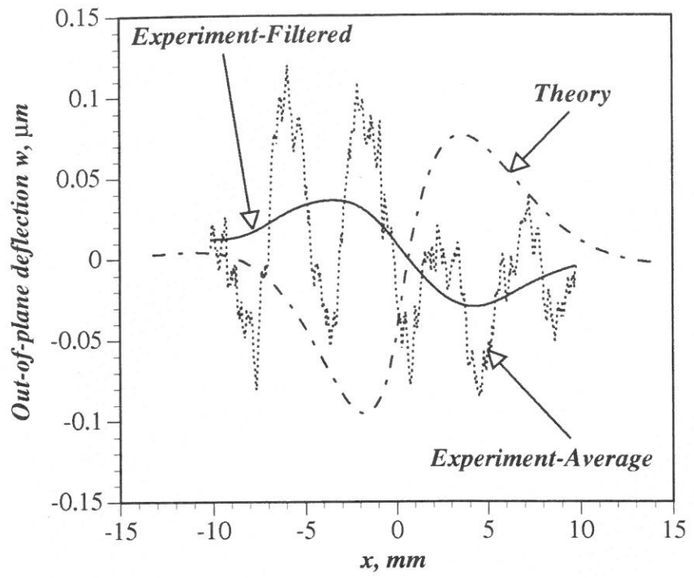

Figure 16. Averaged, "low-pass" filtered and theoretically predicted out-of-plane deflection profiles for sample side s12A. "Off-set" value for averaged and "low-pass" filtered deflection profiles: *-0.230 µm.*

Thus, the comparison of the filtered signal with the theoretically predicted deflection profile shows, that the shape patterns are very close, that the wave-lengths are close, but that the predicted deflection amplitudes are 2.6 times as large as the deflection amplitudes of the filtered signal. Furthermore, there is a considerable phase difference between the predicted and filtered deflection profiles.
Pertaining to the shape of the filtered signal it is seen to be virtually identical to the shape of theoretically predicted signal, and special emphasis should be focused on the fact, that no "distortions" are observed at the ends of the sampling interval (filtered signal). The shape of the filtered signal is so "regular" in this case because the "measurement window" contained a "complete" elastic wave-length, thus displaying no "cut-offs" at the ends of the sampling interval. This provided the filtering algorithm with data, which contained virtually all the information about the "repetition"-sequence of the filtered signal, which again resulted in the very regular and complete pattern displayed in Fig. 16.

s12B:

The specklegram recorded for sample side s12B is shown in Fig. 17, and the size of the "measurement window" is *23.5 mm* (*x*-direction) by *31.3 mm* (*y*-direction). The thickness "drop-off" is positioned along a horizontal line dividing the specklegram in two half's, where the "thin" laminate part corresponds to the lower part of the image. Sample side s12B is a "flat" aspect surface (see section 5.1, Fig. 6), displaying the typical irregularity illustrated in Fig. 7. Comparison of Fig. 17 with the specklegram in Fig. 14 shows that the HC-response, even though visible, is much less pronounced for sample side s12B than for s12A (as expected). As for all the specklegrams, only information about the relative differences between the local minima and maxima is contained in the image (i.e., the displayed absolute deflection level is arbitrarily chosen).
From the data contained in Fig. 17 four out-of-plane deflection profiles parallel with the *x*-axis were selected according to the tests procedure established in section 4.3. The four deflection profiles are shown in Fig. 18.

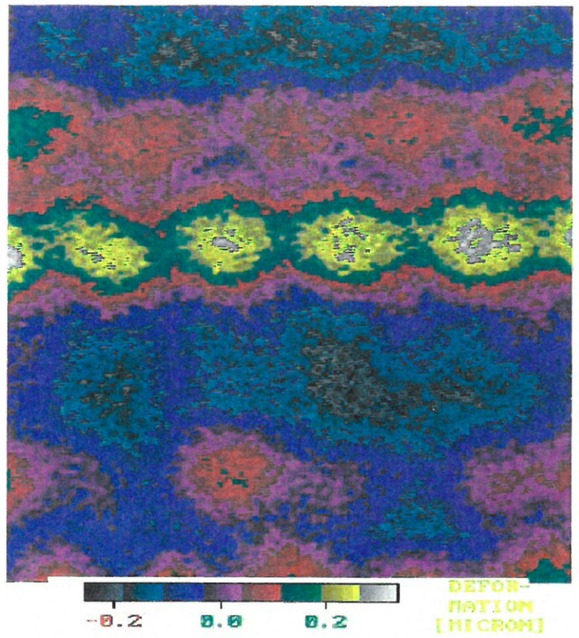

Figure 17. Specklegram (including *440×320* pixels) of sample side s12B recorded for *P=-1.44 N/mm*. "Measurement window": *23.5 mm* (*x*) by *31.3* (*y*) *mm*. The "thin-laminate" part corresponds to the lower half of the image.

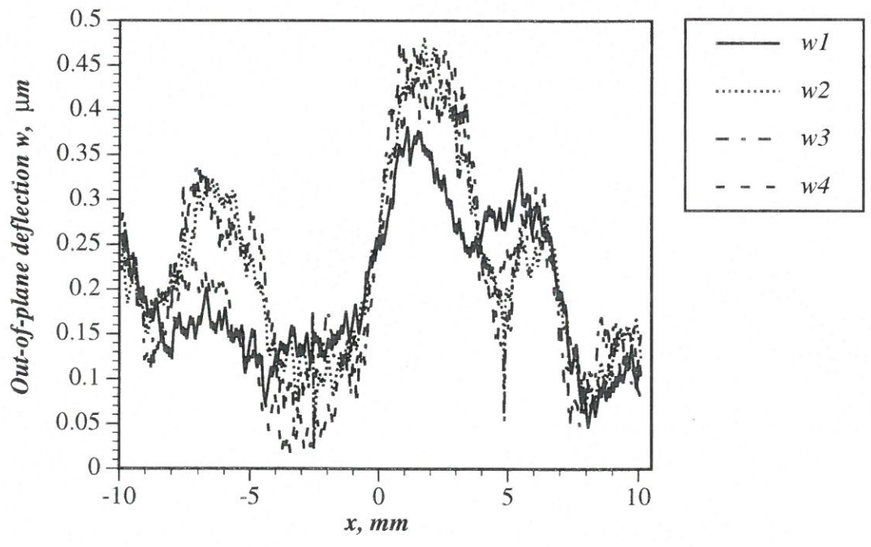

Figure 18. Selected out-of-plane deflection profiles for sample side s12B (*x=0* corresponds to the position of the thickness "drop-off"), where *w1*="*y*-pixel *179*", *w2*="*y*-pixel *222*", *w3*="*y*-pixel *256*" and *w4*="*y*-pixel *289*".

The presence of a LB-response part in the deflection profiles shown in Fig. 18 is easily identified, and is even more clearly seen in the averaged deflection profile displayed in Fig. 19. Fig. 19 also shows the "low-pass" filtered as well as the theoretically predicted out-of-plane deflection profiles. The averaged and filtered deflection profiles in Fig. 19 have been attributed an "off-set" value of *-0.24 µm* as compared to the deflection profiles displayed in Fig. 18.

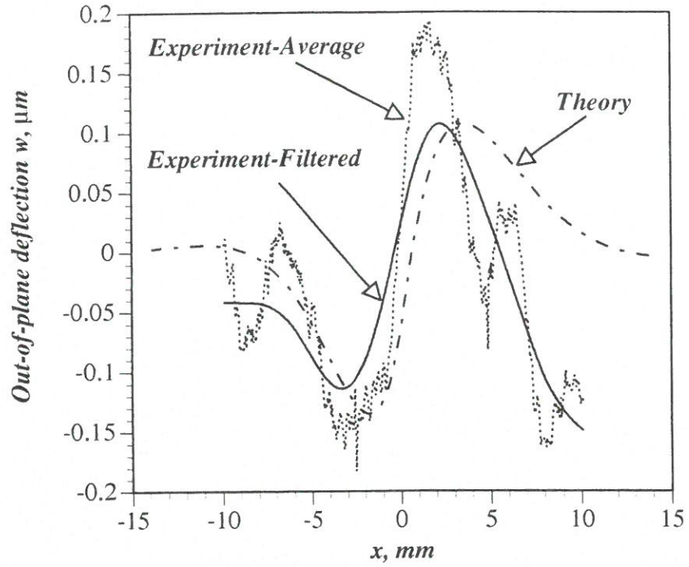

Figure 19. Averaged, "low-pass" filtered and theoretically predicted out-of-plane deflection profiles for sample side s12B. "Off-set" value for averaged and "low-pass" filtered deflection profiles: *-0.240 µm*.

Pertaining to the comparison between the filtered and theoretically predicted out-of-plane deflection profiles, the following key-quantities were computed from the data included in Fig.19:

- Peak distance x_{peak} (filtered profile/theoretical profile): *5.5 mm / 5.5 mm*.
- Phase difference Δx (minimum points/maximum points): *1.5 mm / 1.5 mm*.
- Amplitude |w| (filtered profile/theoretical profile): *0.22 µm / 0.24 µm*.

From the above it is seen, that the match between the filtered and theoretical signals is excellent in terms of all the computed key-quantities (peak distances, amplitudes and phase difference), i.e., the elastic wave-lengths match each other exactly and the amplitudes are nearly identical. However, as for most of the other sample sides the match at the ends of the sampling interval (especially the right side) is not very convincing. However, these discrepancies can be attributed mainly to the limited size of the "measurement window" (the sampling algorithm had to little information about the complete deflectional pattern, i.e., the "repetition"-sequence of the signal).

Comments for sample sides s12A and s12B:

In summary it can be concluded, that the experimental results obtained for test-specimen 1-2 have compared reasonably well with the theoretically predictions. This was especially pronounced for sample side s12B, which displayed almost exact similarity

with the theoretical predictions in terms of elastic wave-length and deflection amplitudes. As for the results obtained for sample side s12A, the predicted deflection amplitude was about 2.6 times larger than the amplitude of the filtered deflection profile, and the theoretical and filtered signals were of almost opposite phases. The overall deflection profile shapes as well as the elastic wave-lengths, however, matched each other well.

5.5.1.3 Concluding remarks for test-specimens of configuration 1

To conclude the comparative studies of the experimental and theoretical results for the CFRP/honeycomb sandwich test-specimens of configuration 1 (base-line laminate $[0°/90°/0°]$; reinforcing laminate $[\pm 45°]$) it can be stated, that the elastic foundation approach (developed in ref. [1]) provided reasonable predictions. The word "reasonable" is used in this context, as the predicted amplitudes for the two sample sides s11A and s12A turned out to be about 2-3 times larger than the amplitudes of the "low-pass" filtered deflection profiles, and as the predicted and filtered deflection profiles for the same two sample sides turned out to be of almost opposite phases. Sample sides s11A and s12A, however, were characterised by the "golf-ball" aspect phenomenon (see Fig. 5), and the observed discrepancies can be attributed to the highly disturbed surface characteristics. Furthermore, it must be considered doubtful whether the "low-pass" filtering algorithm was able to recover the complete LB-response from the experimental data (which were highly dominated by deflectional patterns with wave-length equal to the honeycomb cell size S_c)[18].
With respect to the test-specimens with "flat" aspect surfaces (i.e., s11B and s12B), the comparisons revealed a very fine match on all points, except for some distortions encountered at the ends of the sampling intervals for the filtered deflection profiles. As described, however, these problems are believed to be caused by the limited size of the ESPI "measurement windows".

5.5.2 Configuration 2: $[0°_2/90°]_S + [\pm 45°]_S$

Configuration 2 of the manufactured CFRP/honeycomb sandwich test-specimens represents the configuration, where the LB-responses were expected to be most easily identified beforehand. The reasons for this are:

- Each of the base-line laminates contained six plies ($[0°_2/90°]_S$) and therefore possessed the largest bending stiffnesses of the base-line laminates included in the investigation. As the largest bending stiffness is as also accompanied by the largest elastic wave-length (see eq. (11)), when the core properties are kept fixed, is was expected that the LB-response should be easier to separate from the HC-response than was the case for the specimens of configuration 1.
- Each of the reinforcing laminates contained four plies ($[\pm 45°]_S$) and therefore possessed the largest bending stiffnesses among the reinforcing laminates included in the investigation. This implies that the discontinuous stiffness change at the thickness "drop-off" was also the largest among the test specimen configurations included in the investigation.

Thus, the expected elastic wave-lengths as well as the expected deflection amplitudes should facilitate the identification and quantification of the LB-response parts.

---

18 The specklegrams for sample sides s11A and s12A were also recorded at very low load levels (see Table 9), and (as explained earlier) it was established during the test programme, that the HC-resonse parts were especially pronounced at low load levels (non-linear effect). Thus, the combined effect of "golf-ball" aspect surfaces and low loads is likely to have caused the appearance of very dominant HC-responses.

As for the configuration 1 test-specimens, the specklegrams of highest quality were obtained at the highest load levels. The specklegrams for configuration 2 were recorded under the load conditions specified in Table 10 (see footnote 15 on p. 25 for notation).

Specimen surface	*Reference image recorded at total load: P_{tot}(reference)*	*"Maximum load" image recorded at total load: P_{tot}(maximum)*	*In-plane normal stress resultant corresponding to specklegram: $P=\Delta P_{tot}/(2\times 50\ mm)$*
s21A	*-597 N*	*-781 N*	*-1.84 N/mm*
s21B	*-592 N*	*-777 N*	*-1.85 N/mm*
s22A	*-392 N*	*-782 N*	*-3.90 N/mm*
s22B	*-380 N*	*-785 N*	*-4.05 N/mm*

Table 10. Load conditions for recording of specklegrams for ***configuration 2*** CFRP/honeycomb sandwich test-specimens.

5.5.2.1 Specimen 2-1 (sides s21A and s21B)

s21A:

The specklegram obtained for sample side s21A is shown in Fig. 20, where the "measurement window" size is *28.3 mm* (x-direction) by *37.7 mm* (y-direction). The thickness "drop-off" is positioned along a horizontal line going through the middle of Fig. 20, where the part of the plot above the middle corresponds to the "thin" face-laminate. Sample side s21A is a "golf-ball" aspect surface (as explained in section 5.1; see Fig. 5), and a deflection pattern with doubly-curved local perturbations is clearly recognised in Fig. 20 (most clearly seen in the upper part of the image). By comparing Fig. 20 with Fig. 8 (specklegram for sample side s11A) it is seen, however, that the "golf-ball" deflection pattern for sample side s21A is much less dominating than was the case for sample side s11A. Obviously, this is a consequence of the much larger bending stiffness of the face-laminates of the configuration 2 test-specimens as compared with the test-specimens of configuration 1.
As before, the absolute deflection magnitudes displayed in Fig. 20 only represent information about the relative out-of-plane displacement differences.
From the data contained in Fig. 20, four out-of-plane deflection profiles were selected; two profiles representing maximum deflections (peaks), and two profiles representing minimum deflections (valleys). The selected profiles are displayed in Fig. 21, where $x=0$ corresponds to the location of the thickness "drop-off" (see Fig. 3).
From Fig. 21 is observed, that the response is very homogeneous as compared to the similar results obtained for configuration 1 (see Figs. 9 and 15). Thus, it is seen, that the differences between "peak"- and "valley"-profiles are much smaller than was the case for the "golf-ball" aspect surfaces of configuration 1. Furthermore, it is seen that the HC-response parts are less dominant than in Figs. 9 and 15.

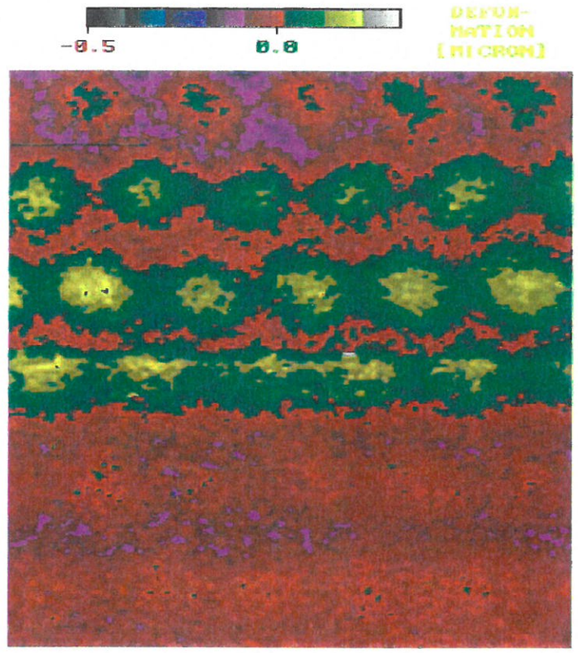

Figure 20. Specklegram (including *440×320* pixels) of sample side s21A recorded for *P=-1.84 N/mm*. "Measurement window": *28.3 mm* (*x*) by *37.7* (*y*) *mm*. The "thin-laminate" part corresponds to the upper half of the image.

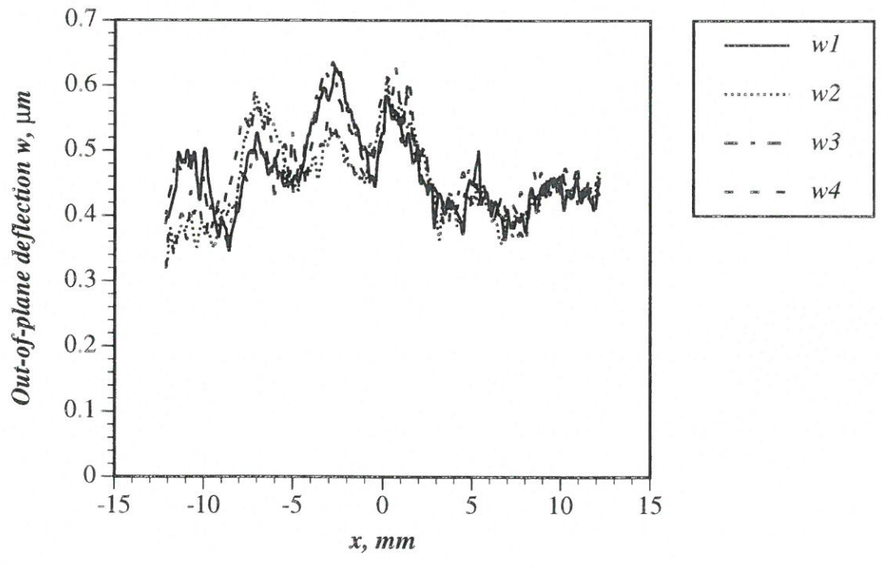

Figure 21. Selected out-of-plane deflection profiles for sample side s21A (*x=0* corresponds to the position of the thickness "drop-off"), where *w1*="*y*-pixel *206*", *w2*="*y*-pixel *236*", *w3*="*y*-pixel *266*" and *w4*="*y*-pixel *295*".

The averaged out-of-plane deflection profile (derived from the four profiles displayed in Fig. 21) is shown in Fig. 22, which also displays the "low-pass" filtered and theoretically predicted deflection profiles. The latter two have been attributed an "off-set" value of *-0.43 µm* compared with the deflection profiles displayed in Fig. 21.

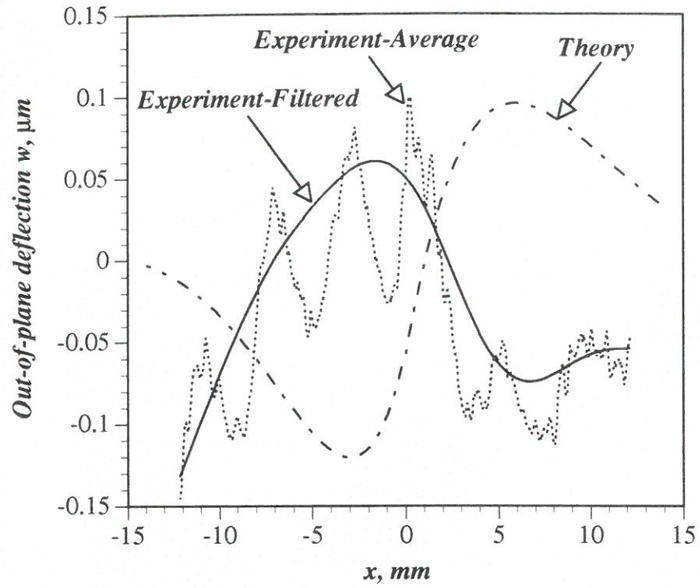

Figure 22. Averaged, "low-pass" filtered and theoretically predicted out-of-plane deflection profiles for sample side s21A. "Off-set" value for averaged and "low-pass" filtered deflection profiles: *-0.430 µm*.

From the data contained in Fig. 22 the following key-quantities have been identified:

- Peak distance x_{peak} (filtered profile/theoretical profile): *8.2 mm / 8.7 mm.*
- Phase difference Δx (minimum points/maximum points): *9.7 mm / 7.2 mm.*
- Amplitude |*w*| (filtered profile/theoretical profile): *0.13 µm / 0.21 µm.*

From Fig. 22 it is seen, that the overall shapes of the filtered and theoretical deflection profiles resemble each other quite well. At the ends of the sampling interval (especially at the left end), however, the filtered signal seems to "dive" much to steeply. Part of the reason for this phenomenon (and believed to be the main reason) is the problem discussed previously pertaining to the limited size of the ESPI "measurement window" used. This problem is especially severe in the present example because the sampling interval (left end) ends in the middle of what appears to be a local HC-response minimum close to a minimum of the LB-response. Furthermore it is seen, that the filtered and theoretical deflection profiles display a phase difference, which is close to one half wave-length (as seen for sample sides s11A and s12A). In other words, the filtered and theoretical deflection profiles are of almost opposite phases. As mentioned previously, this phenomenon is a characteristic feature of the "golf-ball" aspect sample sides, and is a consequence of the highly "disturbed" surface topography induced by the co-curing of the test-specimens.
Comparison of the amplitudes (and discarding the filtered signal at the left end of the sampling interval) reveals, that the theoretically predicted amplitude is about*50 %* larger than the amplitude of the filtered signal.

With respect to the wave-lengths of the filtered and theoretical deflection profiles (evaluated from the peak distance, i.e., the distance between the two neighbouring minimum and maximum values) it is seen, that they match each other quite well.

s21B:

The specklegram obtained for sample side s21B is displayed in Fig. 23. The size of "measurement window" is *28.3 mm* (*x*-direction) by *37.7 mm* (*y*-direction). The thickness "drop-off" is positioned along a horizontal line going through the middle of Fig. 20, where the part of the plot above the middle corresponds to the "thin" face-laminate. Sample side s21B is a "flat" aspect surface (see Fig. 6), with the characteristic irregularity shown in Fig. 7.

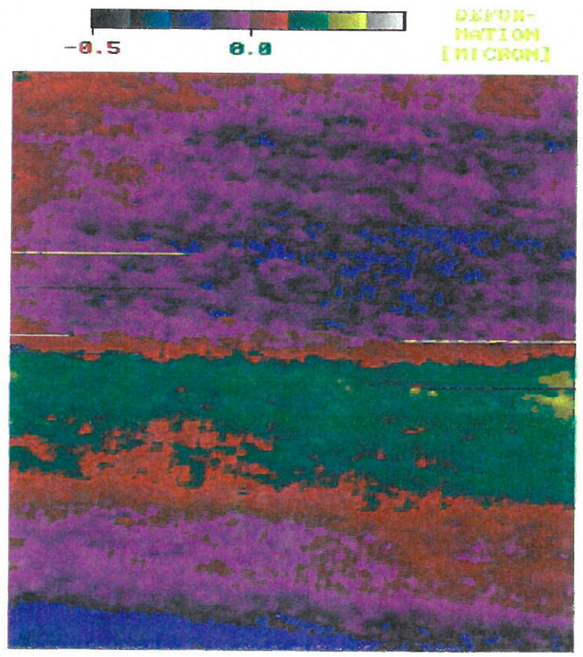

Figure 23. Specklegram (including *440×320* pixels) of sample side s21B recorded for *P=-1.85 N/mm*. "Measurement window": *28.3 mm* (*x*) by *37.7* (*y*) *mm*. The "thin-laminate" part corresponds to the upper half of the image.

Comparing the "B-side" image in Fig. 23 with the corresponding "A-side" image in Fig. 20 it is seen to be more homogeneous in the sense, that a HC-response is virtually impossible to identify. Following the test procedure, four out-of-plane deflection profiles parallel with the *x*-axis were selected from the specklegram displayed in Fig. 23; two "peak"- and two "valley"-profiles (even though it was extremely difficult to point out "peaks" and "valleys"). The selected four deflection profiles are shown in Fig. 24.
From Fig. 24 it is seen (as was also seen from Fig. 23), that the LB-response is very dominant, and it is difficult to identify a HC-response (except in the right side of the deflection profiles). Thus, the primary contributions to the deflection profiles shown in Fig. 24 are the LB-responses overlaid with the usual speckle noise.
The averaged out-of-plane deflection profile (derived from the four selected deflection profiles) is shown in Fig. 25 together with the "low-pass" filtered and theoretically

predicted deflection profiles. The averaged and filtered profiles have been attributed an "off-set" value of *-0.55 μm* compared with the deflection profiles shown in Fig. 24.

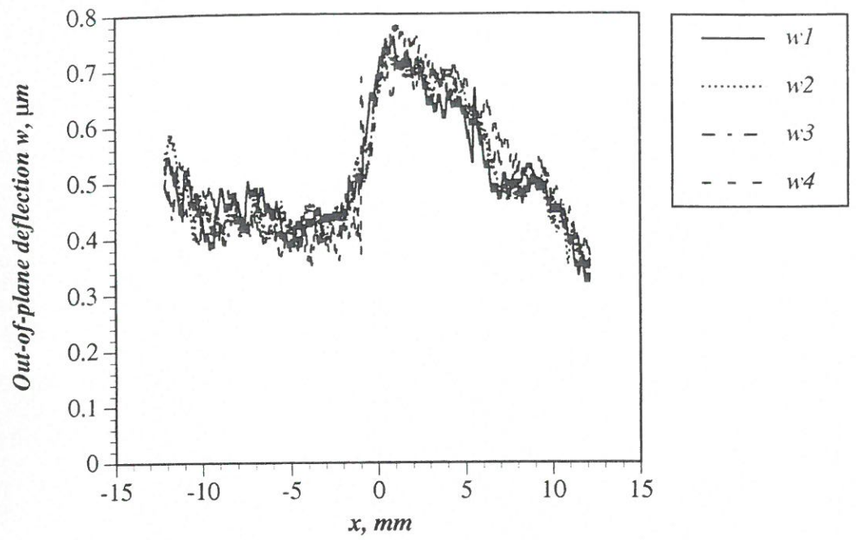

Figure 24. Selected out-of-plane deflection profiles for sample side s21B (*x=0* corresponds to the position of the thickness "drop-off"), where *w1*="*y*-pixel *226*", *w2*="*y*-pixel *256*", *w3*="*y*-pixel *286*" and *w4*="*y*-pixel *316*".

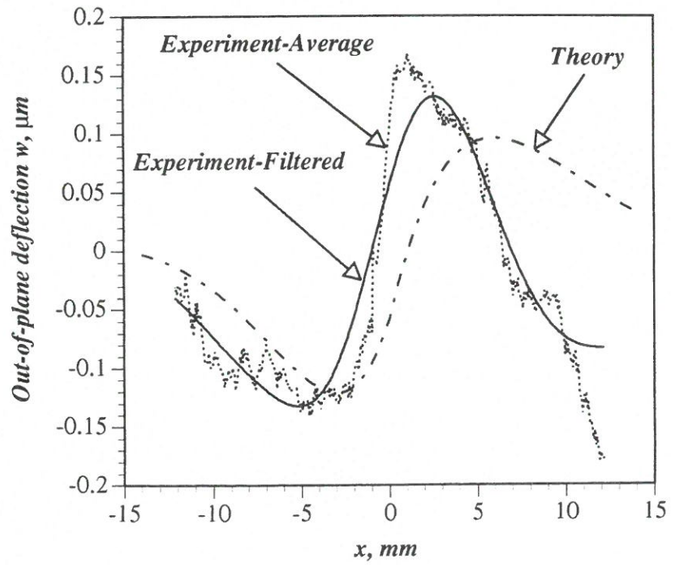

Figure 25. Averaged, "low-pass" filtered and theoretically predicted out-of-plane deflection profiles for sample side s21B. "Off-set" value for averaged and "low-pass" filtered deflection profiles: *-0.550 μm*.

From Fig. 25 it is seen, that the filtered and theoretically predicted profiles are very similar with respect to profile shapes, wave-lengths as well as amplitudes, and the following key-figures have been identified:

- Peak distance x_{peak} (filtered profile/theoretical profile): *7.6 mm / 8.7 mm.*
- Phase difference Δx (minimum points/maximum points): *2.2 mm / 3.3 mm.*
- Amplitude |w| (filtered profile/theoretical profile): *0.26 μm / 0.22 μm.*

Despite the convincing overall match recognised by visual inspection of the deflection profiles, as well as revealed by the key-figures quoted above, it is observed, that the similarity between the filtered and theoretical profiles is rather poor at the right side of the sampling interval (as seen for several of the other sample sides). Thus, it is seen, that the filtered signal tends to "dive" much more than the theoretical signal at the right end. As explained earlier it is believed, that the main reason for these deviations is the fact, that the ESPI "measurement window" was to small to capture a complete wave-length of the elastic response. The consequence of this being, that the filtering algorithm simply lacked the information necessary to identify the "repetition"-sequence of the LB-response.
The above argument is substantiated by the features of the averaged signal (see Fig. 25) at right end of the sampling interval, where the HC-response is clearly visible. It is seen, that the sampling was ended in the middle of a local minimum of the HC-response (in the middle of a honeycomb cell), which at the same time also constituted a minimum (or nearly so) for the LB-response part. Thus, the filtering of the averaged signal caused the filtered signal to "dive" to much at the right end. It should be noted, that the described effect was also detected for sample side s21A; see Fig. 22 (same test-specimen).

Comments for sample sides s21A and s21B:

Pertaining to the results obtained for test-specimen 2-1 the following features should be highlighted. The overall match between the filtered and theoretical deflection profiles was generally good, and the match between key-quantities such as peak distance and deflection amplitude was very good.
As expected in advance, the results for sample side s21B ("flat" aspect surface) have proven to be better than the results for sample side s21A ("golf-ball" aspect surface), where the latter displayed a considerable phase difference between the theoretical and filtered deflection profiles (effective of opposite phases). For both sample sides "irregularities" were detected at the ends of the filtered deflection profiles, and it is believed, that the primary reason for these "irregularities" was the limited size of the ESPI "measurement window".

5.5.2.2 *Specimen 2-2 (sides s22A and s22B)*

s22A:

The specklegram recorded for sample side s22A is displayed in Fig. 26, and the size of the ESPI "measurement window" is *28.3 mm* (*x*-direction) by *37.7 mm* (*y*-direction). The thickness "drop-off" is positioned along a horizontal line a little above the middle of the image, where the upper part of the plot corresponds to the "thin" face-laminate. Sample side s22A is a "golf-ball" aspect surface (as explained in section 5.1; see Fig. 5), and a deflection pattern with doubly-curved local perturbations is clearly recognised in the upper part of the image.
It is seen, that the image in Fig. 26 is very similar to the image in Fig. 20 (sample side s21A) except for the deflection amplitude, which is about double the size. This, however, should be expected as the load level for the recording of the specklegram of s22A (*P=-3.90 N/mm*) was about twice as large as the load level for the recording of the specklegram of s21A (*P=-1.84 N/mm*). As before, Fig. 26 only provides information about the relative differences between the minimum and maximum deflection values.

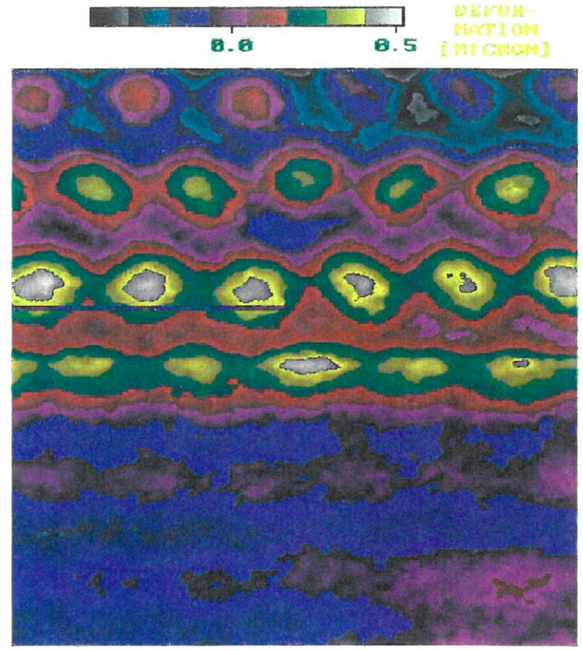

Figure 26. Specklegram (including *440×320* pixels) of sample side s22A recorded for *P=-3.90 N/mm*. "Measurement window": *28.3 mm* (*x*) by *37.7* (*y*) *mm*. The "thin-laminate" part corresponds to the upper half of the image.

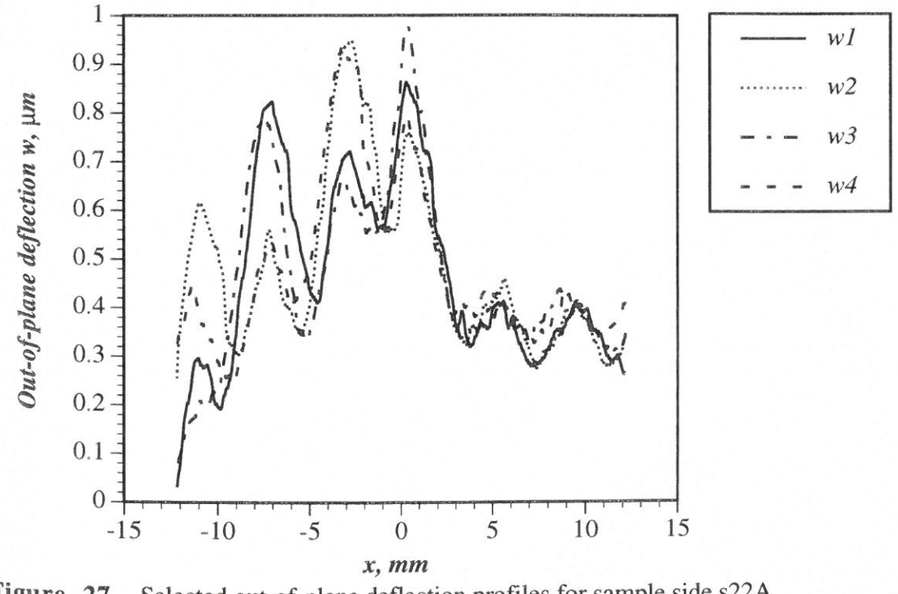

Figure 27. Selected out-of-plane deflection profiles for sample side s22A (*x=0* corresponds to the position of the thickness "drop-off"), where *w1*="*y*-pixel *202*", *w2*="*y*-pixel *232*", *w3*="*y*-pixel *262*" and *w4*="*y*-pixel *292*".

From Fig. 26, four out-of-plane deflection profiles were selected; two profiles representing maximum deflections (peaks), and two profiles representing minimum deflections (valleys). The selected profiles are displayed in Fig. 27, where $x=0$ corresponds to the location of the thickness "drop-off". The averaged out-of-plane deflection profile is displayed in Fig. 28 along with the "low-pass" filtered and the theoretically predicted deflection profiles. The averaged and filtered profiles have been attributed an "off-set" value of *-0.55 μm* compared with Fig. 27.

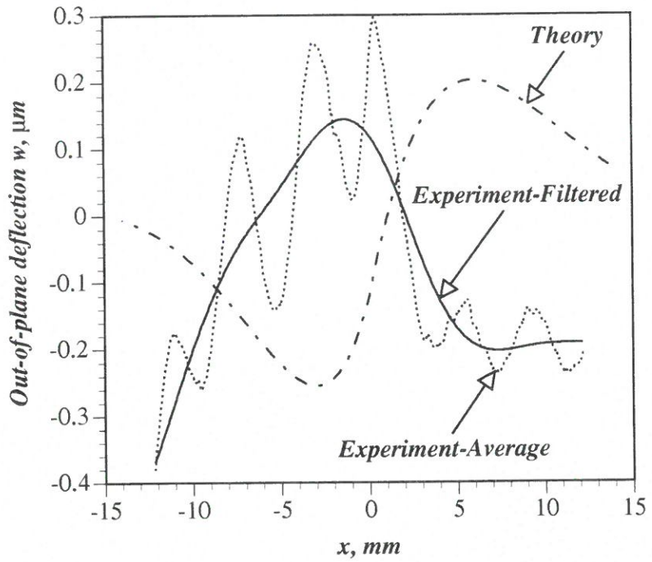

Figure 28. Averaged, "low-pass" filtered and theoretically predicted out-of-plane deflection profiles for sample side s22A. "Off-set" value for averaged and "low-pass" filtered deflection profiles: *-0.550 μm*.

As for the other A-sides, it is observed that a considerable phase difference is present between the theoretical and filtered deflection profiles (effectively of opposite phases). However, the overall shape (except for the regions close to the sampling interval), the deflection amplitude as well as the "peak-distance" of the filtered deflection profile are all seen to be very similar to those of the theoretically predicted profile. The following comparative key-quantities have been derived from the data contained in Fig. 28:

- Peak distance x_{peak} (filtered profile/theoretical profile): *8.5 mm / 8.7 mm.*
- Phase difference Δx (minimum points/maximum points): *10.3 mm / 6.9 mm.*
- Amplitude |w| (filtered profile/theoretical profile): *0.35 μm / 0.46 μm.*

s22B:

The specklegram for the last sample side corresponding to test-specimen configuration 2, i.e., sample side s22B, is shown in Fig. 29. The ESPI "measurement window" is *28.3 mm* (*x*-direction) by *37.7 mm* (*y*-direction). The upper part of the image corresponds to the "thin" face-laminate. Sample side s22B is characterised by having a "flat" aspect surface (see Fig. 6), and it also displays the characteristic irregularity shown in Fig. 7.

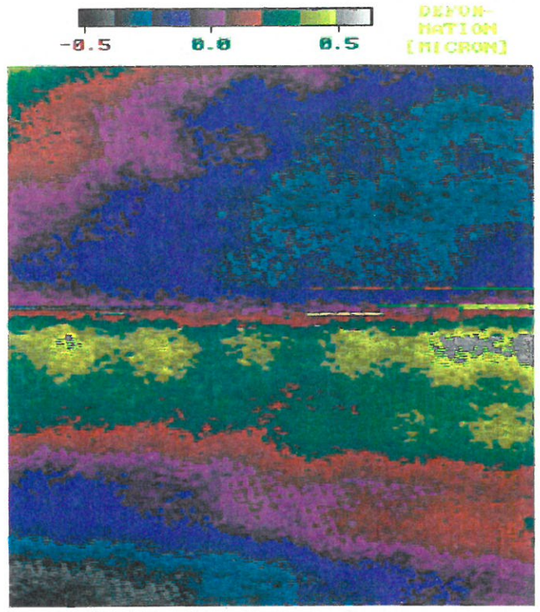

Figure 29. Specklegram (including *440×320* pixels) of sample side s22B recorded for *P=-4.05 N/mm*. "Measurement window": *28.3 mm* (*x*) by *37.7* (*y*) *mm*. The "thin-laminate" part corresponds to the upper half of the image.

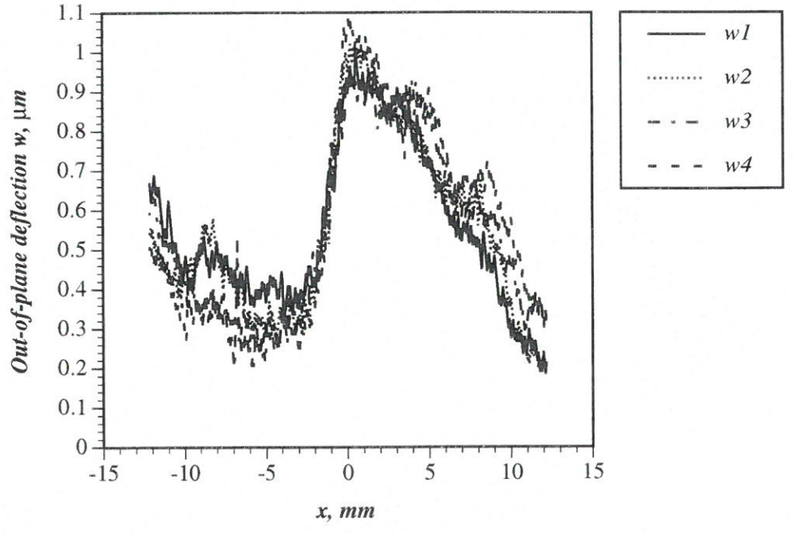

Figure 31. Selected out-of-plane deflection profiles for sample side s22B (*x=0* corresponds to the position of the thickness "drop-off"), where *w1*="*y*-pixel *218*", *w2*="*y*-pixel *248*", *w3*="*y*-pixel *278*" and *w4*="*y*-pixel *308*".

As for the other specklegrams, the information contained in the image only reveals the relative differences between the maximum and minimum out-of-plane deflections. The specklegram is characterised by a very homogeneous deflection pattern in the *y*-direction (see Fig. 3 for reference), which is a consequence of the relatively weak influence of the HC-response for this sample side. As usual, four out-of-plane deflection profiles have been selected from the specklegram; two "peak"- and two "valley"-profiles. Is should be stated, however, that the separation between "peak"- and "valley"-profiles was not very easy due to the homogeneity of the deflection pattern in the *y*-direction. The four selected deflection profiles are displayed in Fig. 31.
Based on the deflection profiles in Fig. 31 an averaged deflection profile was calculated, and this average profile is shown in Fig. 32 together with the "low-pass" filtered and the theoretically predicted deflection profiles.

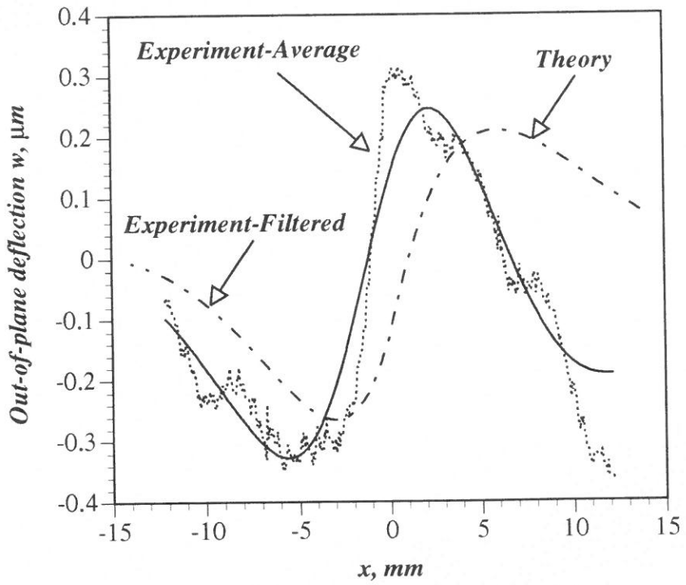

Figure 32. Averaged, "low-pass" filtered and theoretically predicted out-of-plane deflection profiles for sample side s22B. "Off-set" value for averaged and "low-pass" filtered deflection profiles: *-0.650 µm*.

Comparison of the filtered and theoretical profiles in Fig. 32 reveals a very convincing match with respect to signal shapes and wave-lengths (with some phase difference though). With respect to the deflection amplitude it is seen, that the theoretically predicted amplitude is about *14 %* lower than the amplitude of the filtered signal. The derived key-note comparative quantities are as follows:

- Peak distance x_{peak} (filtered profile/theoretical profile): *7.9 mm / 8.7 mm.*
- Phase difference Δx (minimum points/maximum points): *2.7 mm / 3.5 mm.*
- Amplitude |w| (filtered profile/theoretical profile): *0.56 µm / 0.48 µm.*

With respect to the "usual" problems with the filtered deflection profile close to the ends of the sampling interval it is seen, that they are much less pronounced than observed for the other sample sides belonging to the test-specimens of configuration 2. Thus, only slight (if any at all) "problems" can be recognised close to the right end of the sampling interval. The reason why the filtered signal for sample side s22B is of such a high quality is a combination of three circumstances:

- The sampling interval was positioned such that two local extreme points (one "peak" and one "valley") were present (or very closely so) on each side of the thickness "drop-off". This provides the most important information about the "repetition"-sequence of LB-part of the deflection profiles.
- The surface is a "flat" aspect surface.
- The load level at which the specklegram was recorded (i.e., *P=-4.05 N/mm*) is relatively high, and is in fact the highest load level which could be achieved for any of the specimens without causing a complete "break-down" of the image processing (due to excessive global deflections).

Comments for sample sides s22A and s22B:

The results obtained for the sample sides of test-specimen 2-2 have generally demonstrated a good match between the filtered and the theoretically predicted out-of-plane deflection profiles. The good match was especially pronounced for sample side s22B because of its "flat" surface characteristics, but also sample side s22A have provided reasonable comparative results (except for the opposite phases of the theoretical and filtered deflection profiles).
Thus, the signal-shapes, the elastic wave-lengths and the deflection amplitudes were predicted reasonably accurately (the deflection amplitude was "over predicted" by about *30 %* for sample side s22A and "under predicted" by about *14 %* for sample side s22B).

5.5.2.3 Concluding remarks for test-specimens of configuration 2

Summing up the comparative studies of the experimentally and theoretically obtained out-of-plane deflection profiles for the CFRP/honeycomb sandwich test-specimens of configuration 2 (base-line laminate: $[0°_2/90°]_S$; reinforcing laminate: $[\pm 45°]_S$) it has been demonstrated, that the elastic foundation approach (developed and implemented in ref. [1]) is capable of providing a good prediction of the local bending effects encountered in sandwich panels with tapered face-laminates.
The comparative results have generally been better than was seen for the test-specimens of configuration 1 (as expected). This can be attributed to the circumstance, that the face-laminates of configuration 2 possessed bending stiffnesses, which were considerably larger than the face-laminate bending stiffnesses of the test-specimens of configuration 1. The effect of the larger bending stiffnesses being, that the test-specimens were much less sensitive to the HC-response parts in general and the "golf-ball" aspect problems in particular. However, as was seen for the test-specimens belonging to configuration 1, the experimentally obtained deflection profiles obtained for the "flat" aspect surfaces (i.e., the B-sides) generally compared better with the theoretical predictions than the profiles obtained for the "golf-ball" aspect surfaces (i.e., the A-sides), where significant phase differences between the theoretical and filtered out-of-plane deflection profiles were encountered (as they effectively were of opposite phases).
Finally it should be noted, that the problems encountered for configuration 1 with respect to the filtered deflection profiles close to the ends of the sampling intervals, were even more pronounced for configuration 2. This is due to the fact, that the elastic wave-lengths for configuration 2 were about *65-70 %* larger than the elastic wave-lengths for configuration 1, while the size of the ESPI "measurement window" was about the same.

5.5.3 Configuration 3: $[0°_2/90°]_S + [\pm 45°]$

Configuration 3 of the manufactured CFRP/honeycomb sandwich test-specimens represents an intermediate stage compared to configurations 1 and 2. This is to be understood in the way, that it was expected beforehand to be easier to detect the LB-response parts for configuration 3 than for configuration 1 (due to a "thicker"/"stiffer"

base-line laminate), while it was expected to be more difficult than for configuration 2 (due to a "thinner"/"less stiff" reinforcing laminate).
As for the other test-specimen configurations, the specklegrams of highest quality were those recorded at the highest (absolute as well as relative) load levels, and the specklegrams for configuration 3 were recorded under the load conditions specified in Table 11 (see footnote 15 on p. 25 for notation).

Specimen surface	*Reference image recorded at total load: P_{tot}(reference)*	*"Maximum load" image recorded at total load: P_{tot}(maximum)*	*In-plane normal stress resultant corresponding to specklegram: $P=\Delta P_{tot}/(2\times 50\ mm)$*
s31A	*-1340 N*	*-1630 N*	*-2.90 N/mm*
s31B	*-1467 N*	*-1605 N*	*-1.38 N/mm*
s32A	*-1323 N*	*-1602 N*	*-2.79 N/mm*
s32B	*-1324 N*	*-1605 N*	*-2.81 N/mm*

Table 11. Load conditions for recording of specklegrams for ***configuration 3*** CFRP/honeycomb sandwich test-specimens.

5.5.3.1 Specimen 3-1 (sides s31A and s31B)

s31A:

The specklegram recorded for sample side s31A is shown in Fig. 33, where the size of the ESPI "measurement window" is *28.3 mm* (*x*-direction) by *37.3* mm (*y*-direction). The thickness "drop-off" is positioned along a horizontal line across the centre of the image, where the upper part of the plot corresponds to the "thin" face-laminate. Sample side s31A is a "golf-ball" aspect surface (as explained in section 5.1; see Fig. 5), and a deflection pattern with the characteristic doubly-curved local perturbations is clearly recognised. As before, Fig. 33 only provides information about the relative differences between the minimum and maximum deflections.
According to the established procedure, four out-of-plane deflection profiles parallel with the *x*-axis were selected; two "peak" and two "valley"-profiles. These profiles are shown in Fig. 34, from which it is observed, that the HC-parts of the responses are of significant magnitudes. Thus it is difficult, by pure visual inspection, to recognise any distinct LB-response parts in Fig. 34.
From the selected deflection profiles an averaged deflection profile was calculated. The resulting averaged out-of-plane deflection profile is displayed in Fig. 35, which also displays the "low-pass" filtered (averaged) as well as the theoretically predicted out-of-plane deflection profiles. The averaged and filtered deflection profiles shown in Fig. 35 have been attributed an "off-set" value of *-0.385 μm* compared with the deflection profiles shown in Fig. 34. From Fig. 35 it is observed, that the HC-response part of the averaged deflection profile is very significant, but it is possible to identify the contour of the LB-response.

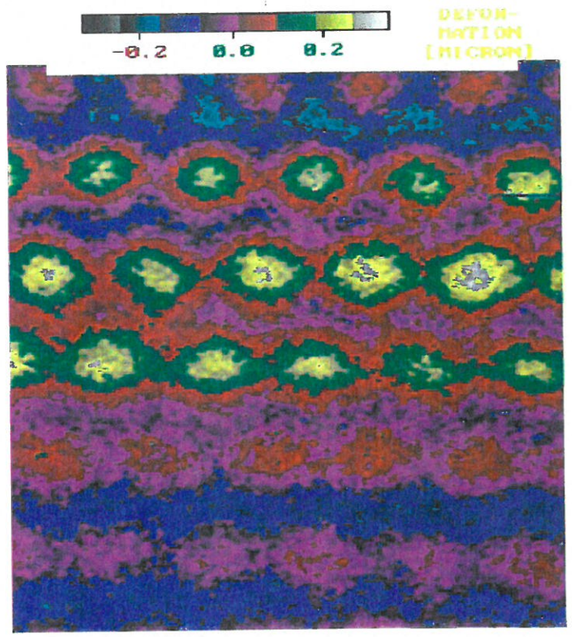

Figure 33. Specklegram (including *440×320* pixels) of sample side s31A recorded for *P=-2.90 N/mm*. "Measurement window": *28.3 mm* (*x*) by *37.7* (*y*) *mm*. The "thin-laminate" part corresponds to the upper half of the image.

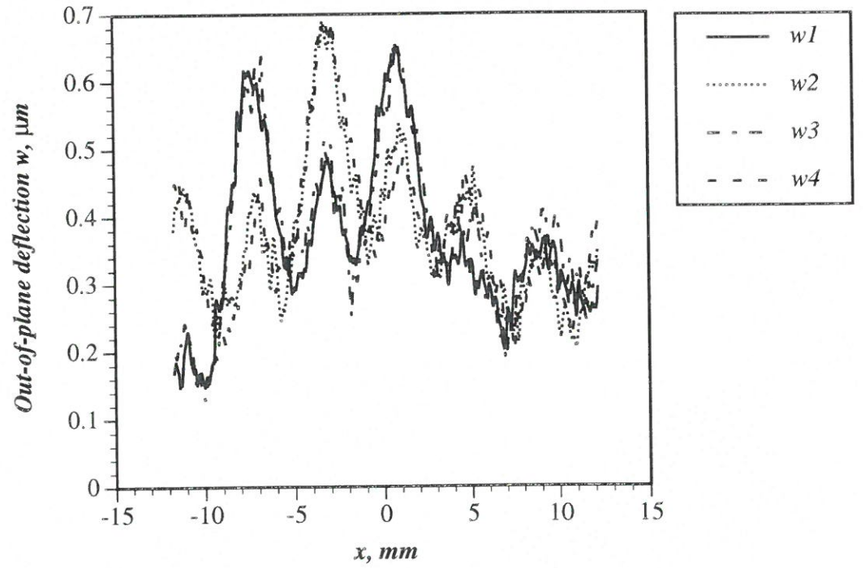

Figure 34. Selected out-of-plane deflection profiles for sample side s31A (*x=0* corresponds to the position of the thickness "drop-off"), where *w1*="*y*-pixel *211*", *w2*="*y*-pixel *242*", *w3*="*y*-pixel *272*" and *w4*="*y*-pixel *304*".

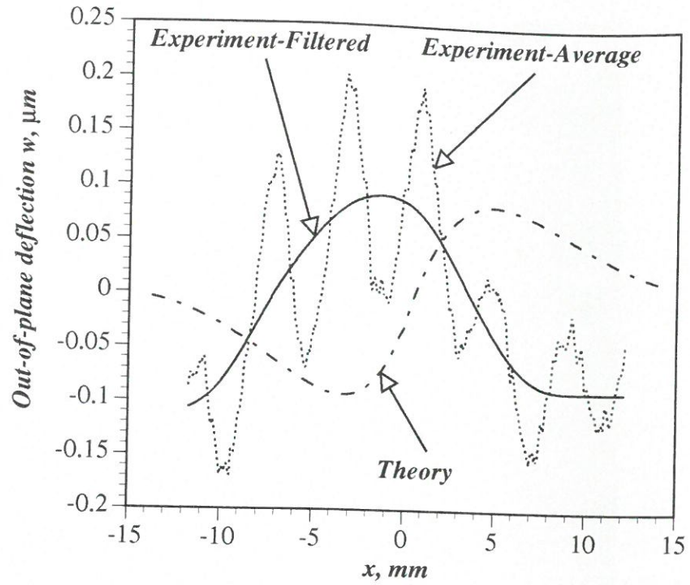

Figure 35. Averaged, "low-pass" filtered and theoretically predicted out-of-plane deflection profiles for sample side s31A. "Off-set" value for averaged and "low-pass" filtered deflection profiles: *-0.385 μm.*

It is further seen from Fig. 35, that the shapes and the amplitudes of the filtered and theoretically predicted deflection profiles resemble each other well in the central part of the sampling interval.
There is however, a significant phase difference between the theoretical and filtered profiles. This phase difference, which was also seen for the other "golf-ball" aspect sample sides, is close to one half elastic wave-length, and the theoretical and filtered signals are effectively of opposite phases. Furthermore it is seen, that the filtered signal displays a somewhat "unrealistic" behaviour close to the ends of the sampling interval (especially at the right end). The primary reason for this is the "well-known" problem with the limited size of the measurement window, which prevents the retrieval of enough sample data to establish the "repetition"-sequence of the signal. Finally there is, as observed often before, some difference between the elastic wave-lengths.
The following comparative key-quantities have been derived from the data contained in Fig. 35:

- Peak distance x_{peak} (filtered profile/theoretical profile): *10.2 mm / 8.2 mm.*
- Phase difference Δx (minimum points/maximum points): *12.2 mm / 6.2 mm.*
- Amplitude |w| (filtered profile/theoretical profile): *0.18 μm / 0.18 μm.*

s31B:

The specklegram recorded for samples side s31B is shown in Fig. 36. The size of the ESPI "measurement window" is *28.3 mm* (*x*-direction) by *37.7 mm* (*y*-direction). The thickness "drop-off" is positioned along a horizontal line across the middle of the image, where the upper part corresponds to the "thin" face-laminate.
Sample side s31B is a "flat" aspect surface (as explained in section 5.1; see Fig. 6), and it is seen to display less HC-influence than was seen in Fig. 33. Fig. 36 only provides information about the relative differences between the "peak"- and "valley"-deflection values.

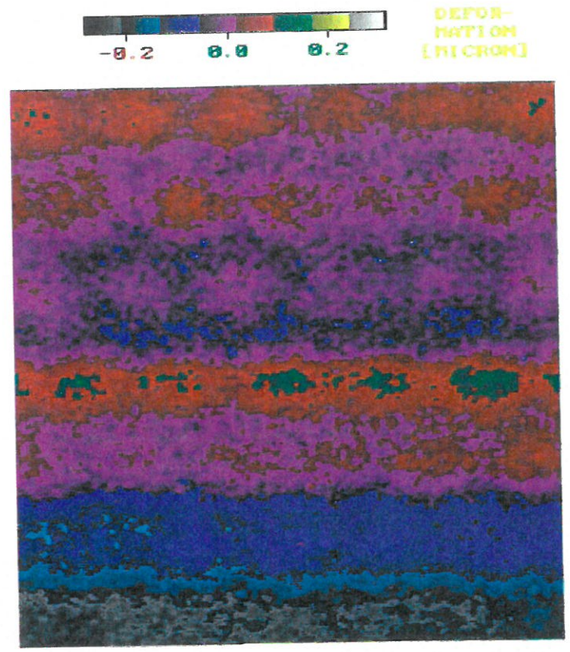

Figure 36. Specklegram (including *440×320* pixels) of sample side s31B recorded for *P=-1.38 N/mm*. "Measurement window": *28.3 mm* (*x*) by *37.7* (*y*) *mm*. The "thin-laminate" part corresponds to the upper half of the image.

Following the usual procedure, four out-of-plane deflection profiles parallel with the *x*-axis were selected; two "peak"- and two "valley"-profiles. These profiles are shown in Fig. 37, from which it is seen, that LB- and HC-response parts are clearly visible. However, compared with Fig. 34 it is seen, that the HC-response parts are less apparent than was the case for sample side s31A (as expected).
The averaged out-of-plane deflection profile (calculated from the profiles displayed in Fig. 37) is shown in Fig. 38, which also displays the "low-pass" filtered (averaged) as well as the theoretically predicted out-of-plane deflection profiles. In Fig. 38, the averaged and filtered profiles have been attributed an "off-set" deflection of *-0.25 μm* compared with Fig. 37.
Considering at first the averaged deflection profile it is seen, that the influence of the HC-response (even though less significant than in Fig. 35) is very pronounced. Thus, the significant "peaks" and "valleys" of the HC-response makes it difficult to recognise the shape of the LB-response part (or rather the "expected" shape).
Considering next the filtered signal it is observed, that the shape as a whole is not very similar to the shape of theoretical deflection profile (may be except for the central part of the sampling interval). The deviations at the ends of the sampling interval are considerable, and even though part of the reason for this is the ESPI "measurement window" size problem (to little information about the signal "repetition"-sequence), this is not sufficient to account for the observed dissimilarities. The behaviour of the filtered signal at especially the right end of the sampling interval is therefore believed to be "essentially" correct, and at least part of the observed differences between the filtered and the theoretical signals must be considered as being "true" for sample side s31B.

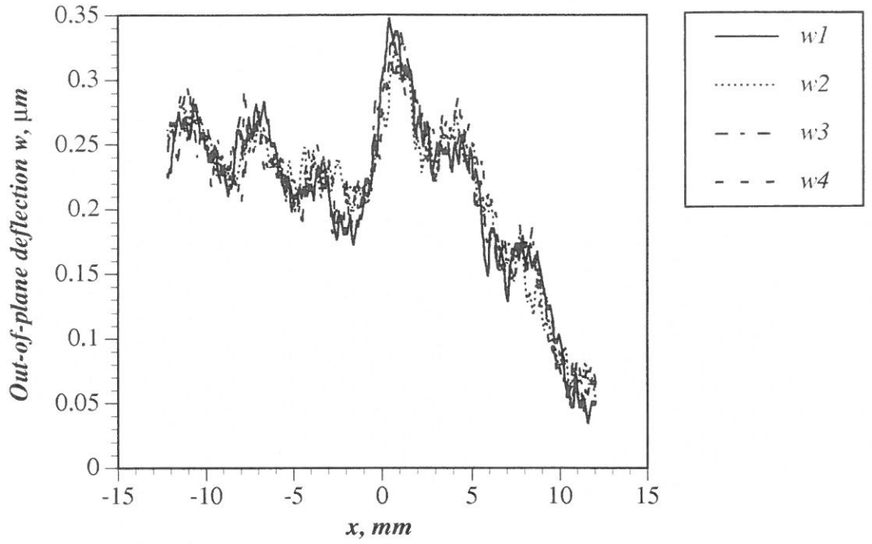

Figure 37. Selected out-of-plane deflection profiles for sample side s31B (*x=0* corresponds to the position of the thickness "drop-off"), where *w1*="*y*-pixel *253*", *w2*="*y*-pixel *282*", *w3*="*y*-pixel *313*" and *w4*="*y*-pixel *341*".

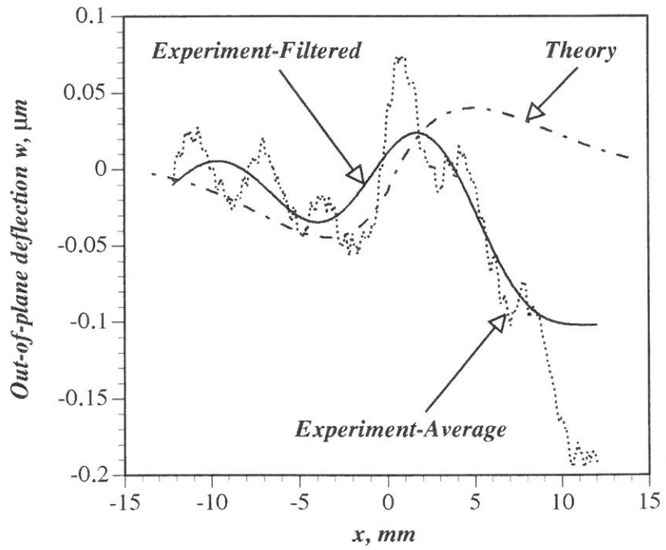

Figure 38. Averaged, "low-pass" filtered and theoretically predicted out-of-plane deflection profiles for sample side s31B. "Off-set" value for averaged and "low-pass" filtered deflection profiles: *-0.250 µm*.

The possible explanations for the observed deviations are difficult to identify precisely, but it is considered likely that the following three effects constitute the main contributions:

- The surface of sample side s31B was characterised by the irregularity displayed in Fig. 7, and this effect caused a slightly more "curvy" LB-response than expected. This effect, by the way, is also likely to have influenced the other B-side responses recorded in this investigation.
- It is likely, that parts of "global" deflections were not been removed completely through the subtraction of the "best-fit" compensating plane in the digital image processing of the recorded specklegram.
- The specklegram was recorded at a rather low load level (*P=-1.38 N/mm*), thus causing the HC-response to be relatively more dominant than for most of the other B-side specimens (this non-linear effect will be discussed later).

Concentrating the comparative efforts on the central parts of the filtered and theoretical signals (and realising that this cannot eliminate the poor overall results of the comparison), the following comparative key-quantities have been derived from the data contained in Fig. 38:

- Peak distance x_{peak} (filtered profile/theoretical profile): *6.1 mm / 8.2 mm.*
- Phase difference Δx (minimum points/maximum points): *1.0 mm / 3.1 mm.*
- Amplitude |*w*| (filtered profile/theoretical profile): *0.06 µm / 0.09 µm.*

Comments for sample sides s31A and s31B:

In general terms, the results obtained for the sample sides of test-specimen 3-1 have not been overly convincing. This observation was true for both sample sides, but the comparative results were especially disappointing for sample side s31B (the possible reasons for this were discussed above), where not even the overall deflection profile shape compared very well. With this made clear, however, it should be noted, that the overall signal shapes, the signal amplitudes and the elastic wave-lengths results for sample side s31A were reasonably good. Thus, the only significant deviation between theory and experiment for sample side s31A was the "phase difference" problem associated with all the "golf-ball" aspect sample sides.

5.5.3.2 Specimen 3-2 (sides s32A and s32B)

s32A:

The specklegram recorded for sample side s32A is displayed in Fig. 39, where the size of the ESPI "measurement window" is *28.3 mm* (*x*-direction) by *37.7 mm* (*y*-direction). The thickness "drop-off" is positioned along a horizontal line across the centre of the image, where the upper part of the plot corresponds to the "thin" face-laminate. Sample side s32A is a "golf-ball" aspect surface (as explained in section 5.1; see Fig. 5), as is clearly indicated by the doubly-curved local perturbations seen in the image. Fig. 39 only provides information about the relative differences between the minimum and maximum deflections.
As usual, four out-of-plane deflection profiles parallel with the *x*-axis were selected; two "peak"- and two "valley"-profiles. The selected profiles are shown in Fig. 40, from which it is observed, that the HC-response parts are of significant magnitude. From the selected deflection profiles an averaged deflection profile was calculated. The resulting averaged out-of-plane deflection profile is displayed in Fig. 41, which also displays the "low-pass" filtered (averaged) as well as the theoretically predicted out-of-plane deflection profiles. The averaged and filtered deflection profiles shown in Fig. 41 have been attributed an "off-set" value of *-0.38 µm* compared with the deflection profiles shown in Fig. 40. From Fig. 41 it is observed, that the HC-response part of the averaged deflection profile is very significant (induced by the "golf-ball" aspect problem), and it is quite difficult to identify the LB-response.

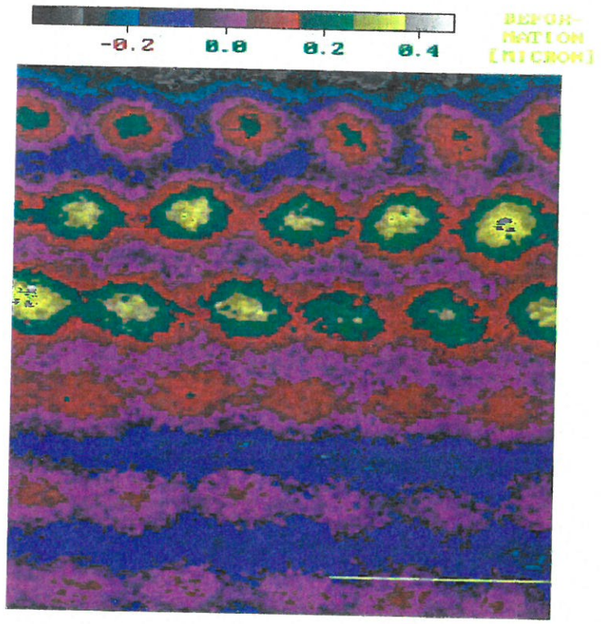

Figure 39. Specklegram (including *440×320* pixels) of sample side s32A recorded for *P=-2.79 N/mm*. "Measurement window": *28.3 mm* (*x*) by *37.7* (*y*) *mm*. The "thin-laminate" part corresponds to the upper half of the image.

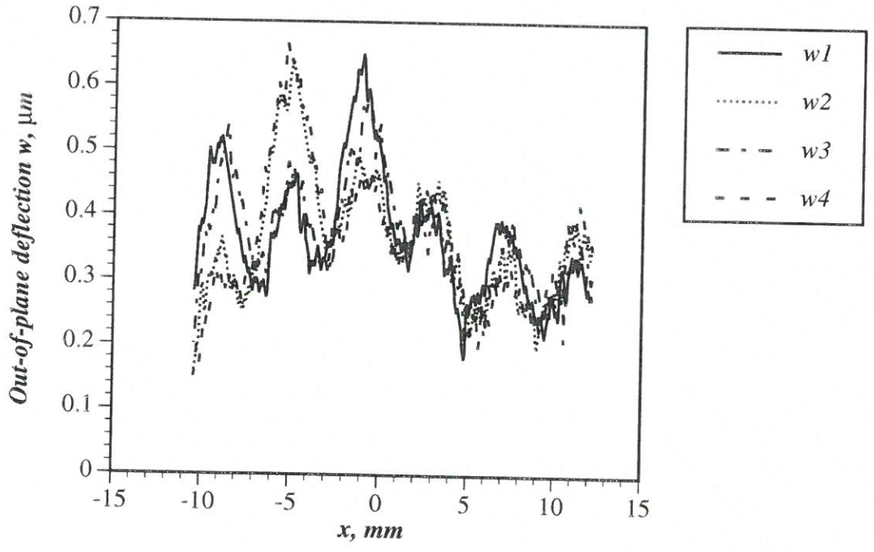

Figure 40. Selected out-of-plane deflection profiles for sample side s32A (*x=0* corresponds to the position of the thickness "drop-off"), where *w1*="*y*-pixel *234*", *w2*="*y*-pixel *265*", *w3*="*y*-pixel *296*" and *w4*="*y*-pixel *324*".

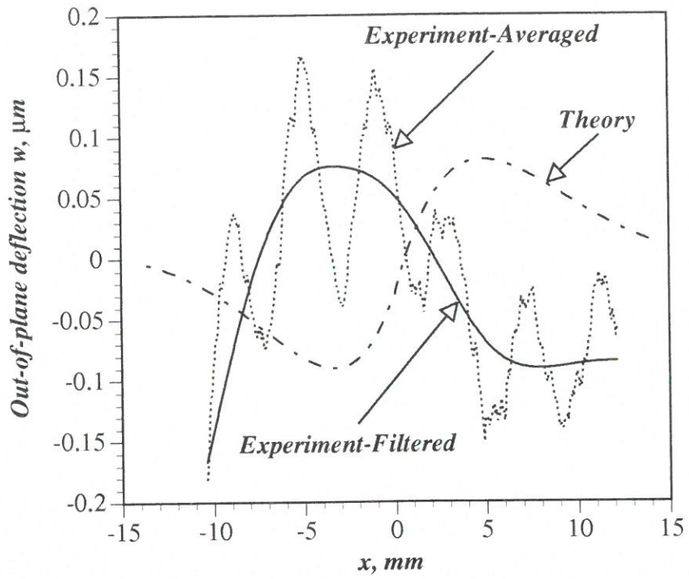

Figure 41. Averaged, "low-pass" filtered and theoretically predicted out-of-plane deflection profiles for sample side s32A. "Off-set" value for averaged and "low-pass" filtered deflection profiles: *-0.38 µm*.

Comparison of the filtered and theoretically predicted out-of-plane deflection profiles reveals a good match with respect to "shape" in the central part of the sampling interval. Close to the ends of the sampling interval (especially at the left end) it is observed that the filtered signal displays an "unrealistic" behaviour. The primary reason for this is believed to be the earlier discussed problems with the limited size of the ESPI "measurement window", which effectively prevented the filtering algorithm in providing reasonable results at the ends of the sampling interval. This belief is substantiated by the appearance of the filtered signal at the left end of the sampling interval, where a very steep "dive" of the deflection curve is observed. The obvious reason for the "dive" is, that the data sampling sequence was cut off at a point of steep decrease of the both the LB- and the HC-part of the averaged signal, thus providing the filtering algorithm with insufficient information pertaining to the "true" pattern of the averaged signal.
Furthermore, as for all the other A-sides, a considerable phase difference between the theoretical and the filtered deflection profiles is observed. Thus, the theoretical and filtered profiles are almost of opposite phases.
By disregarding the "problem areas" close to the ends of the sampling interval, the following key-quantities have been computed on the basis of the filtered and the theoretical signals shown in Fig. 41:

- Peak distance x_{peak} (filtered profile/theoretical profile): *11.0 mm / 8.2 mm.*
- Phase difference Δx (minimum points/maximum points): *11.0 mm / 8.2 mm.*
- Amplitude |*w*| (filtered profile/theoretical profile): *0.16 µm / 0.17 µm.*

From the quoted key-quantities it is seen, that the match between the amplitudes is excellent and that the match between the elastic wave-lengths is reasonably good.

s32B:

The final specklegram to be included in this report is shown in Fig. 42. The specklegram was recorded for sample side s32B, with an ESPI "measurement window" size of *28.3 mm* (*x*-direction) by *37.7 mm* (*y*-direction). The thickness "drop-off" is positioned along a horizontal line across the middle of the image, where the upper part corresponds to the "thin" face-laminate. Sample side s32B is a "flat" aspect surface (see Fig. 6), and the HC-parts of the response are seen to be less dominating than for sample side s32A (see Fig. 39). Fig. 42 only provides information about the relative differences between the "peak"- and "valley"-deflection values.

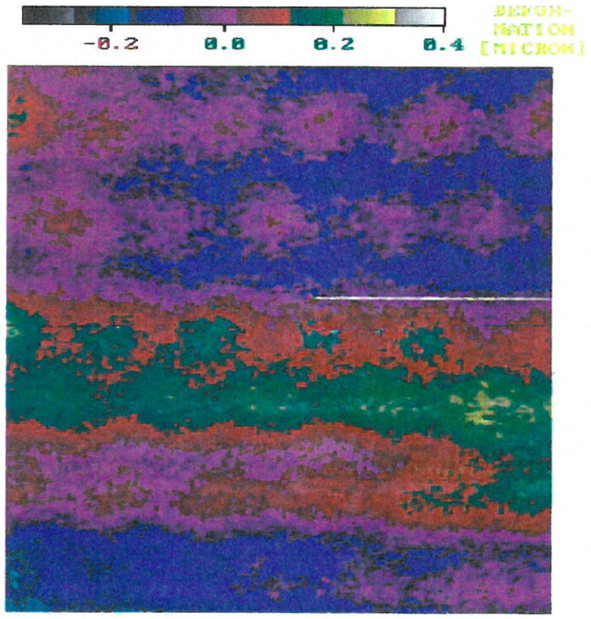

Figure 42. Specklegram (including *440×320* pixels) of sample side s32B recorded for *P=-2.81 N/mm*. "Measurement window": *28.3 mm* (*x*) by *37.7* (*y*) *mm*. The "thin-laminate" part corresponds to the upper half of the image.

From the data contained in Fig. 42, four out-of-plane deflection profiles were selected according to the usual procedure, i.e., two profiles representing minimum points and two representing maximum points. The four deflection profiles are shown in Fig. 43 from which it is recognised, that the difference between the signals is small, i.e., the variation in the specimen *y*-direction is insignificant (also seen from the specklegram).
The averaged deflection profile (calculated from the four deflection profiles shown in Fig. 43) is displayed in Fig. 44 together with the "low-pass" filtered (averaged) and the theoretically predicted out-of-plane deflection profiles. The averaged and the filtered deflection profiles have been attributed an "off-set" value of *-0.40 μm* compared with the deflection profiles shown in Fig. 43.
From Fig. 44 it is seen, that the match between the filtered and the theoretical signals is more favourable than was seen in Fig. 41 for sample side s32A. This is no surprise (as sample side s31A was characterised by the "golf-ball" aspect surface), and the improved comparative results can be attributed (mainly) to the better surface quality of sample side s32B as compared to sample side s32A. The fine match between the filtered and the theoretical deflection profiles for sample side s32B is seen for the overall profile shapes,

the deflection amplitudes and the wave-lengths. Furthermore, only a relatively small phase difference between the theoretical and filtered profiles is seen to be present.

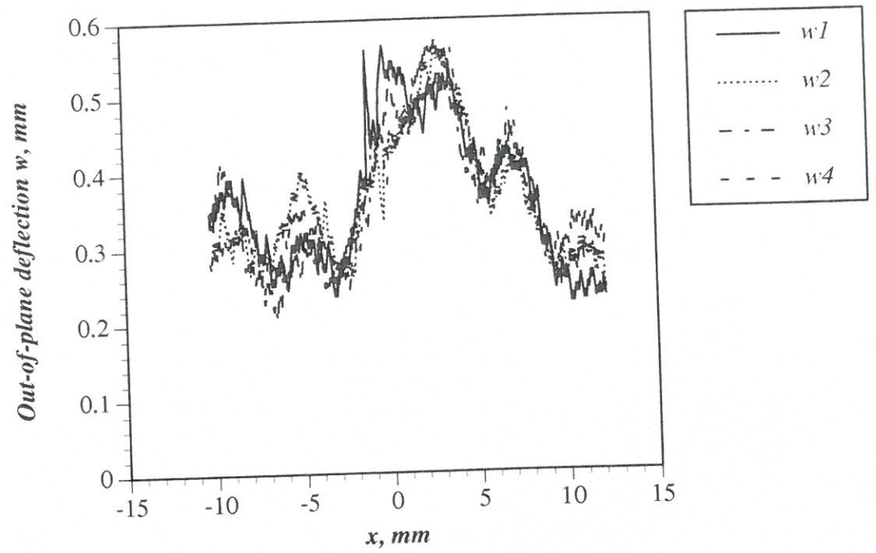

Figure 43. Selected out-of-plane deflection profiles for sample side s32B (*x=0* corresponds to the position of the thickness "drop-off"), where *w1*="*y*-pixel *216*", *w2*="*y*-pixel *248*", *w3*="*y*-pixel *279*" and *w4*="*y*-pixel *313*".

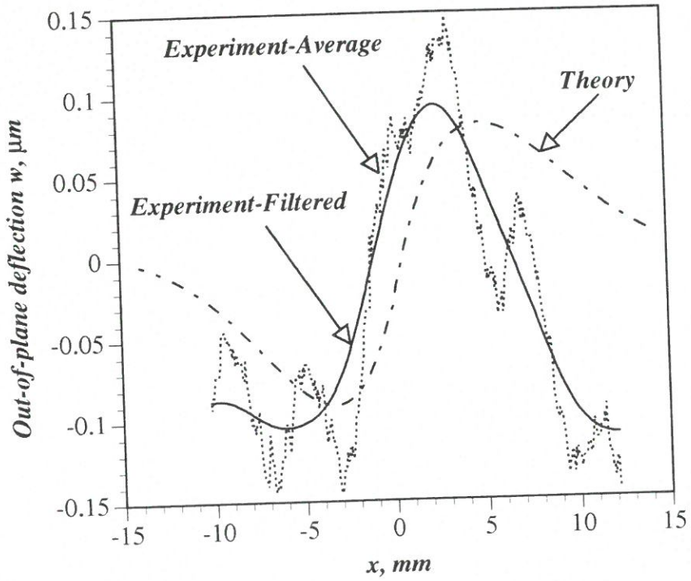

Figure 44. Averaged, "low-pass" filtered and theoretically predicted out-of-plane deflection profiles for sample side s32B. "Off-set" value for averaged and "low-pass" filtered deflection profiles: *-0.40 μm*.

Despite the convincing overall match between the filtered and the theoretical deflection profiles, the "well-known" mismatch problem close to the ends of the sampling interval (ESPI "measurement window" size problem) is seen to be present in Fig. 44. Thus, considerable deviations between the filtered and theoretical deflection amplitudes are seen close to the right end of the sampling interval (the filtered signal "dives" much more than the theoretical signal).
Discarding the filtered signal close to the ends of the sampling interval, and basing the comparison on the central parts of the deflection profiles, the following key-figures have been derived from the data in Fig. 44:

- Peak distance x_{peak} (filtered profile/theoretical profile): *8.2 mm / 8.2 mm.*
- Phase difference Δx (minimum points/maximum points): *2.7 mm / 2.7 mm.*
- Amplitude $|w|$ (filtered profile/theoretical profile): *0.20 μm / 0.17 μm.*

Comments for sample sides s32A and s32B:

The results obtained for the sample sides of test-specimen 3-2 have generally demonstrated a reasonably good correlation between the filtered and the theoretically predicted out-of-plane deflection profiles. The correlation was especially convincing for sample side s32B because of its "flat" aspect surface characteristics, but also sample side s32A has provided comparative results of reasonably quality (especially when the "phase difference" and ESPI "measurement window" problems were taken into account).
Thus, the deflection profile shapes, the elastic wave-lengths and the deflection amplitudes were predicted rather accurately by use of the analysis method presented in ref. [1]. For sample side s32A a significant phase difference between the predicted and the filtered deflection profiles was detected (effectively of opposite phases).

5.5.3.3 Concluding remarks for test-specimens of configuration 3

Summing up the primary findings, pertaining to the comparison between the theoretically and the experimentally obtained out-of-plane deflection profiles for the CFRP/honeycomb sandwich test-specimens of configuration 3 (base-line laminate: $[0°_2/90°]_S$; reinforcing laminate: $[\pm 45°]$), it has been demonstrated, that the elastic foundation approach (ref. [1]) provides a reasonably good estimate of the local bending effects induced around face-laminate thickness "drop-off's".
The results obtained for the sample sides of test-specimen 3-2 demonstrated a better correlation with the theoretical predictions than was the case for the sample sides of test-specimen 3-1, where especially the results obtained for sample side s31B were "disappointing". The primary reason for this is believed to be the considerably lower load at which, the specklegram of sample side s31B was recorded, compared with the load levels used in the investigation of the other sample sides of configuration 3[19]. The low load level effectively caused the LB-response to be "drowned" in the HC-response for s31B.
Apart from the problems associated with the low load level used for the investigation of sample side s31B, the results obtained for the other sample sides have shown a good correlation between the filtered and the theoretically predicted out-of-plane deflection profiles. The comparative results obtained for sample side s32B ("flat" aspect surface) were especially good, whereas the results obtained for sample sides s31A and s32A ("golf-ball" aspect surfaces) were of poorer quality ("phase difference" problem). For all the measured deflection profiles, however, the ESPI "measurement window" size problem described earlier caused the filtered signals to behave "unreliably" close to the ends of the sampling intervals.

19 About half the magnitude of the loads applied in the recording of the specklegrams for sample sides s31A, s32A and s32B; see Table 11, p. 48.

6.0 DISCUSSION OF RESULTS

This chapter will present a summary of the main findings of the investigation (contents of chapter 5), and the most important features of the measured as opposed to the theoretically predicted out-of-plane deflection profiles will be discussed. The chapter will be concluded with a brief discussion of possible future experimental investigations of ply "drop-off" effects in CFRP/honeycomb sandwich panels based on the experience gained from the present investigation (i.e., "lessons learned").

6.1 Non-linear effects

The presence of non-linear effects has been discussed sporadically in the presentation of the results in sections 5.5.1 to 5.5.3. The observed non-linear effects have been associated with the part of the bending response induced by the discrete support supplied by the honeycomb core cells (i.e., the HC-response), where the non-linear nature of this response part was revealed by two features (where only the first has been commented on before):

- The appearance of the deflection profiles (specklegrams) was (highly) dependent of the "off-set" compressive load applied to the test-specimens.
- In some of the specklegrams, the doubly-curved local perturbations caused by the honeycomb cells ("golf-ball" deflection pattern) were seen to be more dominant in the reinforced part of the face-laminates than in the not reinforced laminate parts (i.e., in the "thin" or base-line laminates).

Discussing the former effect first, it should be recalled from the description of the experimental procedure (section 4.3), that specklegrams were recorded at a number of different "off-set" load levels. Thus, a reference image was recorded at a certain absolute compressive load level (referred to as the "off-set" load), say P_1, the load was increased to a level P_2, and a new image was captured. From the images recorded at the two load levels P_1 and P_2 a phase image was computed, and from this phase image the out-of-plane deflections corresponding to the compressive load $P=P_2-P_1$ were computed. This procedure was repeated four times in average for each sample side (i.e., for four different "off-set" loads P_1). Provided the relative compressive loads (i.e., P) were the same for all the recordings (i.e., that P_2-P_1=constant), the out-of-plane deflections obtained for each "off-set" load value P_1 should be the same in the ideal world of linear mechanics. This, however, was not the case, as the magnitudes of the HC-response parts were seen to be dependent of the "off-set" load P_1 (especially for the "golf-ball" aspect sample sides). The influence of the HC-response parts generally decreased with increasing "off-set" load level, and for this reason the specklegrams included in this report represents the interferometric information recorded at the highest "off-set" loads. Unfortunately it was not possible to use even higher "off-set" load levels, as this caused the inducement of an excessive amount of fringes (extensive global and local deformations) and thereby making it impossible to process/analyse the images.

Pertaining to the second non-linear effect mentioned, the phenomenon was encountered exclusively for five of the "flat" aspect surface sample sides; s11B, s12B, s22B, s31B and s32B. The phenomenon is probably most clearly seen in Fig. 17, which displays the specklegram recorded for sample side s12B (load: *P=-1.44 N/mm*). The upper half of the image displayed in Fig. 17 corresponds to the reinforced laminate part (thick laminate), and it is seen, that the honeycomb cells are most "visible" in the reinforced laminate areas (i.e., just above the middle of the specklegram). This observation is rather surprising, as it should have been expected, that the HC-response part would be seen more clearly in the regions of the "thin" face-laminates. What appears to be the most reasonable explanation for the phenomena is presented in the following.

Initially (i.e., no loading), the face-laminates were indented slightly into the honeycomb cells (even for the "flat" aspect sample sides) which caused the face-sheets to appear as "shallow shells" locally (prestressed in bending). Upon application of the overall compressive load (i.e., P), different mechanisms were activated in the "thin" and "reinforced" laminate areas, respectively.
In the "thin" laminate area the overall pattern was that of negative out-of-plane deflections (i.e., indentation into the core), which caused the "cell indentations" to increase. However, due to the initial indentation (i.e., the "shallow shell" characteristics) of the face-laminates within the cell boundaries, the response of the face-laminate was effectively moved into the geometrically non-linear range (i.e., "stiffening"), and the induced deflections were comparatively smaller than could be expected.
In the area of the reinforced laminate the overall pattern upon application of the compressive load was that of positive out-of-plane deflections (i.e., outwards), thus tending to counteract the initial "cell indentations". This forced the face-laminates to "straighten out" within the cell boundaries. Thus, the "shallow shell" characteristics of the laminates within the cell boundaries were forced back into (or close to) "flat" plate characteristics, which again moved the elastic response back into the geometrically linear range (i.e., "softening").
The overall result was, that the out-of-plane deflections encountered within the honeycomb cell boundaries were larger in the reinforced laminate region than in the "thin" laminate region despite of the lower face-laminate bending stiffnesses in the latter region. This effect again caused the HC-response parts to appear to be more dominant in the reinforced laminate regions than in the "thin" laminate regions.
The reason why the above mentioned non-linear effect was observed exclusively for the "flat" aspect surfaces is not known precisely, but it seems likely to be connected with the fact, that the HC-response parts were excessively dominating for the "golf-ball" aspect sample sides (effectively "drowning" all the other response parts).

6.2 Elastic foundation moduli K_x, K_z: linear or exponential decay ?

As was discussed in sections 3.2 and 5.3, the successful application of the elastic foundation approach presented in ref. [1] is highly dependent of the adopted assumptions pertaining to the decay of the local bending effects through the thickness of the core material. Two different decay functions were treated in section 3.2, a simple "linear decay" assumption, and a more complicated "exponential decay" assumption (the corresponding expressions for K_x, K_z were given in eqs. (7) and (9)). In ref. [1] the latter approach was adopted, together with a "characteristic decay length" $\alpha=0.5\ mm$ (the "characteristic decay length" α is an inherent quantity), where the resulting expressions for K_x, K_z were given in eqs. (10).
As described in section 5.3 it was clear, after the analysis of some preliminary results of the experimental investigation, that the expressions used for the elastic foundation moduli K_x, K_z in ref. [1] were over-predicting the stiffness of the honeycomb core material (foundation). The actual shape and general characteristics of the measured deflection profiles, however, complied well with the predictions (especially for the "flat" aspect sample sides). Thus, the apparent (preliminary) mismatch between the experimental and theoretical results was attributed to the choice of expressions for K_x, K_z.
As was discussed in section 3.2 (see also ref. [4]), the general advice pertaining to the choice of "decay function" (i.e., linear or exponential) is, that the exponential decay approach is superior to the linear decay approach. The exponential decay approach, however, suffers the drawback, that the "characteristic decay length" should be specified "a priori". For the present case it is considered likely, that the choice of "characteristic decay length" α could be adjusted such, that the theoretical and experimental results

would match each other better[20]. However, as the amount of experimental data was limited and associated with considerable scatter, it was decided to use the expressions for K_x, K_z derived by assuming a linear decay function (i.e., eqs. (7)).

Test-specimen/Sample side	*Deflection amplitude difference (absolute value):* $\Delta\|w\|=\|w\|_{theory}-\|w\|_{experiment}$	*Deflection amplitude difference in %* $(\Delta\|w\|/\|w\|_{experiment})$
s11A	*0.20 μm*	*181.8 %*
s11B	*0.08 μm*	*26.7 %*
s12A	*0.10 μm*	*142.9 %*
s12B	*0.02 μm*	*9.1 %*
s21A	*0.08 μm*	*61.5 %*
s21B	*-0.04 μm*	*-15.4 %*
s22A	*0.11 μm*	*30.4 %*
s22B	*-0.08 μm*	*-14.3 %*
s31A	*0.00 μm*	*0.0 %*
s31B	*0.03 μm*	*50.0 %*
s32A	*0.01 μm*	*6.3 %*
s32B	*-0.03 μm*	*-15.0 %*

Table 12. Differences between experimental (filtered) and theoretically predicted deflection amplitudes (summary of results from sections 5.5.1 to 5.5.3).

As was seen from the comparative results presented in section 5.5 (specklegrams and out-of-plane deflection profiles for the twelve sample sides), it was generally found that

---

20 A relation expressing the "characteristic decay length" α should probably be related to the geometrical quantities c (core thickness), t_1 (thickness of base-line laminate), t_2 (thickness of reinforcing laminate) and possibly also the cell size S_c.

the predicted (based on the linear decay function) and the experimental deflection profiles (filtered) matched each other rather well. The results, however, were associated with considerable scatter, as it was very difficult (impossible) to eliminate the influence of all the error sources[21] from the experimentally obtained out-of-plane deflection profiles.
Based on the results obtained it is very difficult to justify any further adjustments of the expressions for K_X, K_Z. This conclusion is drawn from the observed discrepancies between theory and experiment, where especially the difference between the predicted and the measured deflection amplitudes provides a convenient measure for the "match"/"mismatch". Table 12 shows the differences between the measured and the predicted deflection amplitudes (i.e., $\Delta|w| = |w|_{theory} - |w|_{experiment}$; with $|w|$ defined from eq. (14)).
From the figures included in Table 12 it is seen, that the encountered deviations are most apparent for the sample sides belonging to test-specimen configuration 1, as well as for the sample sides with "golf-ball" aspect surfaces (A-sides). It is further seen, that the differences between the theoretically and experimentally obtained deflection amplitudes are less than or equal to *30 %* for eight sample sides and less than or equal to *15 %* for six sample sides, where the latter results are considered to be very good in the present context.
Focusing the attention to the eight sample sides where the differences between the theoretical predictions and the experimental results were less than or equal to *30 %* (i.e., s11B, s12B, s21B, s22A, s22B, s31A, s32A and s32B) it is seen, that the theory over-predicts the deflection amplitudes for four of the sample sides (s11B, s12B, s22A and s32A), that the theory under-predicts the deflection amplitudes for three sample sides (s21B, s22B and s32B) and, finally, that theory and experiment match each other exactly (at least within the two decimal digits displayed in Table 12) for one sample side (s31A).
From the above observations it is clear, that it will be very difficult to suggest any adjustments to the theory. Thus, it is impossible on the basis of the figures displayed in Table 12 to specify whether the theory generally over-predicts or under-predicts the deflection amplitudes, or in other words whether the magnitudes of the elastic foundation moduli are predicted to be to small (i.e., core to flexible) or to large (i.e., core to stiff).
Based on the results obtained it seems, that the expressions chosen for K_X and K_Z are in fact very close to being "optimal" in the present context. Thus it is concluded, that the choice of the expressions for K_X and K_Z, which are based on the linear decay assumption (eqs. (6) and (7)) have proven to be justified.

6.3 Summary and discussion of experimental results

In the previous section the issue of the appropriate choice of elastic foundation moduli was discussed, and the differences between the experimentally obtained (filtered) and theoretically predicted deflection amplitudes $|w|$ (as defined by eq. (14)) were used for the evaluation. The deflection amplitudes, however, are not the only quantities of importance in determining the match between the experimentally and theoretically obtained deflection profiles. Thus, features/quantities such as overall shapes, wave-lengths of elastic response (evaluated through the deflection "peak distance" x_{peak} as defined by eq. (12)) and phase difference (Δx as defined by eq. (13)) between the filtered and theoretical deflection profiles were also used for the comparisons presented in sections 5.5.1 to 5.5.3.
Thus, for the sake of "completeness", Table 13 summarises the results derived in sections 5.5.1 to 5.5.3 pertaining to the differences between the measured and the

[21] Among the most important "disturbances"/"error sources" were: "global" deformations of the test-specimens in the test-rig (eliminated by digital image analysis), the "golf-ball" aspect surface problem (caused by co-curing), difficulties with separation of the LB- and HC-response parts at low load levels (primarily a problem for configuration 1), possible distortions caused by the filtering of the averaged deflection profiles (filtering algorithm), and finally the limited size of the ESPI "measurement window" (especially a problem for configurations 2 and 3).

predicted deflection "peak distances" x_{peak} (see eq. (12)) as well as the average phase difference Δx_{avg} (see eq. (13) and Table 13 for exact definition of Δx_{avg}) encountered between the measured and the theoretical deflection profiles.

Test-specimen/Sample side	$[\{x_{peak}\}_{theory} - \{x_{peak}\}_{experiment}]/\{x_{peak}\}_{experiment}$	*Average phase difference:* $\Delta x_{avg} = \{\Delta x(\text{"min. points"}) + \Delta x(\text{"max. points"})\}/2$
s11A	*-9.8 %*	*6.0 mm*
s11B	*-14.1 %*	*3.1 mm*
s12A	*-26.7 %*	*6.5 mm*
s12B	*0.0 %*	*0.0 mm*
s21A	*6.1 %*	*8.5 mm*
s21B	*14.5 %*	*2.8 mm*
s22A	*2.4 %*	*8.6 mm*
s22B	*10.1 %*	*3.1 mm*
s31A	*-19.6 %*	*9.2 mm*
s31B	*34.4 %*	*2.1 mm*
s32A	*-25.5 %*	*9.1 mm*
s32B	*0.0 %*	*0.0 mm*

Table 13. Differences between the experimental (filtered) and theoretically predicted deflection "peak" distances x_{peak} as well as the observed "average" phase differences Δx_{avg} (summary of results from sections 5.5.1 to 5.5.3).

From Table 13 is seen, that the observed differences between the experimental and theoretically predicted elastic wave-lengths (measured in terms of the deflection "peak distance" x_{peak}, eq. (12)) are associated with considerable scatter. However, for most of the sample sides the difference between experiment and theory is less than *15 %* (relative to the experimentally obtained values for x_{peak}). Pertaining to the distribution of the

theoretical predictions relative to the experimental values of x_{peak} is is seen, that five $\{x_{peak}\}_{theory}$-values are smaller than the $\{x_{peak}\}_{experiment}$-values, that five $\{x_{peak}\}_{theory}$-values are larger than the $\{x_{peak}\}_{experiment}$-values, and finally that two $\{x_{peak}\}_{theory}$-values are equal to the corresponding $\{x_{peak}\}_{experiment}$-values (within one decimal digit). Thus the overall conclusion is, that the elastic foundation approach (ref. [1]) is capable of providing rather accurate predictions of the elastic wave-lengths (or rather the deflection "peak distance" x_{peak}).
The second quantity displayed in Table 13, i.e., the average phase difference (denoted by Δx_{avg}), is always positive or zero due to the way Δx was defined (see eq. (13)). It is seen, that the results obtained for the "golf-ball" aspect and the "flat" aspect sample sides differ considerably from each other, as Δx_{avg} is generally much smaller for the "flat" aspect surfaces (i.e., the A-sides). Thus it is observed, that the phase differences between the theoretical and measured deflection profiles encountered for all the "golf-ball" aspect sample sides were in the order of about one half elastic wave-length, which effectively means, that the theoretical and filtered signals were of opposite phases. The reason for this systematic "displacement" of the measured deflection profiles is not known, but as this "opposite phase" problem was seen exclusively for the "golf-ball" aspect sample sides, it seems safe to conclude, that it is a consequence of the highly disturbed surface characteristics induced by the co-curing of the test-specimens.
It is further observed from the left column of Table 13, that small (as compared with the "golf-ball" aspect surface results) phase differences were also encountered for the "flat" aspect surfaces (i.e., the B-sides). The exact reasons for the occurrence of the observed phase differences for the B-sides are not known either, but they are believed to be the result of several contributing factors:

- The definition of the position of the ply "drop-off's" in the specklegrams was associated with some uncertainty. The "drop-off" positions were determined by placing a white sheet of paper at the "drop-off" edges and then establishing the "intensity thresholds" with the image processing system; ref. [9]. The accuracy is estimated to be about *±2* pixels, which effectively means, that the "drop-off" positions were determined with an accuracy of about *±0.10-0.12 mm*.
- The B-sides (i.e., the "flat" aspect surfaces for which the least significant phase differences were generally seen) were all displaying the characteristic "irregularity" shown in Fig. 7 (to a smaller or larger extent). Thus, the base-line laminates were slightly curved adjacent to the ply "drop-off's". The effect of this geometrical irregularity on the elastic responses was, that the deflection amplitudes were decreased slightly ("load path eccentricity" reduced, thus inducing less severe local bending moments) and that the deflection profiles were displaced slightly towards the "thin" laminate-part (i.e., direction of negative x).
- The experimental deflection profiles used for the direct comparisons were derived from the averaged deflection profiles using a digital filter (a "third order Butterworth filter"). Even though the performance of the filter was checked by filtering the theoretical deflection profiles, and no distortions (signal shape, amplitude, wave-length and phase difference) were seen, it cannot be ruled out, that the filtering did cause "distortions" of the LB-response parts of the measured profiles. The likelihood of this is enhanced by the circumstance, that the ESPI "measurement windows" were to small to allow the measurement of a complete wave-length on each side of the ply "drop-off's".

Based on the comparative features presented in sections 5.5.1 to 5.5.3, as well as the discussion presented in this chapter (based on Tables 12 and 13), a complete overview of the comparative results has been prepared. This overview was prepared by evaluating the following four comparative items/quantities:

- Match of overall deflection profile shapes.
- Match of amplitudes (i.e., |w|).
- Match of elastic wave-lengths (or rather the "peak distances" x_{peak}).

- Evaluation of average phase differences (i.e., Δx_{avg}).

The four mentioned comparative items/quantities have been attributed one out of three "grades": *Excellent*, *Good* or *Poor*, where the adopted "grading" system is quantified in Table 14 for the latter three items/quantities. With respect to the first of the comparative items, the "grades" were attributed on the basis of qualitative evaluations of the overall deflection patterns. The complete overview of the comparative results is presented in Table 15.

	Excellent	***Good***	***Poor***
Error on predicted amplitude	*≤15 %*	*≤30 %*	*>30 %*
Error on predicted wave-length (or rather x_{peak})	*≤10 %*	*≤20 %*	*>20 %*
Average phase difference Δx_{avg}	*≤1.5 mm*	*≤3.0 mm*	*>3.0 mm*

Table 14. Quantification of "grading" used in Table 15.

By summarising the comparative features presented in Table 15 it is seen, that the results can conveniently be grouped into two different categories:

- Category 1: Results obtained for the "flat" aspect sample sides (B-sides).
- Category 2: Results obtained for the "golf-ball" aspect sample sides (A-sides).

The results obtained for the first category have generally been very good in the sense, that the experimentally and theoretically obtained deflection profiles compared very well. However, exceptions from this "good" match were encountered for the sample sides, which were subjected to low load levels during the recording of the specklegrams.
The results obtained for the second category were less favourable, as the local bending responses induced by the ply "drop-off" effects (LB-response) were dominated by the presence of local bending effects with a wave-length equal to the honeycomb cell size (HC-response). Furthermore, the theoretical and measured deflection profiles were out-of-phase with about one half elastic wave-length, i.e., they were of opposite phases.
Based on the comparative results discussed in this and the previous sections, the following general conclusions have been drawn:

- The elastic foundation approach derived and implemented in ref. [1] does provide a good description of the local bending effects encountered around ply "drop-off's" in structural CFRP/honeycomb sandwich panels.
- Systematic surface irregularities (i.e., "flatness" deviations) influence the local bending response considerably. Thus it has been demonstrated, that for instance co-curing of sandwich panels causes significant HC-response parts to be induced in the face-laminates characterised as the "golf-ball" aspect sides.
- The investigated test-specimens were of typical "spacecraft composition" in the sense, that they were characterised by thin CFRP face-laminates in combination with a lightweight core. For such configurations the HC-response parts were seen

to be very significant. However, the HC-response parts were seen to decrease with increasing laminate thickness, and are not likely to cause problems in sandwich panels for "non-space" applications (usually characterised by the use of much thicker face-laminates, and often with polymeric foam cores).

Test-specimen/ Sample side	*Match of overall shapes*	*Match of amplitudes*	*Match of elastic wave-lengths*	*Match of phases*	*Comments*
s11A	*Excellent*	*Poor*	*Excellent*	*Poor*	*"Opposite phase" problem*
s11B	*Good*	*Good*	*Good*	*Poor*	*Problems at ends of sampling interval*
s12A	*Excellent*	*Poor*	*Poor*	*Poor*	*"Opposite phase" problem*
s12B	*Good/ Excellent*	*Excellent*	*Excellent*	*Excellent*	*Fine match on nearly all points*
s21A	*Good*	*Poor*	*Excellent*	*Poor*	*"Opposite phase" problem*
s21B	*Excellent*	*Good/ Excellent*	*Good*	*Good*	*Fine match on nearly all points*
s22A	*Good*	*Good/Poor*	*Excellent*	*Poor*	*"Opposite phase" problem*
s22B	*Excellent*	*Excellent*	*Good/ Excellent*	*Good*	*Fine match on nearly all points*
s31A	*Good*	*Excellent*	*Good*	*Poor*	*"Opposite phase" problem*
s31B	*Poor*	*Poor*	*Poor*	*Good*	*Problems at ends of sampling interval*
s32A	*Good/Poor*	*Excellent*	*Poor*	*Poor*	*"Opposite phase" problem*
s32B	*Good/ Excellent*	*Excellent*	*Excellent*	*Excellent*	*Fine match on nearly all points*

Table 15. Summary of comparisons between experimentally obtained (filtered) and theoretical predicted out-of-plane deflection profiles. See Table 14 for quantification of applied "grading" system.

6.4 Future experimental investigation of ply "drop-off" effects in CFRP sandwich panels - "lessons learned"

As described in the previous sections of this report, the results of the experimental investigation have generally demonstrated a convincing match between the experimentally obtained and the theoretically predicted deflection profiles. However, during the period of the test work (conducted by MRC, Bruxelles) as well as during the period of the processing of results, a number of problems were encountered. Some of these problems were anticipated beforehand, while others were not, and on the basis of the gathered experiences a number of recommendations will be given for the purpose of possible future investigations of ply "drop-off" effects in CFRP sandwich panels.
The recommendations will be given separately for three different aspects of the preparation and undertaking of future experimental investigations.

6.4.1 Interferometric technique

Pertaining to the experimental technique chosen and applied in this study, i.e., electronic speckle pattern interferometry or ESPI, there is no doubt, that the method has been very successful in the present case. Thus, the high measuring sensitivity and accuracy of the method were indeed necessary in order to "catch" the very localised ply "drop-off" effects. Other methods, such as holographic interferometry (HI) or phase shifting speckle interferometry (PSSI, ref. [8]) could also have been used for the conduction of the experiments, but the sensitivity and accuracy of these methods are essentially the same as for ESPI.
There is one significant feature of the HI-technique that must be considered as an advantage in the present context. Thus, the HI-technique provides interferometric images of very high resolution with very low noise levels (i.e., no speckle noise as seen in the ESPI-images). The disadvantage is, however, that the capture of a HI-image takes much longer (about one minute using "thermoplastic recording" and much longer using traditional films/film-plates) than the capture of an ESPI-image (about 1/30 second).
Thus, ESPI or one of the other optical interferometric techniques can be recommended for future experimental investigations of ply "drop-off" effects. In fact, there are no realistic alternatives to the optical interferometric techniques due to the extremely localised nature of the problem addressed.
Considering the results obtained from the experimental investigations presented herein, however, it should be noted, that better comparative results could have been obtained if the size of the "measurement window" (i.e., the surface area of the test-specimens where interferometric images were captured) had been somewhat larger. Thus, for future investigations of ply "drop-off" effects (in sandwich panels with similar characteristics) it is recommended to double the size of the "measurement window" (at least in the longitudinal direction). This, obviously, will produce lower resolution images, but will make it possible to capture larger parts of the local bending response (preferably at least one complete wave-length on each side of the ply "drop-off's").

6.4.2 Test-specimens - manufacturing and quality

One of the problems addressed on numerous occasions in this report was the so-called "golf-ball" aspect surface problem. This problem was caused by the (unfortunate) decision of allowing the manufacturing of the CFRP/honeycomb sandwich test-specimens in one cure-cycle (co-curing) instead of two separate cure-cycles as specified in the work statement (see appendix). The result was that one sample side on each test-specimen was predeformed into a characteristic doubly-curved pattern ("golf-ball" aspect

surface, see Fig. 5) where the face-laminates were indented into the honeycomb core cells[22].
The second sample side of each specimen was flat ("flat" aspect surface, see Fig. 6) as it was in direct contact with the mould plate during co-curing. Unfortunately, these surfaces were also displaying a characteristic irregularity (see Fig. 7), which was caused by the fact, that the mould surface was not "stepped" to provide for the change of laminate thickness over the length of the test-specimens.
The combined results of the above mentioned "irregularities" were:

- The deflection profiles obtained for the "golf-ball" aspect sample sides were significantly influenced by the so-called HC-response parts, i.e., the bending response parts induced by the discrete support supplied by the honeycomb core. The local bending response parts induced by the ply "drop-off's" (LB-responses) were therefore especially difficult to identify for these sample sides, and the scatter associated with the experimental results was rather significant. Furthermore, the LB-response parts were displaying a phase difference of about one half elastic wave-length compared with the theoretical predictions.
- For the "flat" aspect surfaces, it is believed that the displayed irregularity had a slightly distorting effect on the out-of-plane deflection profiles (as discussed previously).

Based on the above observations it is recommended, that co-curing should not be used for the manufacturing of CFRP/honeycomb sandwich test-specimens for future investigations, as this effectively will reduce the chances of identifying the LB-response parts clearly. Furthermore, it is recommended to manufacture the tapered face-laminates by use of a specially machined mould with a "step" corresponding to the thickness change of the laminate. Adopting these recommendations in future investigations will ensure a better quality of the test-specimens, and in the end make it possible to place more confidence in the experimental results obtained.

With the above recommendations made clear it should be noted, however, that the comparative results obtained in the present investigation have generally been good even for the "golf-ball" aspect surfaces (except for the "opposite phase" phenomenon). Thus, it has been demonstrated, that the elastic foundation approach suggested in ref. [1] provides a good description even for local bending effects in co-cured CFRP/honeycomb sandwich panels. Considered in this perspective, the "golf-ball" aspect surface problem encountered can be seen as a "fortunate accident"[23].

6.4.3 Test-specimens - characteristic properties

To conclude the discussion pertaining to recommendations for possible future investigations of ply "drop-off" effects in sandwich panels, some comments related to the test-specimen configurations will be given.
In the present experimental investigation three different configurations were included, each with different elastic response characteristics (configurations 1 to 3; see sections 4.2 and 5.3). These different characteristics were obtained by specifying different face-laminate lay-ups, while maintaining the same core material (Hexcel 3/16"-5056-0.0007") and the same UD prepreg system (carbon/epoxy 6T6-145F500 supplied by Hexcel). The three configurations were chosen such that their properties were representative for typical

22 If nothing else, the characteristics of the "golf-ball" aspect surfaces have been demonstrated very clearly, thus revealing why co-curing of sandwich panels should generally be used with great caution (especially for sandwich panels with very thin laminated face-sheets).

23 Moreover, as co-curing is used quite often, the encountered experiences with the "golf-ball" aspect sample sides reflect sandwich panel characteristics, which are very realistic.

space application sandwich panels, i.e., with thin face-laminates (from three to six plies) in conjunction with lightweight/light-gauge honeycomb core.
As described already, the theory worked reasonably well for the investigated sandwich panels, but for the sake of completeness it would be relevant to widen the scopes of a possible future investigation[24]. Thus, one or more of the following features are recommended to be included:

- Sandwich panel configurations with different honeycomb core types (various cell sizes, gauge sizes and core thicknesses).
- Sandwich panel configurations with polymeric foam cores that are used extensively in other industrial areas. The experimental investigation of local bending effects associated with ply "drop-off's" in such sandwich panels will be easier as no HC-response parts will be present (polymeric foam cores supply a continuous support for the face-laminates), and as the wave-lengths of the elastic responses will be longer (due to the lower stiffness of polymeric foam cores as compared with honeycomb cores).
- Sandwich panels with different face-laminate configurations including different material systems (various fibre and resin systems).
- Sandwich panels (test-specimens) with more than one ply "drop-off" station on each sample side in order to investigate interaction effects between adjacent ply "drop-off's".

7.0 CONCLUSIONS

In the present study the results of a combined experimental and theoretical investigation of ply "drop-off" effects in CFRP/honeycomb sandwich panels has been presented. The objective of the study was to adjust and validate a theoretical model suggested and developed in ref. [1]. The theoretical model, which appears as a simple tool for engineering analysis, is based on the adoption of an elastic foundation model for describing the interaction between the face-laminates and the honeycomb core material.
The experimental investigation was carried out using electronic speckle pattern interferometry (or ESPI), which is a very sensitive optical interferometric method providing "whole field" measurements of surface deflections with very high accuracy.
Six CFRP/honeycomb sandwich test-specimens of typical spacecraft application composition (i.e., very thin face-laminates and lightweight/light-gauge honeycomb) were manufactured; three different configurations with two specimens of each, thus providing a total of twelve test-specimen sample sides. The three different test-specimen configurations were characterised by having different elastic response characteristics in the sense, that the face-laminate thicknesses and the "drop-off" sizes were varied. The same honeycomb material (Hexcel 3/16"-5056-0.0007"; core thickness *5/8" = 15.88 mm*) and CFRP/epoxy UD-prepreg system (Hexcel 6T6-145F500; cured ply thickness *0.145 mm*) were maintained for all the test-specimens. The three test-specimen configurations included in the investigation were:

- ***Configuration 1:***
  Base-line laminate: 3-ply symmetric laminate: $[0°/90°/0°]$.
  Reinforcing laminate: 2-ply asymmetric laminate: $[\pm 45°]$.

24 With the objective of providing results of interest in connection with other application types than spacecraft design. Examples could be aircraft, automotive, marine as well as general transportation applications.

- ***Configuration 2:***

  Base-line laminate: 6-ply symmetric laminate: $[0°_2/90°]_S$.

  Reinforcing laminate: 4-ply symmetric laminate: $[\pm 45°]_S$.

- ***Configuration 3:***

  Base-line laminate: 6-ply symmetric laminate: $[0°_2/90°]_S$.

  Reinforcing laminate: 2-ply asymmetric laminate: $[\pm 45°]$.

Each of the CFRP/honeycomb sandwich test-specimens was manufactured in one cure cycle (i.e., co-cured instead of using separate cure-cycles for each face-laminate followed by bonding of the sandwich specimens as requested in the work statement), and the result was, that the surface quality of one sample side of each of the test-specimens was of poor quality ("golf-ball" aspect surface), while the other sample side was essentially flat ("flat" aspect surface). Thus, the quality of the test-specimens was not as good as anticipated (though reflecting realistic surface properties on the other hand).

The experiments were conducted by loading the test-specimens in uni-axial compression, and capturing video images of the sample side surfaces at two different load levels with the ESPI-equipment. From these pictures an interferometric image (specklegram) containing complete information about the out-of-plane deflection pattern (in the form of fringe patterns) was computed for each sample side by digital image processing.

The preliminary results obtained from the experiments demonstrated, that the elastic foundation approach suggested in ref. [1], needed some adjustments in order to provide reasonable predictions of the local deflection amplitudes as well as of the elastic wave-lengths. These adjustments were associated with the expressions used for relating the geometrical and material properties of the constituent materials (i.e., the CFRP face-laminates and the honeycomb core) to the elastic foundation moduli denoted by K_z and K_x, which are needed in the formulation. Thus, the expressions suggested in ref. [1] (based on an assumption of "exponential decay" through the core thickness) turned out to over-predict the stiffness of the core material, and thereby underestimating the out-of-plane deflections. The theory was adjusted by adopting an assumption of "linear decay" through the core thickness, which resulted in new and very simple expressions for K_z and K_x. The results of the adjustments were, that considerably improved predictive capabilities of the elastic foundation approach were achieved with respect to overall deformation patterns, deflection amplitudes as well as elastic wave-lengths.

With respect to the results of the "main" part of the investigation, the essence of the comparative results was presented in dense form in Table 15. The experimental results obtained were associated with considerable scatter, where especially the test-specimen sample sides with "golf-ball" aspect surfaces (co-curing problem) displayed "irregularities" in their elastic response characteristics. The reason for this was, that the local bending responses induced by the ply "drop-off" effects (LB-response parts) were dominated by the presence of local bending effects with a wave-length equal to the honeycomb cell size (HC-response parts). Thus, the initial "curviness" of these surfaces (the "golf-ball" aspect properties) caused the inducement of very significant HC-responses, which effectively "drowned" the LB-response parts for some of the specimens. This effect was seen to be especially pronounced for the measurements conducted at relatively low load levels. Furthermore, the LB-responses for the "golf-ball" aspect sample sides all displayed a phase difference of about one half elastic wave-length as compared with the theoretical predictions (i.e., they were of opposite phases). The reason for the occurrence of this "systematic" displacement of the LB-responses is not understood, but is a consequence of the "flatness" deviations of the sample side surfaces (poor surface quality).
However, it was possible, even for the sample sides with "golf-ball" aspect surfaces, to demonstrate a convincing match between the experimentally obtained and the theoretically

predicted out-of-plane deflection profiles with respect to overall deformation patterns, deflection amplitudes and elastic wave-lengths.
With respect to the measurements performed on the "flat" aspect sample sides, the comparative results were generally very good on all points.

Thus, the main conclusion drawn from the complete investigation is that the elastic foundation approach (with adjusted expressions for the elastic foundation moduli) provides a simple and reasonably accurate description of the local bending effects encountered around ply "drop-off's" in CFRP/honeycomb sandwich panels. Moreover, as the developed engineering analysis and design model (ref. [1]) is very simple (describing the face-laminate/honeycomb core interaction in terms of two constants), the obtained results are considered as very satisfactory.
Performing an analysis with the capability of capturing the complete elastic response including LB-response parts, HC-response parts as well as the various geometric "irregularities" would involve much more refined modelling of the problem. Thus the model should include the discrete nature of the honeycomb material, the initial "curviness" of the face-laminates, coupling effects in the laminates, and finally the interaction between the two face-laminates of the sandwich panels. Obviously, such a model would be capable of providing much more accurate results, but would also be "orders of magnitude" more complicated than the simple elastic foundation approach suggested in ref. [1]. Thus, a model with the potential of predicting the full elastic response (most likely an elaborate finite element model) is not likely to be suitable for engineering analysis and design purposes merely because of its complexity.

ACKNOWLEDGEMENT

The contents of this report represent parts of the work carried out during the period of an ESA research fellowship awarded with the Structures and Mechanisms Division, Structural Engineering Section (YME) at the European Space Research and Technology Centre (ESTEC) in Noordwijk the Netherlands.

REFERENCES

1. Thomsen, O. T., *Analysis of Thickness-Change Induced Local Bending Problems in CFRP-Sandwich Panels.* ESTEC Working Paper EWP-1787, The Netherlands, June 1994.
2. Thomsen, O. T., Analysis of local bending effects in sandwich plates with orthotropic face layers subjected to localised loads. *Composite Structures* **25** (1993) pp. 511-520.
3. Thomsen, O. T., Theoretical and experimental investigation of local bending effects in sandwich plates. *Composite Structures* **30** (1995) pp. 85-101.
4. Vlasov, V. Z. and Leont'ev, N. N., *Beams, Plates and Shells on Elastic Foundations.* Moscow 1960 (English translation by Israel Programme for Scientific Translation, Jerusalem 1966).
5. Hétenyi, M., *Beams on Elastic Foundations,* The University of Michigan Press, Ann Arbor, Michigan, 1946.
6. Kerr, A. D., Elastic and viscoelastic foundation models, *Journal of Applied Mechanics*, Sept. 1964, pp. 491-498.
7. Zhaohua, F and Cook, R. D., Beam elements on tw0-parameter elastic foundations, *ASCE Journal of Engineering Mechanics*, **vol. 109**, No. 6, Dec. 1983, pp.1390-1402.

8. Maas, A. M., *Phase Shifting Speckle Interferometry*, Ph.D. Thesis, Technical University of Delft, The Netherlands, 1991.
9. FINAL REPORT: *Experimental Investigation of Thickness Drop-Off Effects in CFRP-Sandwich Panels*, ESTEC Contract No. 10.983/94/NL/PP (prepared by Dupont, O. and Queekers, P.), Microgravity Research Center, Université Libre de Bruxelles, May 1995.
10. Zenkert, D., *An Introduction to Sandwich Construction*, Royal Institute of Technology, Stockholm, 1993.
11. MATLAB®, version 4.1, *User's Guide (For UNIX Workstation's)*, The MATH WORKS Inc., 1993.
12. Signal Processing TOOLBOX, For Use with MATLAB®, version 4.1., *User's Guide*, The MATH WORKS Inc., 1994.

APPENDIX

STATEMENT OF WORK FOR

EXPERIMENTAL INVESTIGATION OF THICKNESS DROP-OFF EFFECTS IN CFRP-SANDWICH PANELS

prepared by

O. T. Thomsen
ESA/ESTEC/YME
December 1, 1994

under

ESTEC CONTRACT NO. 10.983/94/NL/PP.

Contractor: Microgravity Research Center (MRC),
Université Libre de Bruxelles,
Avenue F. D. Roosevelt 50,
B-1050 Bruxelles CP 165,
Belgium.

Project manager: Dr. Olivier Dupont.

Subcontractor for MRC: C. R. I. F. Technologie des Matériaux,
Parc Scientifique de la Cense Rouge,
Rue du Bois Saint-Jean 12,
B-4102 Ougree, Seraing,
Belgium.

EXPERIMENTAL INVESTIGATION OF THICKNESS DROP-OFF EFFECTS IN CFRP-SANDWICH PANELS

1. INTRODUCTION

This work statement defines the experimental investigation of local bending effects in compression loaded CFRP-sandwich panel samples with a CFRP face-sheet laminate drop-off. The objective of the investigation is to measure the out-of-plane displacements around the CFRP-facesheet thickness drop-off zones of typical lightweight CFRP-honeycomb sandwich panels for space applications.

The work required consists of:

1. Manufacturing of six (6) sandwich panel test-specimens with a CFRP-facesheet thickness drop-off.
2. Measurement of elastic engineering constants E_x, E_y and ν_{xy} for two (2) CFRP-laminates.
3. Measurement of out-of-plane displacements around thickness drop-off zones under compression load.

2. TECHNICAL SPECIFICATIONS

2.1 Manufacturing of test-specimens

Six (6) sandwich panel test-specimens, with geometry as shown in figure 1, needs to be manufactured. Two (2) samples of each of the following three (3) CFRP-laminate/honeycomb-core sandwich configurations are required:

Config. 1:

Face 1 (baseline laminate):
- 3-ply (symmetric) laminate: [0°/90°/0°].
- laminate thickness: t_1=0.411 mm.

Face 2 (reinforcing laminate):
- 2-ply asymmetric laminate: [±45°].
- laminate thickness: t_2=0.274 mm.

Config. 2:

Face 1 (baseline laminate):
- 6-ply symmetric laminate: $[0_2°,90°]_S$.
- laminate thickness: t_1=0.822 mm.

Face 2 (reinforcing laminate):
- 4-ply symmetric laminate: $[±45°]_S$.
- laminate thickness: t_2=0.548 mm.

Config. 3:

Face 1 (baseline laminate):
- 6-ply symmetric laminate: $[0_2°,90°]_S$.

- laminate thickness: t_1=0.822 mm.

Face 2 (reinforcing laminate):
- 2-ply asymmetric laminate: [±45°].
- laminate thickness: t_2=0.274 mm.

The following materials are to be used:

UD-prepreg: 6T6-145F500 carbon fibre/epoxy system;
curing temperature: 250 °F (120 °C);
cured ply-thickness: 0.137 mm (61.1 fibre vol. %).

Honeycomb: HEXCEL Aluminium 3/16"-5056-0.0007"; core thickness: 10 mm (or 20 mm if that turns out to be more convenient).

The CFRP-laminates with thickness drop-offs will be cured separately. The CFRP-laminates will be bonded to the honeycomb cores in a separate cycle. The test-specimens will be provided with epoxy end-taps with faces perpendicular to the CFRP face-sheet laminates.

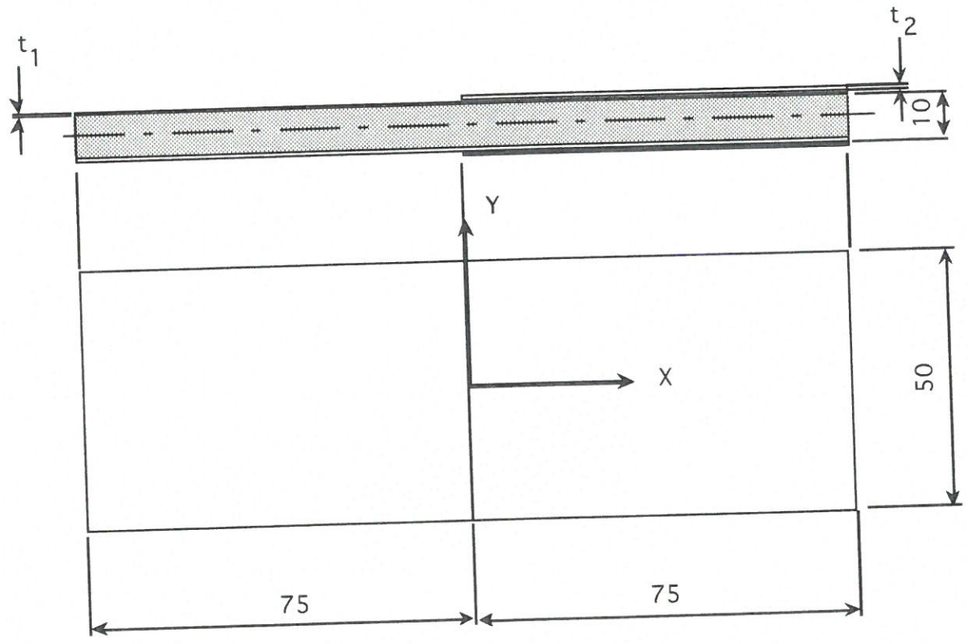

Figure 1. Test-specimen geometry ("end-taps" not shown).

2.2 Measurement of engineering constants

In order to validate the material data supplied by the manufacturer, it is required that the in-plane elastic engineering constants E_x, E_y and ν_{xy} are measured for the base-line laminates (face 1) of configurations 1 and 2. The measurements shall be performed on four (4) tensile test-specimens for each of the base-line face-laminates:

Test-config. 1; face 1: two (2) tensile specimens for measuring E_x and ν_{xy};
two (2) tensile specimens (off-axis) for measuring E_y.

Test-config. 2; face 1: two (2) tensile specimens for measuring E_x and ν_{xy};
two (2) tensile specimens (off-axis) for measuring E_y.

2.3 Loading device

ULB will modify an existing loading device in order to comply with the loads expected to be needed to obtain out-of-plane displacements of about 100 nm.

Expected in-plane compressive load for test-config.1: P_{c1}=550 N.
Expected in-plane compressive load for test-config.2: P_{c2}=770 N.
Expected in-plane compressive load for test-config.3: P_{c3}=1600 N.

3. MEASUREMENT OF OUT-OF-PLANE DISPLACEMENTS

ULB will measure the out-of-plane displacements on the twelve (12) sample sides around the thickness drop-offs of the 6 test-samples under compressive load. The out-of-plane displacements will be measured using the ESPI (electronic speckle pattern interferometry) technique together with digital image processing.

4. REPORTING

ULB will produce a report containing all relevant test-data, and a description of the test set-up and test-procedure. The derived out-of-plane displacement distributions will also be supplied on 1.4" floppy diskettes (as ASCII-data files).

5. TIME-SCHEDULE

ULB will start the test programme in calendar week 1 of 1995, and the tasks will be carried out such that the full programme can be completed at the end of February 1995.
The test programme shall foresee two (2) meetings at ESTEC, Noordwijk, The Netherlands.

6. FINAL PROPOSAL

The final proposal shall include a total price breakdown (specified on the ESA PSS-A2 sheet).

7. CONTRACT

The contract will be arranged through ERA Technology Ltd., Cleeve Road, Leatherhead, Surrey KT22 7SA, United Kingdom, contact person: David Bashford (direct telephone: +44 (0) 1372 367062; direct fax: +44 (0) 1372 377927).